From the School of Physical Sciences,
Dublin City University,Glasnevin,
Dublin 9, Ireland

"On The Growth and Characterisation of Zinc Oxide"

by A.J. Meaney, B.Sc.

Under the supervision of Prof. Martin Henry

July-2010

Für Ricarda,
schöner Götterfunken,
Tochter aus Elysium.

Declaration:

I hereby certify that this material, which I now submit for assessment on the programme of study leading to the award of Dr. of Philosophy in Physics is entirely my own work, that I have exercised reasonable care to ensure that the work is original, and does not to the best of my knowledge breach any law of copyright, and has not been taken from the work of others save and to the extent that such work has been cited and acknowledged within the text of my work.

Signed: _____ ID No.: 99502658

July-2010

Table of Contents

Ch. 3: Growth and Preparation

Ch. 4: Thin Films and Nano-Structures

Ch. 5: Doped ZnO Thin Films

On The Growth and Characterisation of Zinc Oxide

A.J. Meaney

Abstract:

Optical, electrical and structural properties of ZnO grown via grown via PLD and VPT were examined. Both growth techniques were successful in producing nano-structured ZnO with thin films also produced with PLD. An epitaxial relationship to the substrate was found for all materials. A temperature-stepping growth process was identified as beneficial to overall material quality. Good quality nominally un-doped material with sharp near band edge (NBE) emission was achieved, demonstrating a FWHM of 1.9meV, compared to 0.7meV for single crystal samples. VPT and PLD nano-strucutres displayed a characteristic PL features due to the surface exciton, SX. Doped ZnO demonstrated p-type conductivity, with carrier concentrations as high as $4 * 10^{16} \, cm^{-3}$ under illumination for N-ZnO. P-ZnO displayed a fast-decaying photoconductive effect. High concentrations of dopant were found disadvantageous to crystalline and optical quality, but evidence of ABX emission was observed with as much as 2.5 wt% of dopant. Li and Bi were also employed as dopant sources but neither produced evidence of a p-type film.

Chapter 1 – Introduction

1.1 – A History of Zinc Oxide

Producing technologically advanced devices is often hindered by material availability, or from limitations imposed in material production. The semiconductor physics industry commonly encounters such developmental obstacles for new devices and the difficulty in fabrication of p-type conducting zinc oxide (ZnO) is a prime example. This II-VI semiconductor has long since offered the potential for new devices such as blue / UV emitting laser diodes[1] and high-temperature transparent field-effect-transducers (FET). Producing the p-type conducting material required for basic p-n junctions necessary to realise these devices has eluded many across the globe.

ZnO is a very desirable semiconductor for fabrication of many of these devices as it provides superior qualities in comparison to others. It exhibits a high piezoelectric coefficient (1.2 cm^{-2}), larger thermal conductivity than its counterparts (some 0.05 $WK^{-1} cm^{-1}$ more than gallium arsenide), the largest exciton binding energy of the II-VI and III-V semiconductors at 60 meV and a band gap of 3.437 eV at 1.6 K [1]. These properties and the prospect of ZnO-based devices being realised led to a rapid expansion in theoretical, fabrication, characterisation and application based research in the latter half of the 20th century leading to recent realisation of ZnO-based devices [2].

ZnO had been studied extensively for a number of decades, with reviews of the electrical [3] and optical [4] properties available as early as the 1950's describing, for example, the stubborn n-type conductivity, showing absorption spectra, electro-luminescence decay parameters, and so forth. The first period of notable growth in ZnO research occurred in the mid 1960's with a series of highly-cited theoretical and characterisation works. The nature of the excitonic molecule in semiconductors was extensively discussed by Haynes [5], aiding a key publication by Park *et al* concerning the observation of excitonic emission in ZnO [6]. A definitive paper from Reynolds *et al* [7] concerning Zeeman splitting in ZnO absorption lines introduced the canonical *I*-line nomenclature, assigning the near band-edge spectral lines to excitonic complexes. An important contribution from Damen and Porto[2] [8] identified ZnO phonon energies in 1966 from Raman Effect studies.

---

[1] Together with the applications these would allow; high capacity data discs, image scanning / printing, lasing, etc.

[2] Preliminary studies of these phenomena appeared earlier in [9] and [10], though these were of far less impact.

The higher-profile works[3] in the 1970's concentrated mainly on manufacture and characterisation of simpler ZnO devices [11-14]. Reasonably high-purity polycrystalline ZnO was available but not large area, good quality bulk material. Because of this, device application was limited to the development of ceramic varistors, phosphors and piezoelectric transducers or others that involved neither epitaxial nor single crystal material required to realise the full technological impact of this promising semiconductor.

Theoretical and experimental work also continued to offer further insight into the optical and electrical character of the material through a variety of techniques: cathodoluminescence (CL) [15], capacitance-voltage studies (CV) [16], electrical conduction [17] and further work on Raman scattering [18]. This characterisation, as with device development, was again restricted to working with polycrystalline ZnO or performing electrical studies on the simpler ceramic devices but the interest in ZnO continued to grow. Overall, from 1950 to 1970 there was an order of magnitude increase in the number of publications per year, as shown in figure 1.i.

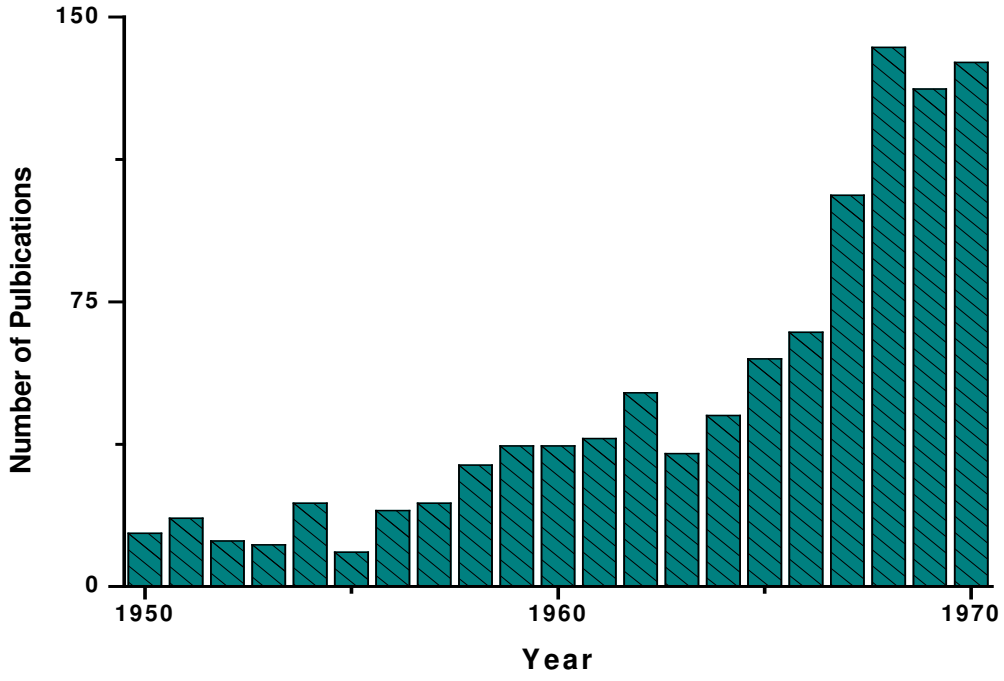

Fig. 1.i: ZnO journal publications year-on-year from 1950-1980.
Source: ISI Web of Knowledge.

Publications concerning ZnO continued with many concentrating on similar research to the 1970's, expanding on areas such as varistor characterisation [20], deep

[3] Based on citation volume.

defects [21] and electrical studies [22]. The 1980's led to a departure from such characterisation studies of the simpler ZnO-based devices. Many growth procedures were examined in the quest for high-quality thin films. Metallo-organic chemical vapour deposition (MOCVD) [23], spray pyrolysis [24] and radio-frequency (RF) magnetron sputtering [25] were discussed extensively in 1980s publications as viable techniques for growing good quality ZnO.

The principal papers concerning ZnO growth mechanisms concentrated on sputtering techniques discussed originally by Shiosaki *et al* [26]. Some other studies involving ZnO doped with group-III [27] or group-V [28] elements were published but the 1980's also saw the beginning of the now extensive ZnO nano-structure growth. A paper on quantum-size particle growth has become a highly influential work [29], as did characterisation of high-quality ZnO thin films [30]. In addition, other work tackling the p-type issue with doping of thin films [31] fuelled interest in ZnO. Much of the research in the 1980's attempted to resolve issues concerning a lack of satisfactory material for device fabrication but the number of papers published each year remained fairly constant, showing a drastic slowing in the growth of this field as seen in figure 1.ii. The quality of material available seems the most likely cause of this plateau.

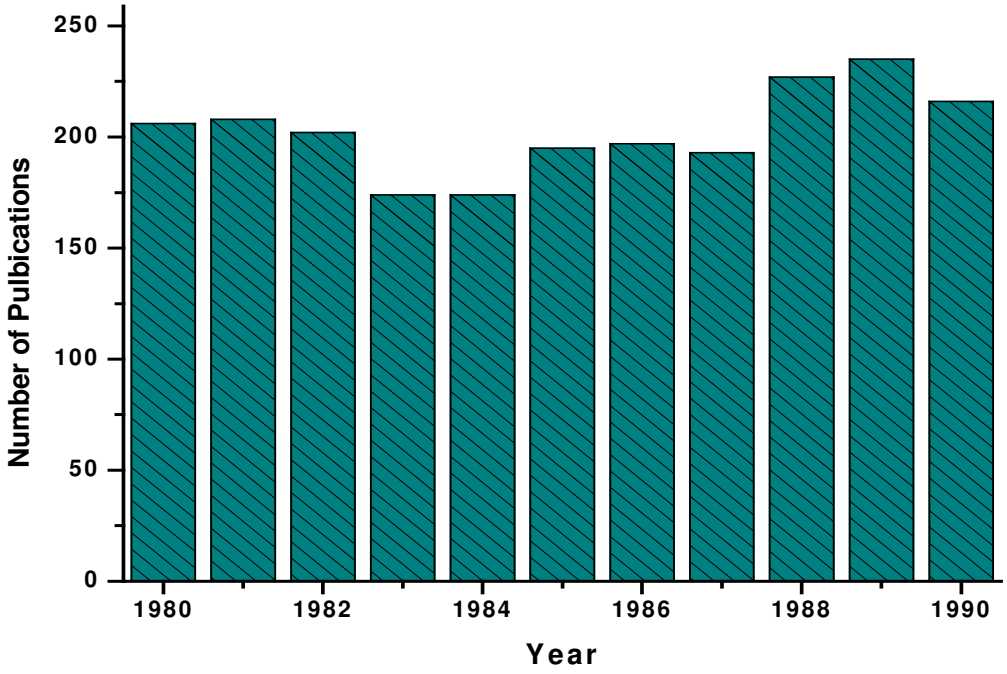

Fig. 1.ii: ZnO journal publications year-on-year from 1980-1990.
Source: ISI Web of Knowledge.

The dramatic explosion in ZnO research began in the 1990s, as evidenced in figure 1.iii. The community saw similar growth rate as from 1950 to 1980 with an order of magnitude increase in publications to some 5000 plus publications per annum.

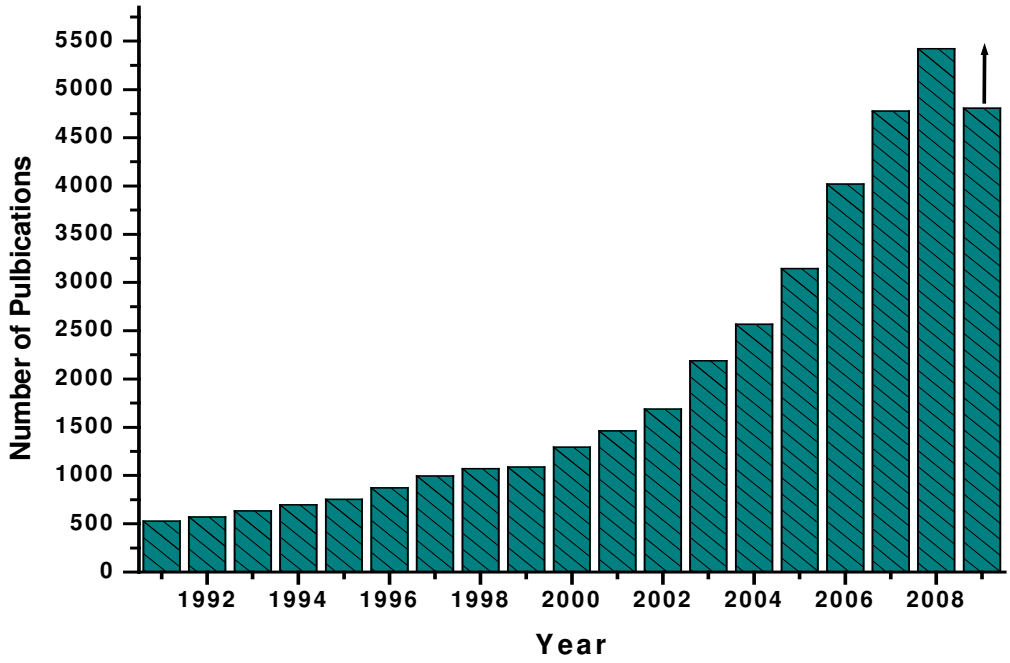

Fig. 1.iii: ZnO journal publications year-on-year from 1990 - winter 2009.
Source: ISI Web of Knowledge.

The level of interest in ZnO over the four previous decades had grown but not as markedly as in the 1990's. There was a steady flow of publications concerning growth techniques and characterisation, but only one significant milestone in increase in year-on-year publication numbers that came from 1966-67. The near doubling of interest as seen in the 1960's again occurred in 1990-91. The appeal of ZnO has soared since, with now several thousand publications per annum.

The plethora of works from 1990 onward focused on high-quality growth [32], doping studies directed toward p-type ZnO [33], electrical [34], optical [35] and structural characterisation [36], device fabrication [37] and the persistent question of the green-band luminescence [38]. Much of this was hampered by the continuing lack of high quality material, even from the promising growth mechanisms pursued in the 1980's. Characterisation processes were not limited to determining fundamental ZnO properties or identifying a particular defect, but rather used as a tool to verify quality. Many known growth techniques provided hetero-epitaxial thin films of reasonable optical, structural and electrical quality. High-quality, high-purity material however, is

necessary to realise the potential of homo-epitaxial ZnO, to act as a benchmark for thin film quality and to allow reduction of unintentional impurities or defects.

In the 1990's, newer growth methods were used including pulsed laser deposition (PLD) [39] and molecular-beam epitaxy (MBE) [40]. D.C. Look *et al* [34] worked toward fabricating high-purity bulk ZnO wafers and had success in 1998 with the vapour-phase-transport growth method. That work, with colleagues at the Eagle Pitcher Company (E.P. ™), resulted for the first time in commercially available single crystal ZnO. Bulk ZnO had been manufactured and studied since the 50s [41] but large-scale commercial material only came to the forefront of ZnO research in the late 1990s. The numbers of citations of publications involving single crystal ZnO dramatically increased with commercial availability of single crystals, as shown in the figure 1.iv with the inset showing the steady increase of publications concerning singe-crystal ZnO since its inception.

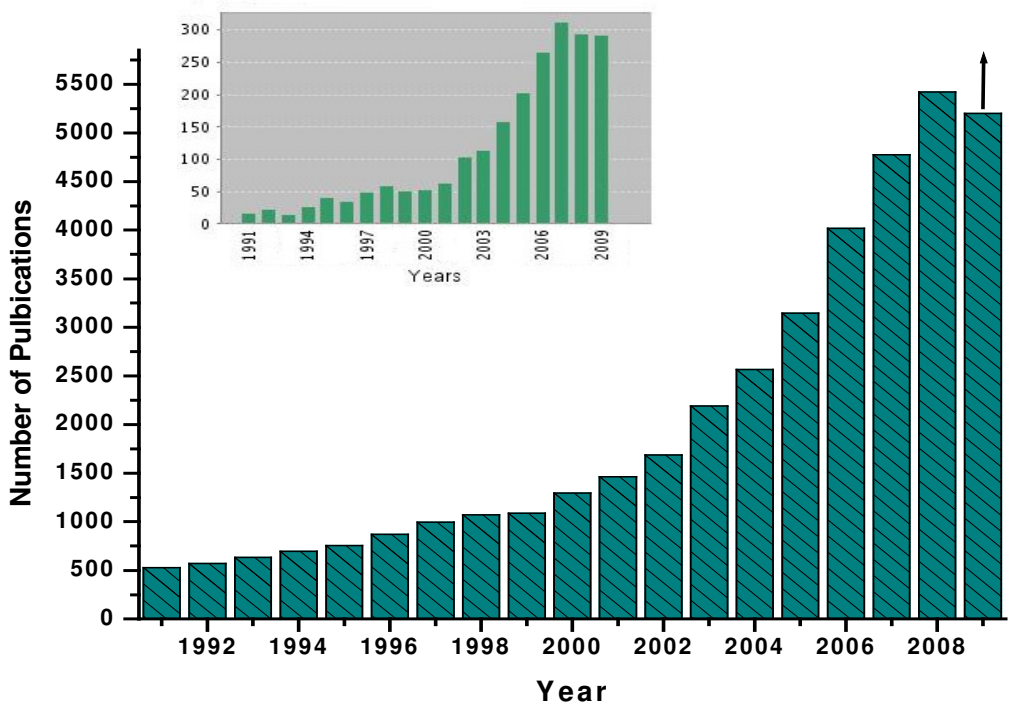

Fig. 1.iv: Year-on-year citation numbers concerning single crystal ZnO from 1990 - winter 2009. Source: ISI Web of Knowledge.

Work in the early part of the 2000s focused mainly on growth mechanisms and parameters. The nature of native defects incorporated from growth was studied [42, 43]; potential p-type dopants and the difficulties encountered in their incorporation examined extensively [44-47], together with the fundamental optical [1, 48] and

electrical [49] properties, and the initial breakthrough of ZnO-based light emitters achieved [50, 51, 52]. Several review articles appeared, showing much of the state-of-the-art knowledge of ZnO. Özgür *et al* [53] and Klingshirn *et al* [54] independently produced papers with extensive discussion on band structure, thermal, mechanical, optical and electrical properties, doping, contacting, growth and devices. The number of research areas in ZnO had mushroomed, but amongst the goals being pursued the production of high quality, reproducible, p-type conducting ZnO for device application was perennial.

1.2 – Doping

Improvement and adjustment of a semiconductor's electrical properties is achieved with addition of a discrete amount of dopant atoms, producing an excess or deficiency of electrons determined by the valence of dopant employed. The doping of ZnO with pentavalent impurity atoms (antimony, phosphorous and nitrogen for example) on an oxygen site or mono-valent impurity atoms (hydrogen, lithium) on a zinc site can create acceptor states, producing p-type conducting ZnO. In successful doping regimes non-native states are produced, either high-energy states lying below the conduction band (CB) edge in the case of donors, or for acceptor states, deep levels close to the VB maximum. A consequence of the Fermi Energy (E_f) remaining the highest possible energy state at 0K, it will reside above any new donor states or below newly created acceptor states, providing levels for donor e^- to be thermally excited to the CB and e^- capture by acceptors above the valence band (VB) to satisfy local bonding.

For semiconductors with native majority hole carriers, electrons can be added by the incorporation of dopant atoms of higher valence than the native atoms to creating n-type material. The latter is not required in ZnO as it presents natural n-type conductivity ZnO. Donor defects such as V_O, Zn_O and Zn_i are commonly present [55] and although V_O displays the lowest formation enthalpy of the native donors, recent consensus is that Zn_i is the dominant donor in as-grown ZnO [56,57]. Recent publications have pointed to the interaction of these native centres with dopants and the subsequent complexes formed as the primary barrier in the p-type doping difficulty for ZnO [58,59].

1.3 – References

[1] B.K. Meyer, H. Alves, D.M. Hofmann, W. Kriegseis, D. Forster, F. Bertram, J. Christen, A. Hoffmann, M. Strassburg, M. Dworzak, U. Haboeck, A.V. Rodina, *Phys. Stat. Sol. (b),* **241**, 2, 231-260 (2004)

[2] M. Law, L.E. Greene, J.C. Johnson, R. Saykally, P.D. Yang, *Nature Materials*, **4**, 6, 455-459 (2005)

[3] A.R. Hutson, *Phys. Rev.* **108**, 2, 222-230 (1957)

[4] G. Heiland, E. Mollwo, F. Stockmann, *Solid State Phys.* **8**,193 (1959)

[5] J.R. Haynes, *Phys. Rev. Lett.* **17**, 16 (1966)

[6] Y.S. Park, C.W. Litton, T.C. Collins, D.C. Reynolds, *Phys. Rev.* **143**, 2 (1966)

[7] D.C. Reynolds, C.W. Litton, T.C. Collins, *Phys. Rev.* **140**, 5A (1965)

[8] T. Damen, S.P.S. Porto, B. Tell, *Phys. Rev.* **142**, 2 (1966)

[9] D.G. Thomas, *J. Phys. Chem. Solids*, **15**, 86 (1960)

[10] S.S. Mitra, J.I. Bryant, *Bull. Am. Phys. Soc.* **10**, 333 (1965)

[11] M. Matsuoka, *J. J. App. Phys.* **10**, 6, 736 (1971)

[12] P.R. Emtage, *J. App. Phys.* **48**, 10, 4372-4384 (1977)

[13] M. Inada, *J. J. App. Phys.* **17**, 1, 1-10 (1978)

[14] F.S. Hickerne, *J. App. Phys.* **44**, 3, 1061-1071 (1973)

[15] E.G. Bylander, *J. App. Phys.* **49**, 3, 1188-1195 (1978)

[16] K. Mukae, K. Tsuda, I. Nagasawa*, J. App. Phys.* **50**, 6, 4475-4476 (1979)

[17] G.D. Mahan, L.M. Levinson, H.R. Phillip, *J. App. Phys.* 50, 2799 (1979)

[18] J.M. Calleja, M. Cardona, *Phys. Rev. B.* **16**, 8, 3753-3761 (1977)

[19] C. Klingshirn, *Phys. Stat. Sol. (b)*, **71**, 2, 547-556 (1975)

[20] L.M. Levinson, H.R. Philipp, *Am. Cer. Soc.* **65**, 4, 639-646 (1986)

[21] A. Kobayashi, O. F. Sankey, S. M. Volz, J. D. Dow, *Phys. Rev. B.* **28**, 2, 946-956 (1983)

[22] W. Gopel, U. Lampe, *Phys. Rev. B*, **22**, 12, 6446-6462 (1980)

[23] S.K. Tiku, C.K. Lau, K.M. Lakin, *App. Phys. Lett.* **35**, 4, 318-320 (1980)

[24] C. Eberspacher, A.L. Fahrenbruch, R.H. Bube, *Thin Solid Films*, **136**, 1, 1-10 (1986)

[25] P.F. Carcia, R.S. McLean, M.H. Reily, G. Nunes Jr. *App. Phys. Lett.* **82**, 7 (2003)

[26] T. Shiosaki, M. Ooishi, S. Ohnishi, A. Kawabata, *Ferroelec.* **19**, 3-4, 166 (1978)

[27] T. Minami, H. Sato, H. Nanto, S. Takata, *J. J. App. Phys. 2*, **24**, 10, L781-L784 (1985)

[28] J. Kim, T. Kimurat, T. Yamaguchi, *J. Mater. Sci.* **24**, 1, 2581-2586 (1989)

[29] D.W. Bahnemann, C. Kormann, M.R. Hoffmann, *J. Phys. Chem.* **91**, 14, 3789-3798 (1987)

[30] S. Benthke, H. Pan, W. Wessles, *App. Phys. Lett.* **52**, 2 (1988)

[31] Z-C. Jin, I. Hamberg, C.G. Granqvist, *J. App. Phys.* **64**, 10 (1988)

[32] F.C.M. Vandepol, *Am. Cer. Soc.* **69**, 12, 1959-1965 (1990)

[33] K. Minegishi, Y. Koiwai, Y. Kikuchi, K. Yano, M. Kasuga, A. Simizu, *J. J. App. Phys.* **2**, 36, 11a, L1453 (1997)

[34] D.C. Look, D.C. Reynolds, J.R. Sizelove, R.L. Jones, C.W. Litton, G. Cantwe11, W.C. Harsch, *Solid Stat. Comm.* **105**, 6, 399-401 (1998)

[35] X. W. Sun, H.S. Kwok, *J. App. Phys.* **86**, 1, 408-411 (1999)

[36] K.H. Kim, K.C. Park, D.Y. Ma, *J. App. Phys.* **81**, 12 , 7764-7762 (1997)

[37] D.M. Bagnall, Y.F. Chen, Z. Zhu, T. Yao, S. Koyama, M.Y. Shen, T. Goto, *App. Phys. Lett.* **70**, 17, 2230-2232 (1997)

[38] K. Vanheusden, C.H. Seager, W.L. Warren, D.R. Tallent, J.A. Voigt, *App. Phys. Lett.* **68**, 3, 403-405 (1996)

[39] N.J. Ianno, L. McConville, N. Shaikh, S. Pittal, P.G. Snyder, *Thin Sol. Films*, **220**, 1-2, 92-99 (1992)

[40] T.V. Butkhuzi, A.V. Bureyev, A.N. Georgebiani, N.P. Kekelidze, T.G. Khulordava, J. Crys. Growth, 117, 1-4, 366-369 (1992)

[41] L. Lucas, *Proceedings: Phys. Soc. Lon. A*, **64**, 383, 943 (1951)

[42] A.F. Kohan, G. Ceder, D. Morgan, C. G. Van de Walle, *Phys. Rev. B*, **61**, 22, 15019 (2000)

[43] S.B. Zhang, S.-H. Wei, A. Zunger, *Phys. Rev. B.* **63,** 075205 (2001)

[44] C. G. Van de Walle, *Phys. Rev. Lett.* **85**, 5 (2000)

[45] T. Aoki, Y. Shimizu, A. Miyake, A. Nakamura, Y. Nakanishi, Y. Hatanaka, *Phys. Stat. Sol. (b)*, **229**, 2, 911-914 (2002)

[46] D. M. Hofmann, A. Hofstaetter, F. Leiter, H. Zhou, F. Henecker, B. K. Meyer, S. B. Orlinskii, J. Schmidt, P. G. Baranov, *Phys. Rev. Lett.* **88**, 4 (2002)

[47] F.X. Xiu, Z. Yang, L.J. Mandalapu, J.L. Liu, W.P. Beyermann, *App. Phys. Lett.* **88**, 052106 (2006)

[48] K. Thonke, Th. Gruber, N. Teofilov, R. Schnfelder, A. Waag, R. Sauer, *Physica B*, **308-310,** 945-948 (2001)

[49] D. C. Look, *Semiconductor Sci. & Techn*. **20,** S55-S61, (2005)

[50] M.H. Huang, S. Mao, H. Feick, *Science*, 292, 5523, 1897-1899 (2001)

[51] A. Tsukazi, A. Ohtomo, T. Onuma, M. Ohtani, T. Makino, M. Sumiya, K. Ohtani, S.F. Chichibu, S. Fuke, Y. Segawa, H. Ohno, H. Koinuma, M. Kawasaki, *Nature Materials*, **4**, 42-46 (2005)

[52] D-K. Hwang, S.-H. Kang, J.-H. Lim, E.-J. Yang, J.-H Yang, J.-H. Yang, S.-J. Park, *App. Phys. Lett.* **86**, 222101 (2005)

[53] Ü. Özgür, Ya. I. Alivov, C. Liu, A.Teke, M.A. Reschikov, S. Doğan, V. Avrutin, S-J. Cho, H. Morkoç, *J. App. Phys.* **98**, 041301 (2005)

[54] C. Klingshirn, R. Hauschild, H. Priller, M. Decker, J. Zeller, H. Kalt, *Superlatt. and Micro.* **38**, 209-222 (2005)

[55] A. Janotti, C.G. Van de Walle, *J. Crys. Growth.* 287, 58-65 (2006)

[56] D.C. Look, J.W. Hemsky, J.R. Sizelove, *Phys. Rev. Lett.* **82**, 12 (1999)

[57] F. Oba, S. R. Nishitani, S. Iostani, H. Adachi, I. Tanaka, *J. App. Phys.* **90**, 2 (2001)

[58] C.H. Park, S.B. Zhang, Su-Huai Wei, *Phys. Rev. B*, **66**, 073202 (2002)

[59] M.D. McCluskey, S.J. Jokela, *J. App. Phys.* **106**, 071101 (2009)

Chapter 2 – ZnO Characterisation

2.1 – Characterisation Techniques

ZnO semiconductor research is undertaken mainly with a view to device application based on p-n junctions for which p-type conducting material is vital. Undoped ZnO notoriously displays only n-type conduction. It is crucial to have techniques available to readily identify any p-type properties in doped material. The features relating to acceptor incorporation are searched for using a wide range of techniques. Photoluminescence (PL) or cathodoluminescence (CL) measurements are employed for optical studies with Hall measurements for electrical characterisation. Insight into deep energy states not probed well with other techniques is available with DLTS (Deep-level transient spectroscopy) with XRD (X-ray diffraction) or SIMS (secondary ion mass spectroscopy) and AFM (atomic force microscopy) used for structural and surface-based characterisation respectively.

PL is the primary optical characterisation technique employed here, due mainly to the technique's ability to aid in defect identification over wide-ranging energies with high resolution, typically from 0.5 eV to 3.5 eV for ZnO.To obtain such spectra, a Spex 1704 1-meter long spectrometer was used, with a Thorn FACT50 photomultiplier set to photon counting mode. Calibrations to Cd or Hg discharge lamp spectra were performed as necessary, to maintain reliability in the ZnO spectra. A helium closed cycle SHI 950 D cryostat, produced by the Janis Corporation, in conjunction with a Sumitomo CKW-21A helium compressor allowed low temperatures to be reached and maintained.

Spectral features are compared with theoretical predictions and classification from experiment for both nominally undoped and doped materials. There is still some controversy in the assignment of ZnO emission lines, though the impurities responsible for some near band edge emission have been chemically identified [1,2]. In electrical studies, a Hall system is employed which provides characteristics of Hall voltage, mobility, carrier concentration and resistivity. Ohmic and Shottky contacting issues [3,4] together with difficulty in measurement conditions can raise questions over the validity of electrical data [5]. Important XRD and AFM data are correlated with optical and / or electrical data in this work, providing insight into crystalline quality and surface morphology.

Optical and electrical measurements are commonly performed over a wide range of temperatures, aiding in identification of material characteristics and allowing demonstration of properties at temperatures necessary for potential device application,

RT excitonic processes for example. The following sections detail the characterisation technique, including examples of material characteristics afforded from each.

2.2– Photoluminescence

Optical excitation of electrons from the VB occurs upon sample illumination from an excitation source of greater energy than the band gap. This is typically laser illumination with a 325nm HeCd laser used for ZnO PL. Coulomb interaction between electrons excited to the CB and VB holes leads to the formation of electron-hole pairs, or excitons. Pair annihilation occurs from recombination and resultant photon emission of energy $\hbar\omega = E_{Gap} - E_{B_{Ex}}$ where $E_{B_{Ex}}$ is the exciton binding energy, 60 meV for ZnO. This is a free excitonic (FX) emission process, resulting in a spectral feature at ~3.347 eV. Such emission is an indication of high quality ZnO, as few defects exist to trap the exciton, resulting in a high probability of direct band-to-band recombination.

Native or impurity related defect sites in imperfect ZnO provide energy states within the gap at which excitons may become localised. Recombination of excitons bound to such defects results in bound exciton emission that usually dominates the ZnO spectrum at low temperature, with analysis providing much information about them. PL features common to ZnO are listed in table 2.i together with some non-excitonic processes, which also occur.

Emission Feature	Process
Donor / Acceptor-Bound-Exciton. (DBX / ABX)	Recombination of exciton bound to acceptor/donor.
Donor-Acceptor Pair (DAP)	Recombination of donor electron and acceptor hole.
Free exciton (FX)	Direct excitonic recombination.
Free Electron to Acceptor (e^-A)	CB electron to acceptor transition.
Intragap-Defect.	Excited to ground state transition in impurity (may be non-radiative).
Longitudinal Optical Phonon (LO)	Exciton recombination coupled with photon emission and phonon(s) creation. Photon energy shifted downward by ~72 meV per emitted phonon.
Two-Electron-Satellite (TES)	Recombination of a bound-exciton electron leaving neutral donor electron in 2s or 2p state.

Table 2.i: A summary of common optical transitions in ZnO

The above transitions are shown in a band gap schematic in figure 2.i demonstrating the variation in energies involved in each:

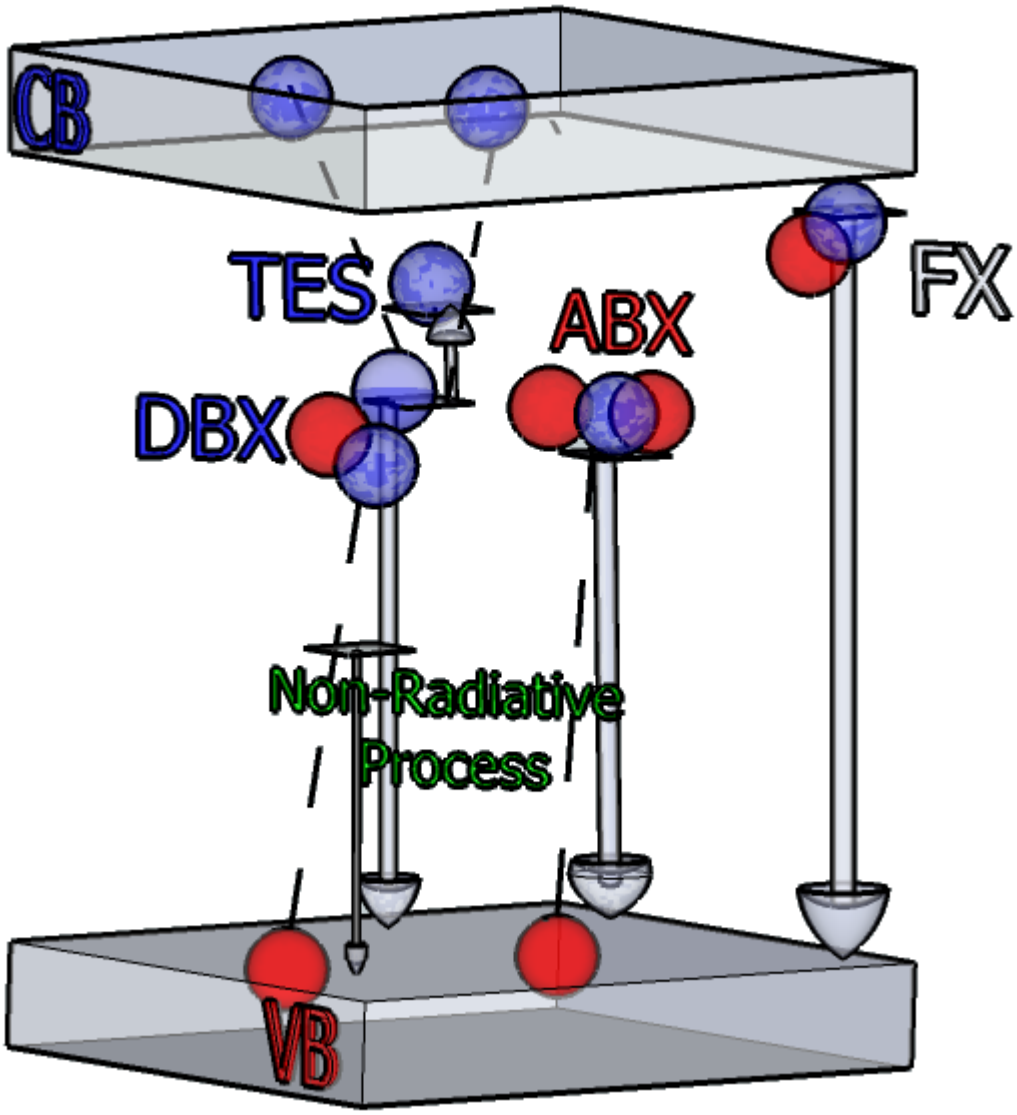

Fig. 2.i: Representation of PL transitions. Energy levels not to scale for 3.44 eV gap,

2.2.1 - Typical ZnO PL Emission

Donor impurities are most common in ZnO with native V_o and Zn_i defects and hydrogen or common group III impurities contributing to n-type conductivity. Considering an exciton bound to a donor such as an In impurity, the recombination of an electron-hole pair from this complex will produce a spectral feature described as DBX emission and is a common signature in nominally undoped ZnO. An example of the DBX emission, which often dominates spectra of ZnO, is shown in figure 2.ii.

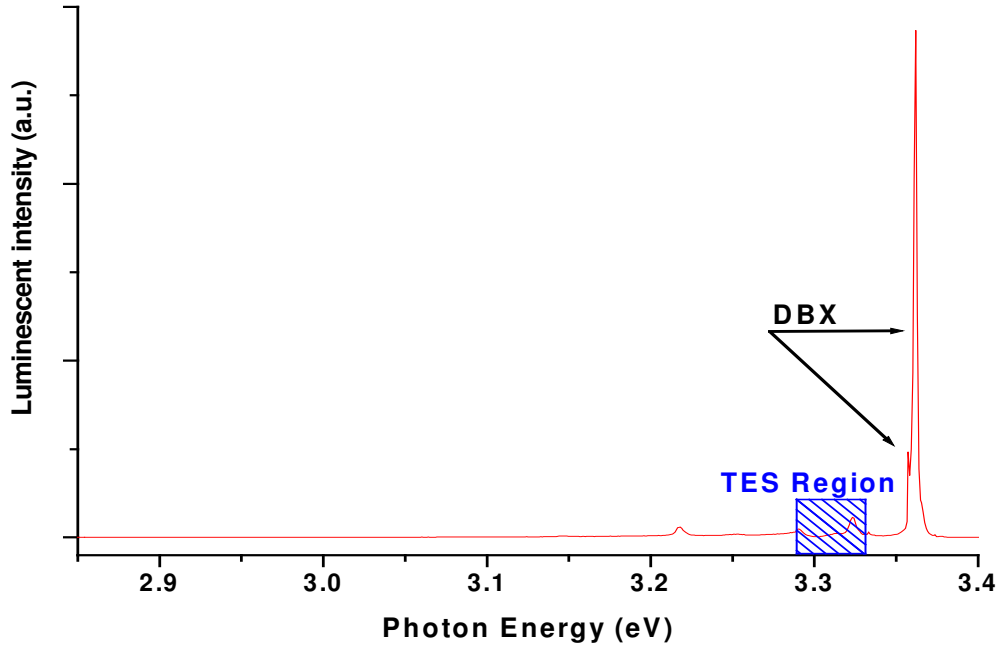

Fig. 2.ii: Typical PL spectrum of single crystal ZnO. Emission almost totally dominated by DBX line at ~3.365 eV.

Typical spectral features of good-quality ZnO may include excitonic emission due to the FX transition, TES, high energy exciton rotator states and respective LO phonon replicas, as well as non-excitonic features such as electron to acceptor or hole to donor transitions, donor-acceptor recombination, or intra-band transitions. Though generally weaker than the DBX emission, these features are often present in ZnO. Scaling figure 2.ii logarithmically shows examples of such features present in this DBX dominated spectrum, revealing other emission lines such as FX and LO replica as in figure 2.iii.

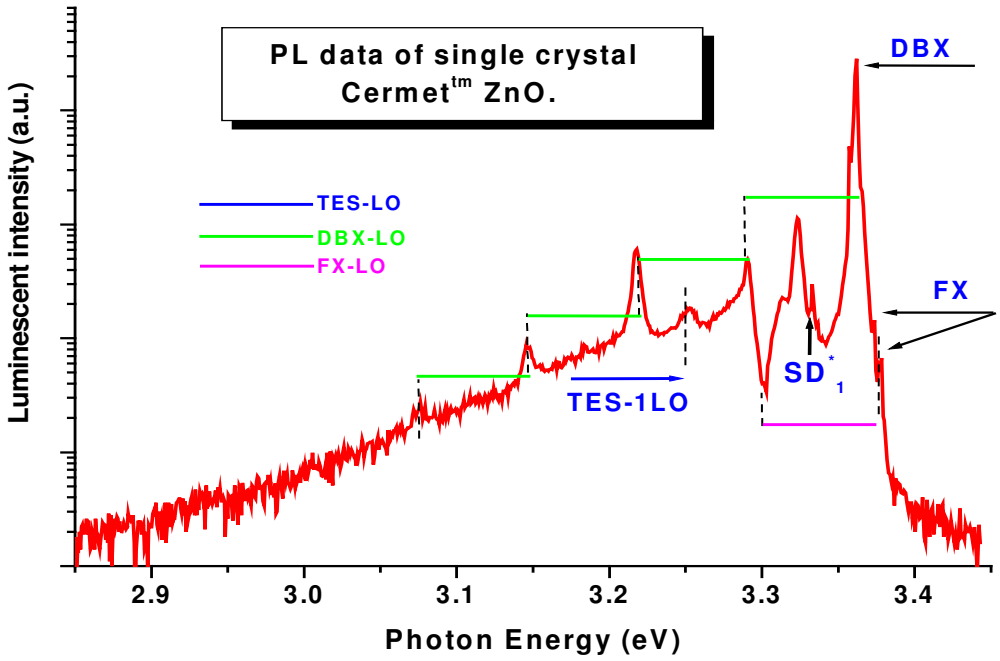

Fig. 2.iii: As figure 2.ii, scaled to show non-DBX features. - see section 4.4.2*

The ZnO sample for which this spectrum was taken was of good quality, as evidenced by the presence of FX emission. The dominant DBX emission appears to be the typical H-related I_4 although other DBX lines are present, but not significantly resolved to allow confident assignment. The high quality of the material is emphasised with distinguishable FX_A and FX_B contributions. The FX energies differ as a consequence of VB splitting from crystal field and spin orbit interaction. Table 2.ii lists the energies of each feature in fig. 2.iii.

Cerment™ ZnO Emission Feature	Energy (eV)
FX_A, FX_B	3.3737, 3.3783
DBX	3.3618
DBX -1, -2, -3, -4 LO	3.291, 3.2173, 3.1464, 3.076
TES	3.3232
TES -1, -2 LO	3.2512

Table 2.ii: Emission processes from spectrum of typical commercial ZnO.

These emission lines are common to many ZnO PL spectra, due mainly to native defects or impurities incorporated within the structure. Familiarity with features native

to nominally undoped, high quality ZnO aids in identification of defects that may be directly related to a doping process.

2.2.2 – Identification of Spectral Features

2.2.2.i – Comparative Analysis

PL emission of a single crystal commercial ZnO sample from E.P.™ is shown in figure 2.iv, from ~3.3 eV to the band edge. A large number of near band edge (NBE) emission processes result in a series of well-defined DBX lines. The real value of PL becomes apparent in such a high-resolution spectrum. In a PL study of undoped ZnO [2], the chemical origin of some more common ZnO features were listed; Ga at 3.3567 eV, In at 3.3598 eV, Al at 3.3607 eV and H at 3.3628 eV. In another extensive study of DBX emission in bulk ZnO [7], energy ranges from various sources of six common NBE spectral features were listed which included those above. Differences of up to 1.2 meV in photon energy of a particular *I*-line were identified. These ranges are shown in figure 2.iv demonstrating good agreement with initial assignment.

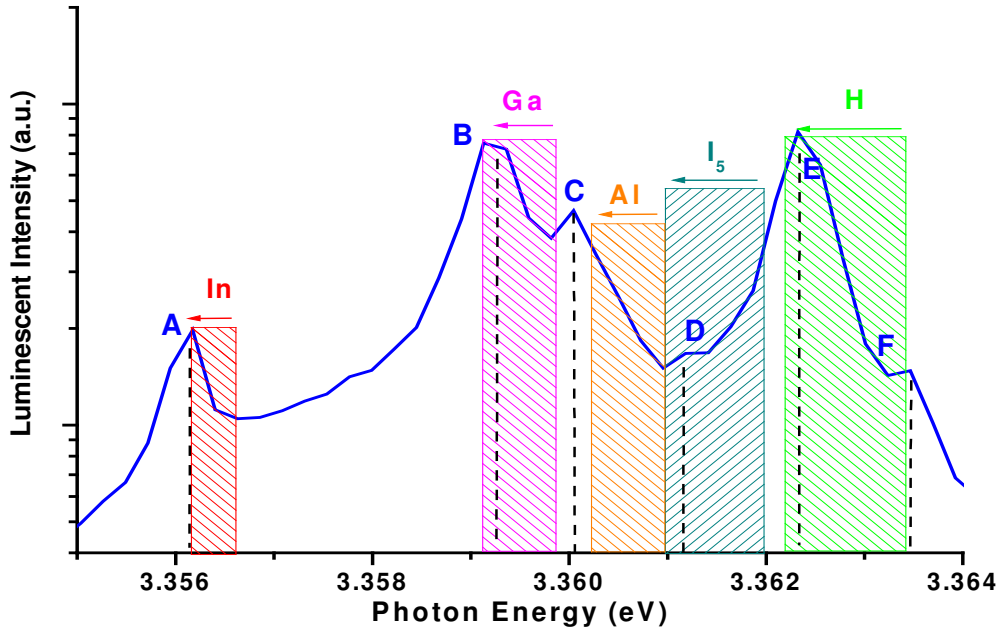

Fig. 2.iv: PL of E.P.™ single crystal ZnO, corrected with 2.1 meV red shift. Energy ranges for In (red), Ga (pink) and H (green) contributions shown, coinciding with peaks A, B and E respectively.

For peak A, a range of 3.3562 eV [8] to 3.3566 eV [9] is listed in [7]. The data presented here shows peak intensity for this emission line at just below 3.3562 eV and so assignment to the In-related defect in ZnO for peak A is justifiable. A similar

argument is applicable to peaks labelled B, D and E with energy values and range listed in table 2.iii.

Peak label	Corresponding I-Line	Line position (eV)	Reported energy range of line (eV)
A	I_9 - In	3.3562	3.3562 [8] - 3.3566 [9]
B	I_8 - Ga	3.3592	3.3592 [10] – 3.3598 [11]
C	$I_{6/6a}$ - Al	3.361	3.3602 [8] – 3.3610 [11]
D	Unclassified	3.3611	3.361 [8] – 3.362 [9]
E	I_4 - H	3.3624	3.3622 [10] – 3.3634 [8]

Table 2.iii: PL energies for DBX lines observed in a spectrum of E.P.™ material, with a range of values for these lines from literature listed.

A picture emerges of a typical PL spectrum for undoped ZnO with a familiar series of sharp *I*-lines in the NBE region. The peak labelled C at just above 3.361 eV deserves attention, appearing between In and Al energy ranges [7]. Its origin emerges in a discussion concerning sapphire substrates in section 4.4.1.

2.2.2.ii – Photon and Binding Energy Calculation

The optical and/or binding energies of many defects in ZnO may be calculated by applying spectral data to the relevant equations such as those below in table 2.iv. Detailed quantitative analysis of PL spectra is afforded by these equations, which incorporate the principal parameters governing the position of PL lines in a spectrum. It is important to note that equations 2.i to 2.vi are dependent on E_{Gap} and so dependent on the temperature as well.

Energy values	Equation	Variables
FX: Eqn 2.i	$E_{FX}(T) = E_{Gap}(T) - E_{B_{Ex}}$	$E_{Gap}(T)$ is the gap energy at temperature T. $E_{B_{Ex}}$ is the temperature independent exciton binding energy.
e^- A Eqn 2.ii	$E_{e^-A} = E_{Gap}(T) - E_{B_A} + k_B T/2$	E_A is the acceptor energy level. E_{e^-A} is the free electron to acceptor energy.
ABX: Eqn 2.iii	$E_{ABX} = E_{FX} - E_{B_A}$	E_{ABX} is the ABX energy. E_{B_A} is the acceptor binding energy.
Donor binding energy: Eqn 2.iv Eqn 2.v	$E_{B_D} = (E_{DBX} - E_{TES})4/3$ $E_{B_D} = E_{ABX} - k_B T/2 - E_{DAP} - \alpha N_D^{1/3}$	E_{B_D} is the donor binding energy. E_{TES} is the TES energy. E_{DBX} is the DBX energy. E_{DAP} is the DAP energy level. $\alpha = 2.7*10^{-8}$ eVcm, proportional to ε_{ZnO}=8.6 N_D is the average donor distance.
DAP energy: Eqn 2.vi	$E_{DAP} = E_{Gap} - E_{B_D} - E_{B_A} + \frac{e^2 \varepsilon_{ZnO} \pi}{4r}$	

Table 2.iv: Equations for calculation of defect energies from PL data.

2.2.3 – The Temperature Dependent Band Gap

The positional dependence of these features on temperature allows much information to be garnered from temperature dependent studies of PL emission, including binding energies and verification of features as acceptor-related. Such useful

data becomes available because the fundamental gap of semiconductors varies with temperature, as described in the Varshni equation [12]:

$$E_{Gap}(T) = E_{Gap}(0) - (\alpha T^2 / T + \beta) \qquad \text{Eqn: 2.vii}$$

with E_{Gap} (0) = 3.440 eV [13] for ZnO, T is the temperature, $\alpha_{ZnO} = 8.2(\pm 0.3)*10^{-4}$ eV / K and β related to Debye temperature as ~ 0.375 θ_D or ~700 $\pm$ 30 K for ZnO. Fitting equation 2.i as a function of temperature shows the range in E_{Gap} at 300 K is 3.36573 eV to 3.3667 eV, as in figure 2.v.

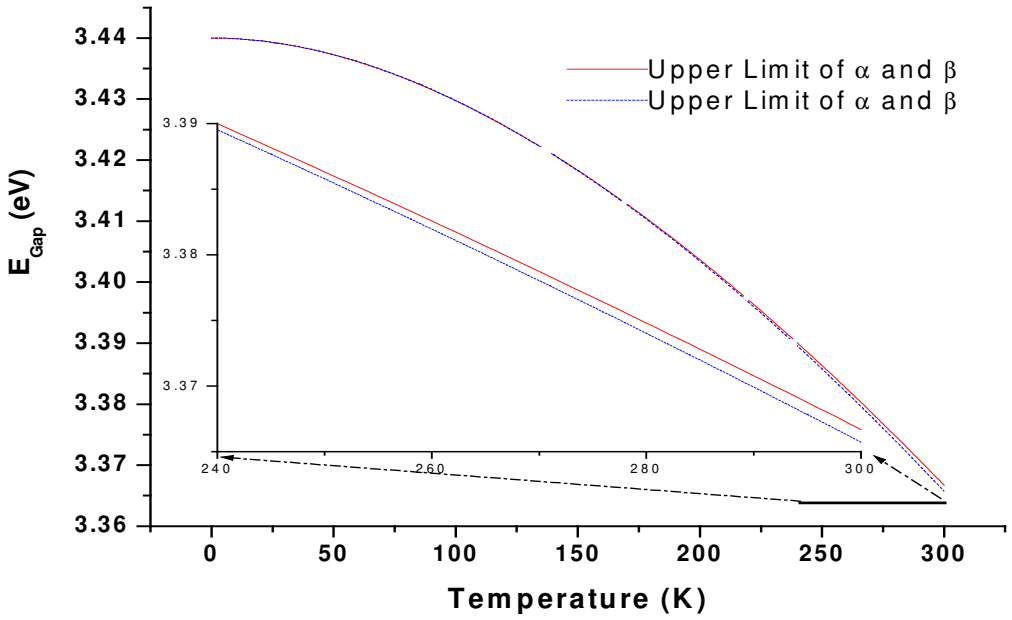

Fig. 2.v: Varshni equation fit for ZnO to RT. Upper and lower limits due to uncertainty in values of α, β shown. Inset: Divergence of limits, as apparent at high T.

The equation parameters are chosen phenomenologically, and indeed there are more recent functions to describe E_{Gap} variation with temperature for ZnO [2], which relate more closely to our experimental data than equation 2.vii.

The intensity of emission lines in a spectrum also varies with temperature. Maxwell-Boltzmann statistics show the relative population of two energy levels above a ground state minimum at a specified T, is proportional to the distribution function $ge^{(-\Delta E / k_B T)}$, where g is the relative degeneracy of the upper level, k_B is the Boltzman constant and ΔE is the energy difference between two levels. Considering such a system, the intensity of an emission line as a function of temperature is related to the distribution function as

$$I(T) = Nf(0)/(1 + ge^{-(E_1 - E_0/k_B T)}) \quad \text{Eqn: 2.viii}$$

where N is the population at a level 1, which is ΔE higher than level 0, and $f(0)$ is the transition probability for a radiative transition from level 0. At temperatures close to T = 0 K it is clear that

$$I_0 = Nf_0 \quad \text{Eqn: 2.ix}$$

with only states in the lower energy level occupied. This allows equation 2.viii to be expressed as

$$I(T) = I(0)/(1 + ge^{-(E_1 - E_0/k_B T)}) \quad \text{Eqn: 2.x}$$

Expressing this equation logarithmically gives

$$Ln((I(0)/I(T)) - 1) = Ln(g) - \Delta E/k_B T \quad \text{Eqn: 2.xi}$$

A plot of $Ln((I(0)/I(T)) - 1)$ as a function of 1/T results in a region of linearity between particular temperature limits, with slope of $\Delta E/k_B$, yielding the defect activation energy ΔE. Considering an exciton bound at a defect of energy E, it can be seen from equation 2.ix that at lower temperatures emission intensity related to it will dramatically increase - and conversely decrease for higher temperatures. Native defect and impurity-related excitonic emission have been observed to quench completely at room temperature [14] although some instances of free excitonic emission has been recorded at RT [15], a signature of very high quality material.

2.2.3.i – Low to High Temperature PL Intensity Variation

ZnO usually exhibits few optical features at higher temperatures [16], with an example of this is shown in figure 2.vi below, taken from studies on good-quality thin films. At higher temperature, emission bands become broad and deep as the temperature increases with a total quenching of DBX features.

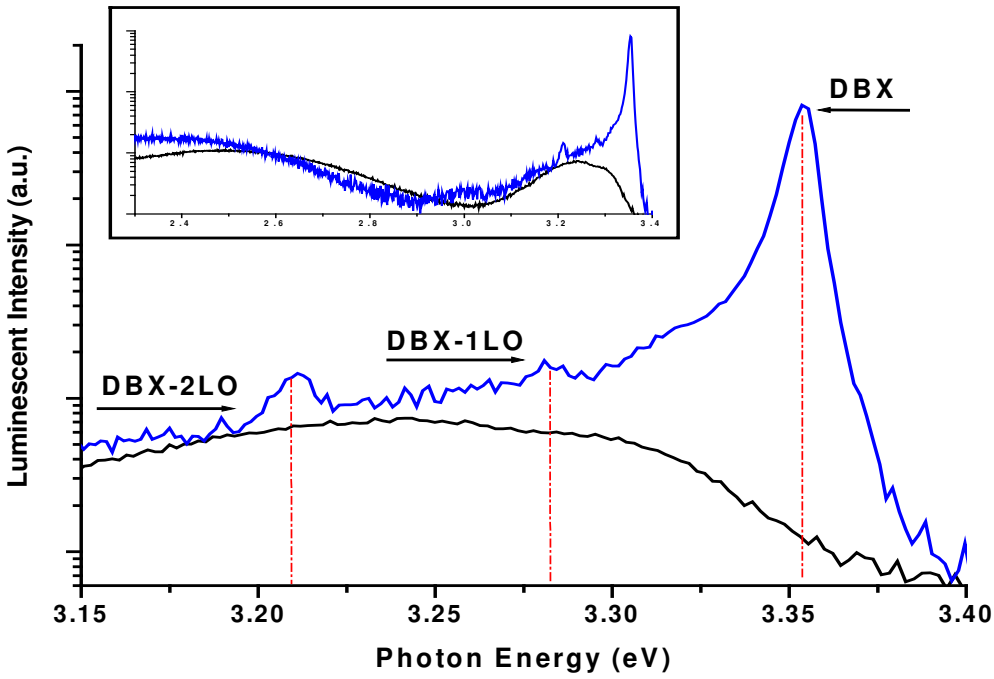

Fig. 2.vi: NBE emission at 9 K (blue) and 300 K (black)- of nominally undoped PLD grown ZnO. Inset: Full spectra to deeper emission.

It is apparent from this data that excitonic-related emission is quite sensitive to temperature change. Increasing temperature results in a lowering of the CB minimum and consequently a lower intensity of DBX emission as in equation 2.ix. Accordingly, as two primary excitonic signatures are emission red shift and reduction in intensity as temperature increases, temperature-dependant (TD-PL) measurements are an excellent method of identifying exciton-related features. Analysis of a particular spectral line's integrated intensity as a function of temperature yields the activation energy for emission quenching, as in equation 2.x.

2.2.3.ii – TD PL

PL examination of nominally undoped ZnO [19] showed a reduction in intensity as a function of increasing temperature as shown in figure 2.vii below. The two NBE emission lines quench over a modest temperature increase of 33 K with the dominant DBX feature decreasing in intensity by an order of magnitude. The data demonstrates a quenching of excitonic emission with temperature, together with red shift in energy position of the emission lines.

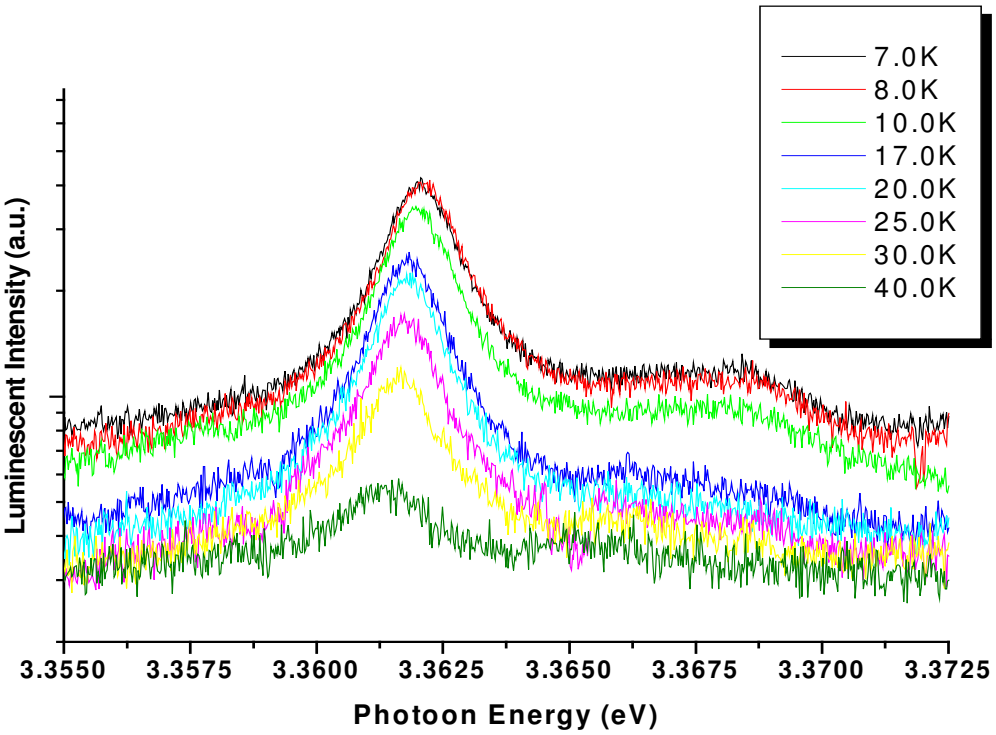

Fig. 2.vii: TD of NBE emission of ZnO thin film grown via PLD on sapphire.

Summing all intensities over a range encompassing the dominant 3.362eV line – with inclusion of appropriate temperature induced red-shift of said range – allows extraction of activation energy for this bound exciton of ~3.8 meV. This indicates that for this material, the intensity of DBX emission is expected to reduce with increasing temperature due to the release of bound excitons. Some exceptions to TD emission quenching are reported in [20].

2.2.3.iii – TD DAP Signature

TD PL measurements enable the identification of DAP emission. Thermal ionisation of the donors occur as the temperature is increased [9 and references therein] resulting in a reduction of the donor population and consequently DAP features reduce in intensity. The e^{-}A transition begin to appear as the DAP diminishes due to an increase in capture probability by the acceptor level of the thermalised CB electrons. The process is shown in figure 2.viii.

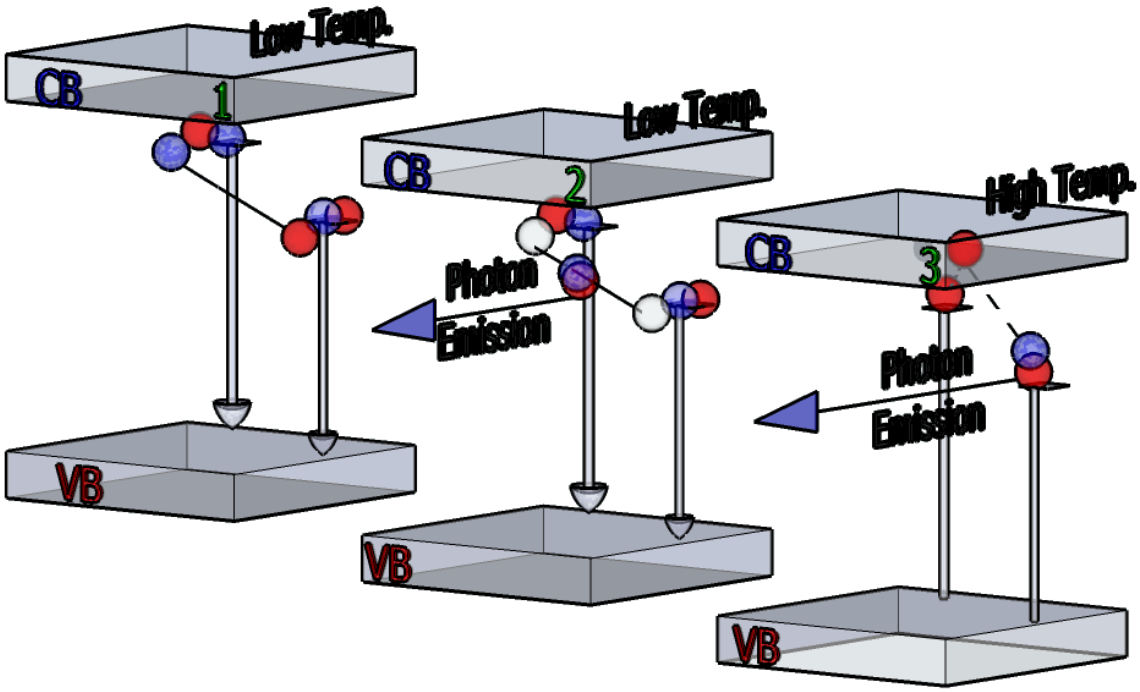

Fig 2.viii: DAP evolution with temperature from Coulombic attraction (1) with DAP emission (2) to ionised donor and $e^{-}A$ emission (3).

Such an intensity inversion was observed an N-doped PLD grown film. Initial comparative analysis of features in this region of the ZnO spectrum suggested assignment to DAP of the 3.24 eV band, as in figure 2.ix.

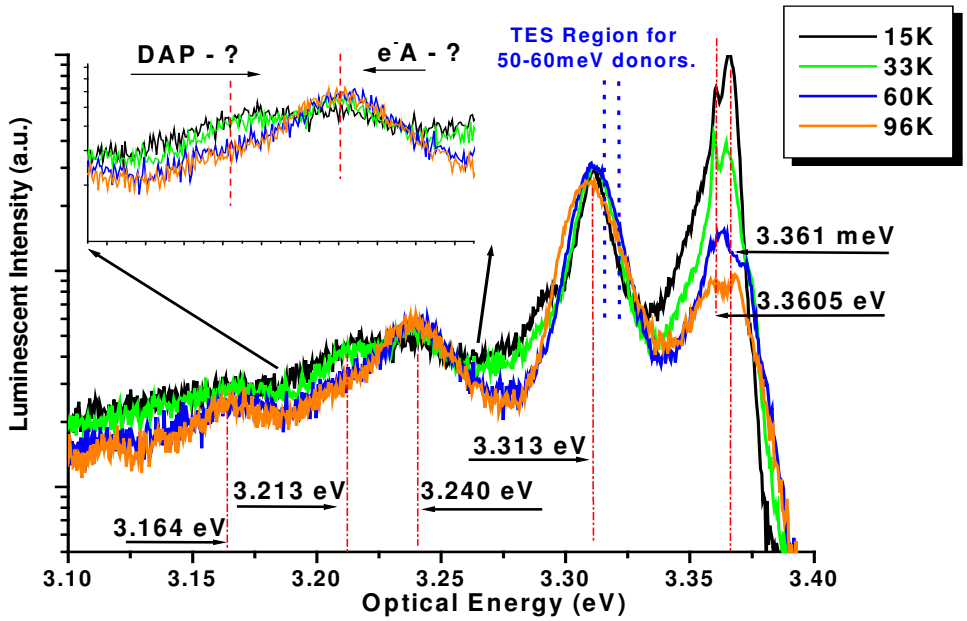

Fig. 2.ix: Spectra of N-doped ZnO thin film. Emission at ~3.2 eV reduces with increase in intensity of high-energy contribution of band with temperature increase.

A temperature increase of 80 K results in quenching the emission at 3.213 eV with the 3.24 eV band growing in intensity. Although displaying only a modest reduction in intensity, there is a marked inversion in relative intensity between these two bands, a prime characteristic of DAP emission.

Typical DBX emission at 3.3605 eV and 3.366 eV observed here appears to quench while the 3.313 eV emission remains relatively stable. The DBX peaks reduce in intensity considerably more than emission assigned to the DAP recombination. Trends in the intensity over 15 K to 96 K were examined with comparison of the integrated areas of both DBX peaks, together with the DAP and e^-A assigned bands. The results are shown in figure 2.x. These data raise doubt over initial assignment to TES, e^-A and DAP emission for peaks at 3.313, 3.240 and 3.213 eV respectively.

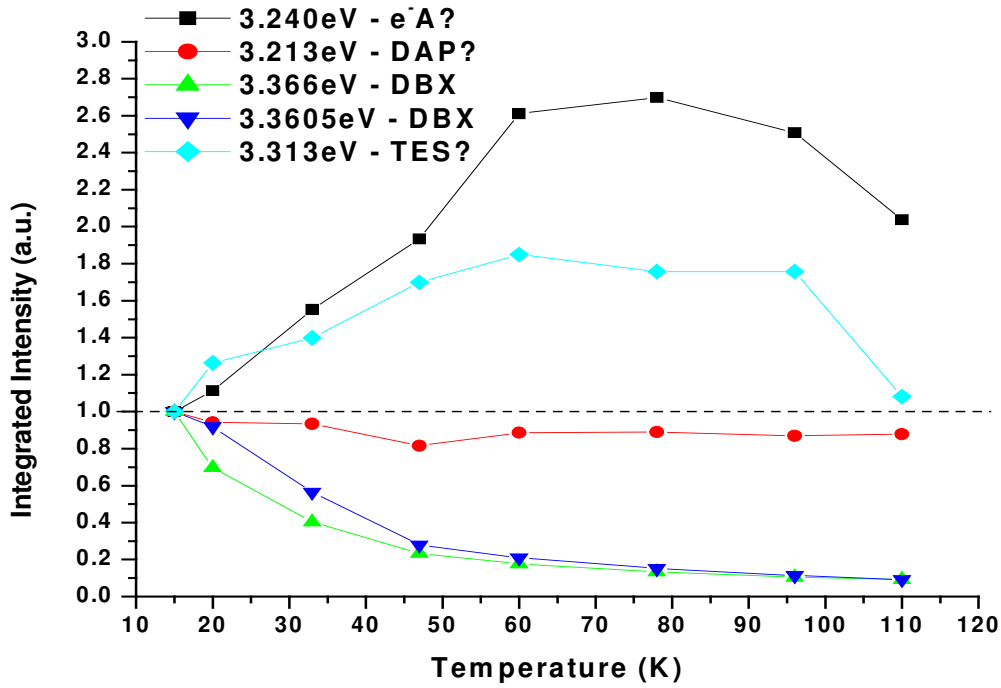

Fig. 2.x: Integrated intensities of emission of ZnO thin film as in figure 2.x, normalised for lowest temperature.

TES emission should exhibit the same reduction in intensity as DBX emission because it is a direct consequence of DBX recombination. This is clearly not observed. Although its relative position in the spectrum as predicted from equation 2.iv[4] lies within the broad band, other contributions besides that of TES must be present as emission persists to higher temperatures. Analysis of integrated intensities over this

[4] $E_{B_D}(T) = (E_{DBX} - E_{TES})4/3$

temperature range shows the feature not only remains, but also tends to increase in intensity, following a similar trend to that of the 3.240 eV emission, suggesting perhaps the latter is a 3.313 eV – 1LO.

The emission at 3.213 eV, initially assigned to the DAP band is near unchanging over the temperature range, retaining some 90% of initial intensity at 110 K. It is clear that features at 3.240 eV, 3.213 eV and 3.313 eV require further examination and they are considered in more detail in section 5.7. The difficulty in classification of a band as DAP emission and sensitivity of various ZnO luminescence peaks to temperature is very apparent from these data.

2.2.3.iv – Excitation Density Dependence (EDD)

Reducing or increasing the energy density of excitation with a change in area of excitation source, or changing the power output of the excitation source directly[5] influences the contributions from occupied donor and acceptor defects in the sample, and consequently the character of DAP emission. The dependence of DAP energy position on mutual Coulomb attraction between donor and acceptor is evident from equation 2.vi - $E_{DAP} = E_{Gap} - E_{DBX} - E_{ABX} + (e^2 \varepsilon_{ZnO} \pi / 4r)$. A higher excitation density increases the number and concentrations of occupied donors and acceptor centres.
This consequently reduces the distance between the pairs resulting in an increase in Columbic term and a blue shift of DAP emission. Higher energy contributions within the DAP band may also become more intense with increased excitation density. This is because they exhibit a lower probability of saturation - due to strong interactions and short decay times between close D-A pairs - allowing for more intense peak with increasing excitation energy.

EDD PL measurement can be a strong technique for identifying the DAP emission band with some reported blue shift of 9 meV over a 6.5 fold change in excitation density [21]. Measurements may also lead to questionable results with the blue shift often exceptionally small, even over order of magnitude changes in excitation density, as low as 0.2 meV [22, 23, 24].

2.3 – Surface Measurements

A good deal of information becomes available concerning a semiconductor and its properties with examination of the material's surface. Verification of growth mechanism, identification of material quality, sample homogeneity or nano-structure

[5]The source used here was a HeCd laser centred at 325 nm.

type and how material varies with growth and / or treatment parameters can be obtained. Atomic force microscopy (AFM) and scanning electron microscopy (SEM) are most commonly used for such analysis employing standard commercial systems[6]. Surface raster scanning capabilities of these techniques allows for collection of data over large areas, including any variation in topography.

2.3.1 – Surface Alteration with Doping

The effect of doping on optical or electrical qualities can often be subtle or ambiguous [5,22]. In the case of surface measurements, the imaging from AFM / SEM acts as a direct visual aid showing changes in sample characteristics. In the following figure 2.xi the sample surfaces are altered with addition of phosphorous dopant from nominally undoped to 5 wt%. The ZnO films here were analysed as grown on *r*-Al_2O_3 for which the c-plane is parallel to the substrate surface.

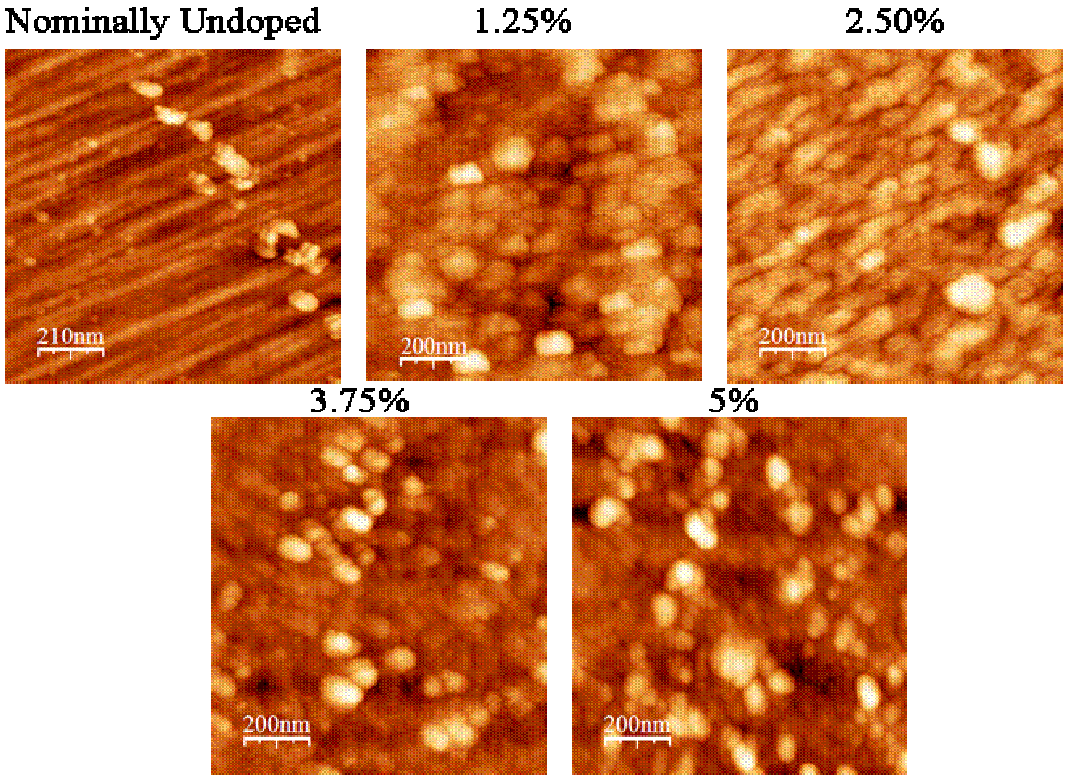

Fig. 2.xi: AFM imaging of P-doped ZnO (various wt% shown) on r-Al_2O_3

Surface striation is observed up to 2.5 wt% of P_2O_5, after which the ZnO deposits cluster at some surface points but leave the sample somewhat porous in others. Such lateral striation is evidence of growth parallel to the substrate *c*-plane [19]. Even at

[6]Instrument used for AFM, SEM, a Leo Stereoscan 440.

relatively high dopant quantities, growth remains directed along the surface plane. Triboulet *et al* discuss such substrate growth copying the substrate morphology, which is indicative of dramatically reduced defect density in the bulk [25]. If such an ordered pattern appears on the film surface due to the substrate, it must also be reproduced throughout the sample. Profilometry measurements compliment the AFM data with r_{rms} (root-mean-squared roughness) of each surface increasing with P-concentration and confirming the large-scale clustering of ZnO particles on the substrate. Figure 2.xii

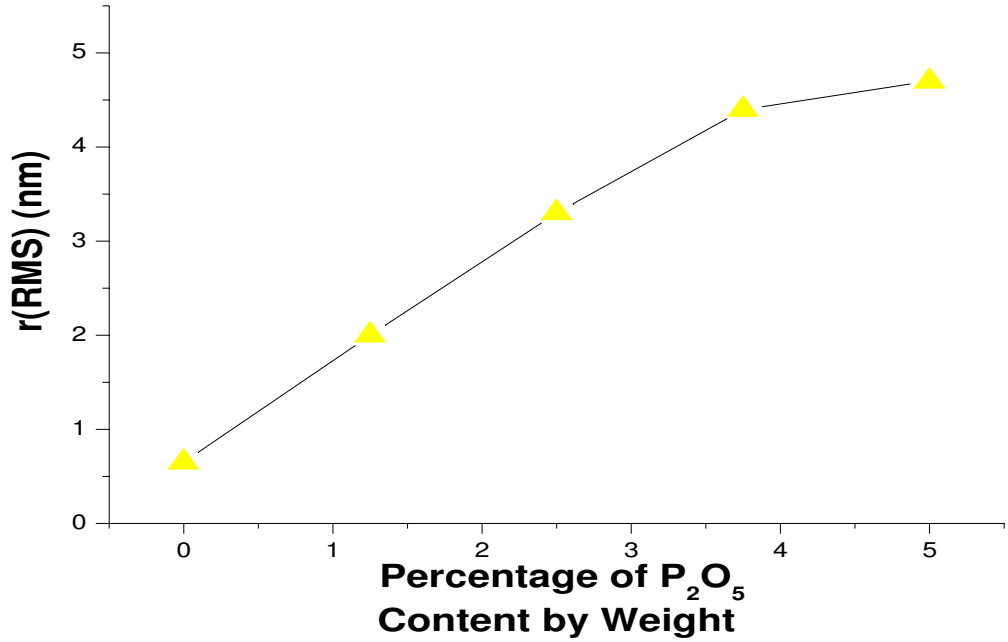

shows how r_{rms} was found to depend on dopant wt%.

Fig. 2.xii: Dependence of surface roughness on P_2O_5 concentration

2.3.2 – Post Growth Treatment Effects on Surface

Annealing conditions have been known to dramatically affect as-grown ZnO, indeed even altering the conductivity type via thermally activated dopants [26, 27]. There has been much discussion in the literature concerning appropriate annealing conditions. Trial and error approaches have been used with some success to establish those that favour improving quality of as-grown ZnO [28, 29]. Annealing conditions are generally appropriate on a sample-by-sample basis but incorrect annealing conditions may have a detrimental affect. The majority of ZnO studied here underwent an *in-situ* annealing process to allow migration of dopant and offset the commonly abundant V_O

with treatment in an O-rich 50 kPa environment at, or near, T_{Grow} of 800 K for 30 minutes.

An additional *ex-situ* annealing process was undertaken to allow comparison of as-grown films before and after annealing in order to determine the effect of an annealing process. This is emphasised later with consideration of optical data. This dedicated treatment was performed at 80 K greater than T_{Grow} for 90 minutes in the same ambient as the *in-situ* treatment. AFM images in figure 2.xiii depict the changing profile of film surface after this annealing. The pre-annealed image is approximately 4% of the post-anneal image's area. This emphasises the extent of surface deterioration from an inappropriate annealing process.

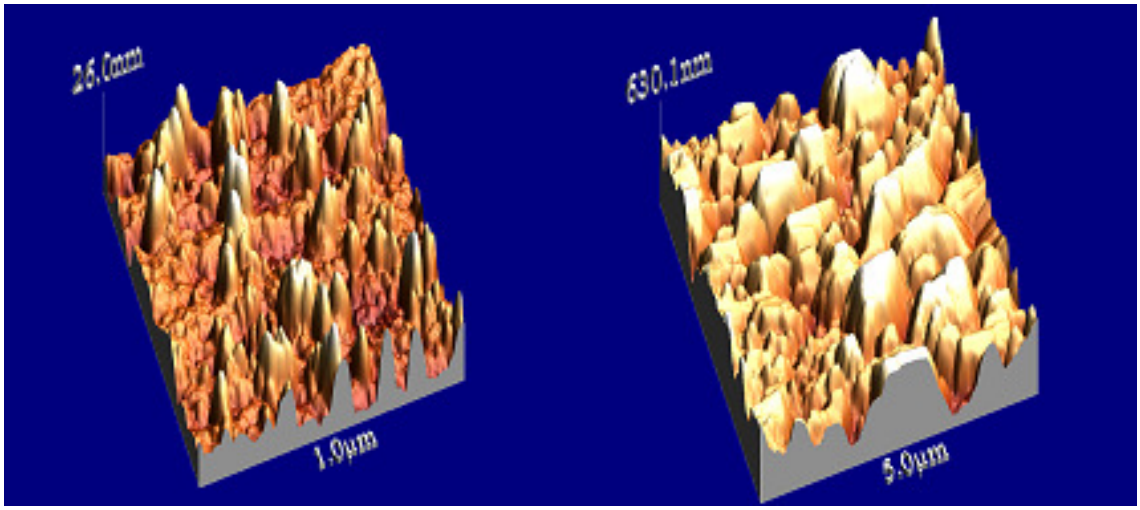

Fig. 2.xiii: 3-D AFM images, pre- and post- anneal of 1.25 wt% P_2O_5.

Coalescing surface features in the annealed sample increased the surface roughness significantly, an indication of a lower crystalline quality of the film bulk [25]. Surface-feature heights of 630 nm are also greater than layer thickness of sequential ZnO / ZnO : P_2O_5 layers used in growth, indicative of a film in which an inhomogeneous distribution of ZnO has occurred. This was further evidenced from profilometry measurement which showed an inhomogeneous and significant clustering of ZnO across the surface of the anneal film. This is shown in figure 2.xiv below. It follows that such a clustering of ZnO / ZnO: P_2O_5 layers and ensuing 50-fold increase in surface feature heights resulted in a thin film of greater volume than that prior to annealing. This greater volume implies a lower density film and as such a larger number of vacancy centres are present post-anneal. Of these, V_O and Zn_i have been identified

as compensation centres for P-type doping [32] and are also expected in greater abundance due to low formation enthalpies [33].

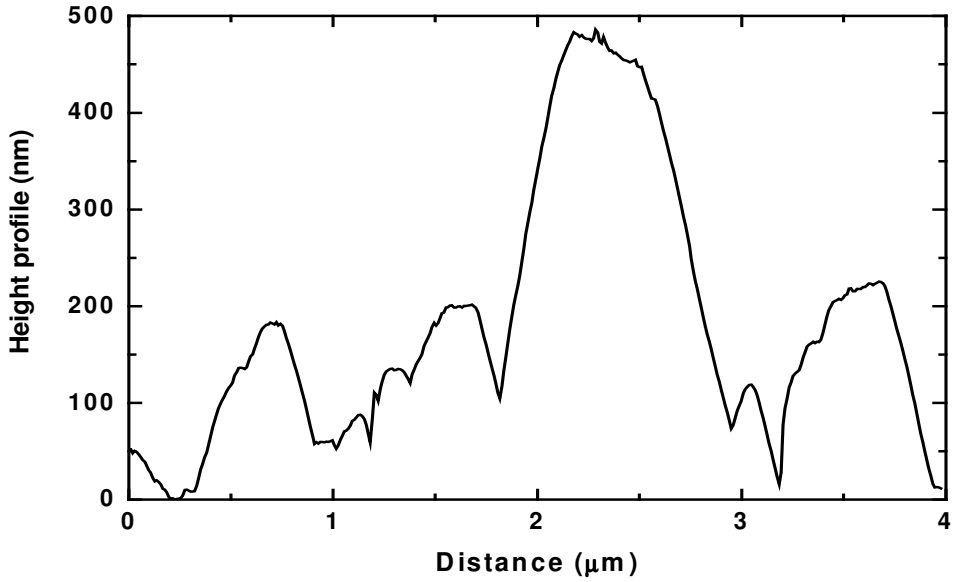

Fig. 2.xiv: Height profile of annealed PLD thin film.

Luminescent data support the argument that these particular sets of annealing conditions were incorrect with deterioration of NBE emission observed. PL data of the P_2O_5 films from figure 2.xiii, which demonstrated that inappropriate annealing processes drastically changed NBE emission are shown in figure 2.xv. The spectra affirm the changes in characteristics after the additional annealing process. The optical data supported the viewpoint that this annealing process resulted in a lower quality sample with a high number of vacancy centres. The origin of the green band remains controversial but there was reasonable evidence from this PL data suggesting native V_o and V_{Zn} centres contributed [34 - 36]. After annealing, the deep energy process at 2.35 eV increased in intensity, one attributed to the V_{Zn} defect [36, 37]. Typical structured emission on the high-energy shoulder of this band supported such classification. The assignment was especially fitting considering the high O-pressure annealing ambient.

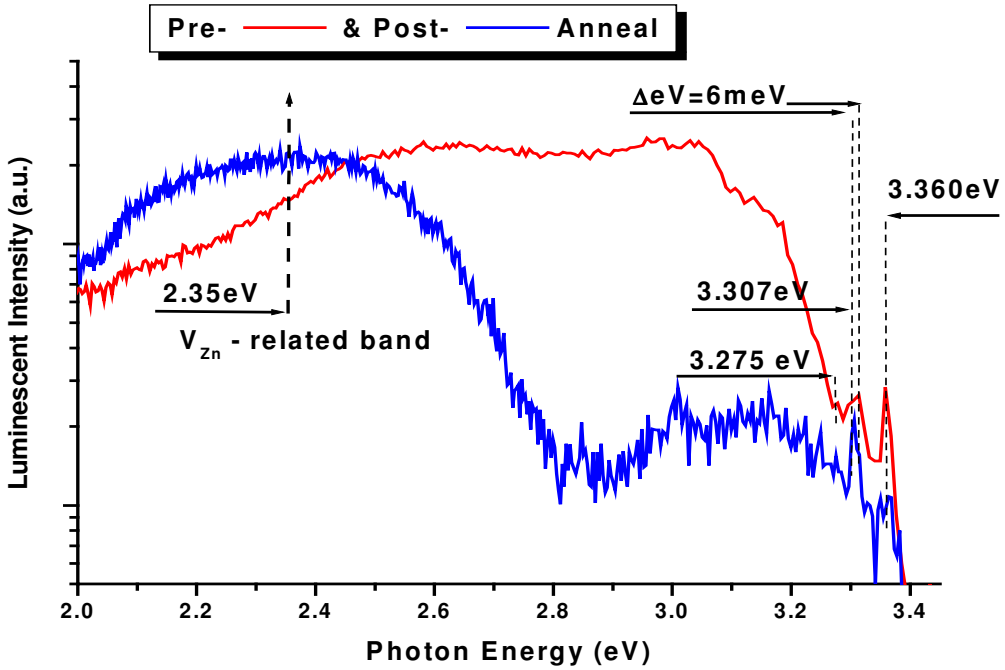

Fig. 2.xv: PL spectra of 1.25 wt% doped ZnO thin films before and after annealing treatment.

A considerable reduction in the 3.05 eV band and its shallower shoulder at 3.145 eV was observed. Classification of these features was difficult however, due to the broad nature and as such, likelihood of a high number of processes contributing such as TES, LO replica or excitonic emission from a structural defect[7]. The Al-related DBX line quenched completely making a coupling of this to a contribution(s) within the 3.05 eV band probable. Conversely, the intensity of a feature at ~3.10 eV was exaggerated with thermal treatment. Due to the presence of P-dopant, and the increase in intensity with *ex-situ* annealing inducing a large number of V_{Zn} centres, a provisional classification to a P-related ABX line was applied with further examination provided in section 5.5.

2.4 – Electrical Characterisation

Electrical characterisation was performed exclusively with a Hall Measurement system. The Hall voltage is one induced when an applied current in the material is subject to a magnetic field. Charge carries are subject to the Lorentz force in the presence of a B-field. This force promotes an asymmetric distribution of charge density throughout the material with accumulation of electrons and holes on opposite faces of

[7]Refer to section 5.5

the semiconductor, perpendicular to both applied B-filed and original current direction. The resulting voltage difference between these faces is the Hall voltage.

The polarity of induced Hall Voltage is determined from the majority carrier and indicates p- or n- type conductivity within the semiconductor. Typical Van der Pauw configuration for Hall Measurement in a small semiconductor film took an averaging from six permutations of 4 symmetrically placed contact points. A schematic of a typical Hall system set-up for one of these permutations appears in figure 2.xvi below with applied current between contact points 2 and 4 with the induced Hall Voltage measured between contact points 1 and 3.

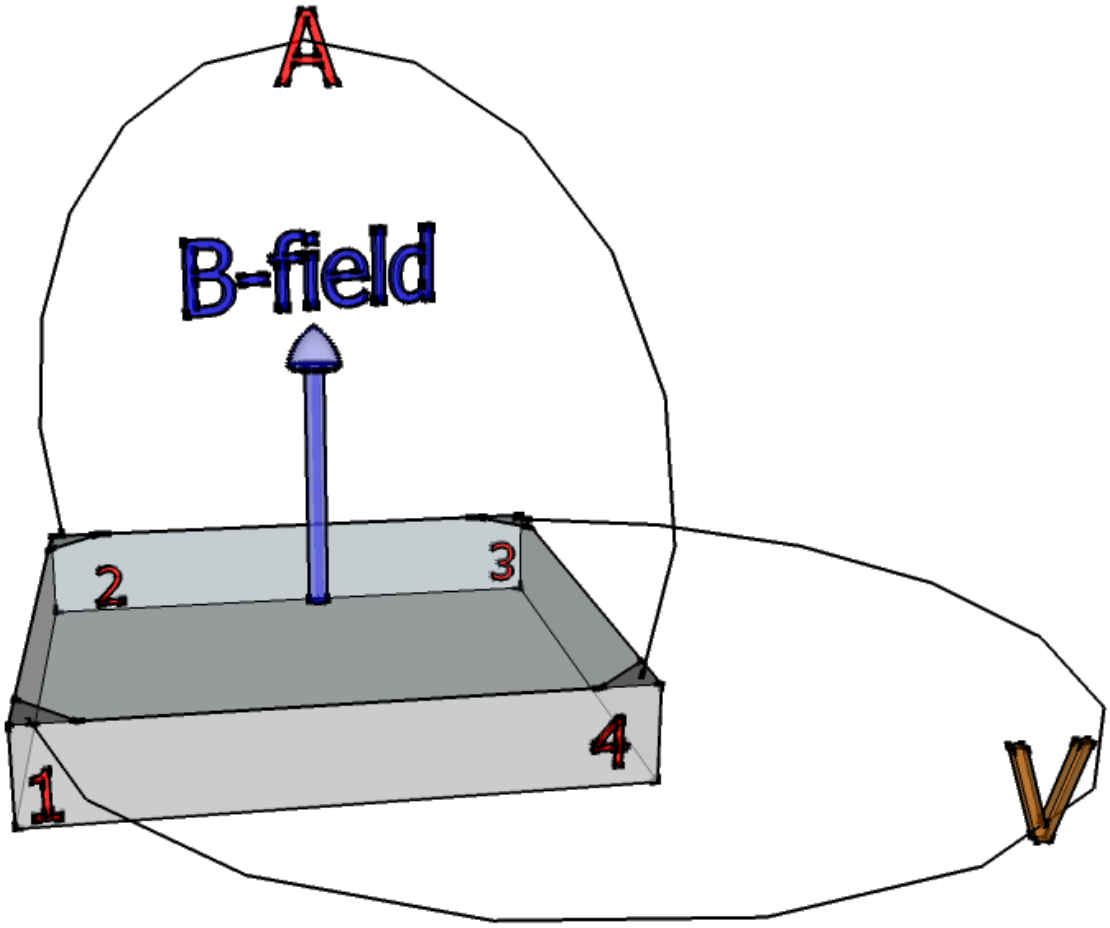

Fig. 2.xvi: Schematic of typical Van der Pauw configuration for Hall Measurement. Combination of contact points used for I application / V measurement rotate.

Hall software employed for these studies also allow calculation of resistivity and mobility as well as carrier concentration, with values calculated from measured Hall Voltage given a set of conditions such as material thickness and electrical permittivity. Unlike optical measurement in which interpretation of data is required, electrical studies of semiconductors offer direct quantitative information with regards to the material properties. The difficulty arises when measurement conditions are considered, with

temperature and ambient playing an important role in the measured characteristics. This is evidenced clearly in the following figure 2.xvii, which shows the resistivity for a 0.01 wt% P_2O_5 film as a function of temperature in both nitrogen and evacuated atmospheres.

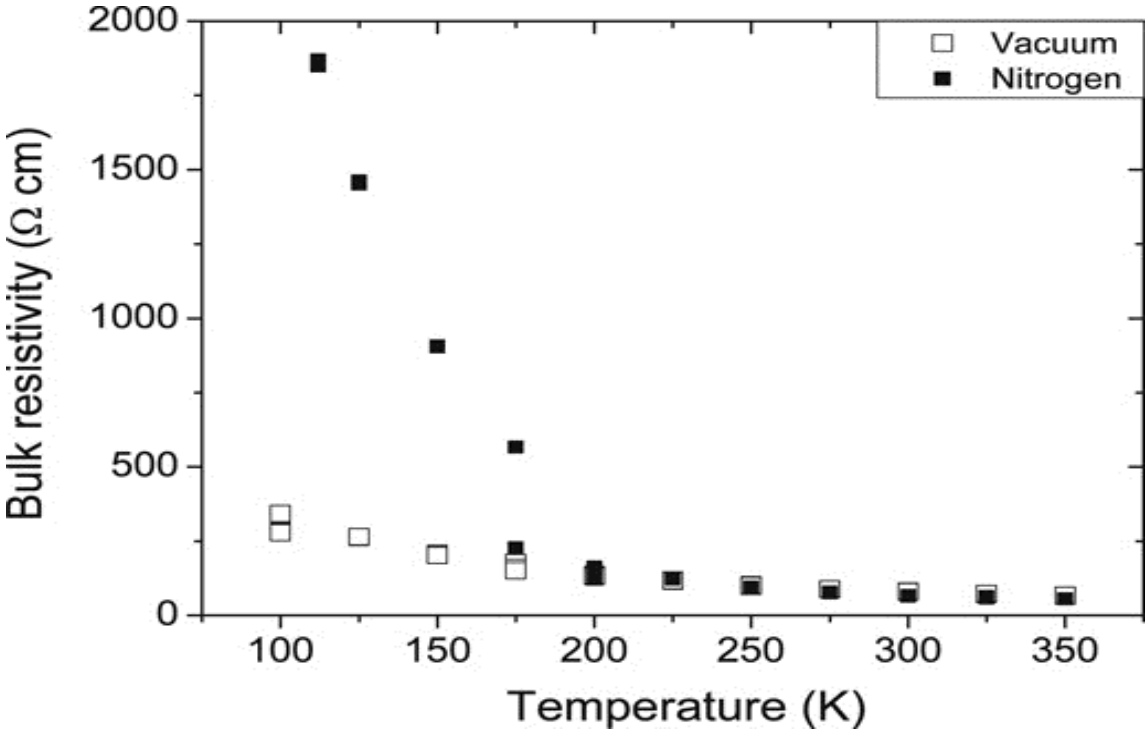

Fig.2.xvii: TD resistivity of N-doped ZnO thin films. N-ambient measurement substantially increased resistivity.

2.4.1 – Persistent Photoconductivity

Photo-induced conductivity has been observed for 0.01 – 1.0 wt% P_2O_5 films, but with short-lived conversion to p-type conductivity in films after exposure to an incandescent source with at 375nm. The intensity at this wavelength was some 3% of the maximum intensity at 576 nm [10]. Typically n-type conduction has been induced / enhanced upon exposure of the ZnO to UV illumination. The current understanding concerns the formation of a charge-trapping layer at the surface due to adsorbed oxygen [38]. Species trapped at surface-vacancies in the form of O_2^-. This is turn becomes passivated by excitonic holes produced from illumination, freeing up the electrons to contribute to conduction. This process continues to dominate conduction even in the absence of illumination, with sometimes very large relaxation times for trapped charges.

This photoconductive effect was observed in nano-structured ZnO and is indeed probably a surface effect, but data from other reports and studies here show the phenomenon for thin films [5, 39, 40]. Look [9] suggests the thin film inhomogeneous

nature, especially on lattice-mismatched substrates, as a cause for another curious electrical phenomenon in ZnO, the dual conductivity. The majority carrier type changing from one locality to another with intermittent regions dominated by e^- or $hole^+$ throughout the measured sample may result in ambiguous data.

The induced p-type photoconductivity here clearly does not originate in an e^- supplying layer of adsorbed oxygen. A model considering both a surface layer interacting with the ambient and an inhomogeneous conductivity in a film may explain the p-type photoconductivity. For N : ZnO films, mobility reduced by some 60% after illumination with bulk resistivity increasing somewhat at low temperature and considerably so in an N-based ambient. Should illumination result in electron traps due to positive species on the surface, perhaps N-related centres, regions of acceptor-related conduction could dominate the bulk. This model is proposed based on qualitative observation and would requires future work to test.

Overall, it is clear that any deviation from discretely controlled Hall measurement, for example fluctuation in applied current, non-symmetry in typical Van Der Pauw contacts positioning – such as contacting perpendicular to the film sides – may all lead to non-reproducible and varying conductivity type measured in a film. Though problematic, these experimental obstacles also offer additional confidence in data. A high level of certainty is afforded to Hall data that demonstrate consistent p-type conducting despite the aforementioned difficulty in measurement.

2.5 – Structural Characterisation

XRD or X-ray diffraction is a prominent tool in measuring and quantifying structural and crystalline characteristics in materials. The data afforded from XRD measurement allow for determination of sample composition from relative plane intensities, identification of lattice parameters, strain, epitaxial quality and impurities, including those of substrate species migration.

X-rays incident on a sample at an angle Θ become diffracted from atoms within the sample and emitted at an angle 2Θ. The prevalence of an atom type within the plane determines the peak intensity. The spacing of atomic planes determines peak position, corresponding to Bragg's law with planes typically identified with Miller Indices (*h-k-l*), with a 4^{th} Bravais index *i* used to distinguish permutation symmetries in hexagonal structures.

A fixed incident beam and sample rotation of $\Theta°$ with detector over $2\Theta°$, or Θ-2Θ measurement allows selection of various planes and assembly of the crystalline

make-up of the sample. An intense XRD spectral peak at an incident angle of ~0.34º for the ZnO (0002) plane for example, is evidence of material with high density of atoms lying in that plane. The following figure 2.xviii shows an example of an XRD spectrum of ZnO grown on *c*- Al_2O_3 with peaks corresponding to the ZnO (0002) and (0004) of comparable intensity to that of the Al_2O_3(0006) plane. The comparable intensity of ZnO and Al_2O_3 planes suggest a high quality herto-strucure.

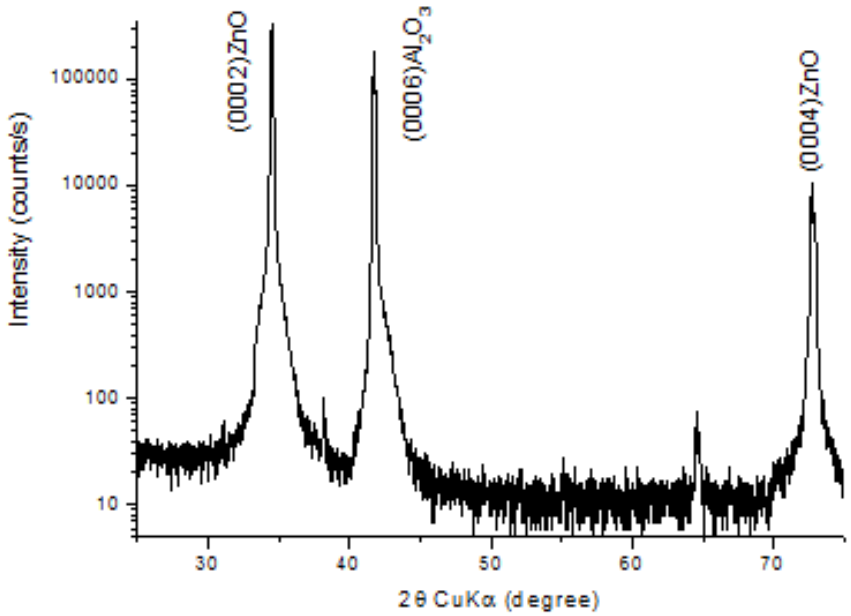

Fig. 2.xviii: Sample XRD spectrum of ZnO on c-Al_2O_3

2.5.1 – Rocking Curve Measurements

Rocking curve measurements focus on a particular XRD diffraction peak. Scans are performed with incident Θ varied but 2Θ fixed which allow for analysis of a single crystalline plane. The peak width, or rocking curve ω_{FWHM}, is directly related to dislocation density of atoms in that plane and as such a good indicator of sample quality.

2.5.2 – Confirmation of Epitaxy to Substrates

Full angle scans across 0º ± 180º allows for confirmation of epitaxial relationships of materials to a substrate. Measurements are taken at different angles of sample rotation about their centre with a fixed 2Θ and varying sample tilt angles, or azimuths. Confirmation of epitaxial relationship of sample to substrate is achieved from identification of a close matching or symmetrical relationship between azimuths from the substrate growth plane and those from the deposited material.

2.6 – References

[1] D.C. Look, D.C. Reynolds, C.W. Litton, R.L. Jones, D.B. Eason, G. Cantwell, *App. Phys. Lett*, **81**, 10 (2002)

[2] B.K. Meyer, H. Alves, D.M. Hofmann, W. Kriegseis, D. Forster, F. Bertram, J. Christen, A. Hoffmann, M. Strassburg, M. Dworzak, U. Haboeck, A.V. Rodina, *Phys. Stat. Sol. (b),* **241**, 2, 231-260 (2004)

[3] K. Ip, G.T. Thaler, H. Yang, S.Y. Han, Y. Li, D.P. Norton, S.J. Pearton, S. Jang, F. Ren, *J. Crys. Growth,* 287, 149-156 (2006)

[4] G. Xiong, J. Wilkinson, B. Mischuck, S. Tzemen, K.B. Ucer, R.T. Williams, *App. Phys. Lett.* **80**, 7 (2002)

[5] B. Clafin, D.C. Look, S.J. Park, G. Cantwell, *J. Crys. Growth,* **287**, 16-22 (2006)

[6] M.W. Cho, C. Harada, H. Suzuki, T. Minegishi, T. Yao, H. Ko, K. Maeda, I. Nikura, *Superlatt. and Micro.* **38**, 349-363 (2005)

[7] Ü. Özgür, Ya. I. Alivov, C. Liu, A.Teke, M.A. Reschikov, S. Doğan, V. Avrutin, S-J. Cho, H. Morkoç, *J. App. Phys.* **98**, 041301 (2005)

[8] D.C. Reynolds, D.C. Look, B. Jogai, C.W. Litton, T.C. Collins, W. Harsch, G. Cantwell, *Phys. Rev. B*. **57**, 19, 12151-12155 (1998)

[9] K. Thonke, T.H. Gruber, N. Teofilov, R. Schonfelder, A. Waag, R. Sauer, *Phsyica B,* **308 – 310**, 945 – 948 (2001)

[10] C. Boemare, T. Monteiro, M. J. Soares, J. G. Guilherme, and E. Alves, *Physica B*, **308–310**, 985 (2001)

[11] A. Teke, Ü. Özgür, S. Doğan, X. Gu, H. Morkoç, B. Nemeth, J. Nause, H. O. Everitt, *Phys. Rev. B*, **70**, 195207 (2004)

[12] Y.P. Varshni, *Physica A*, **34**, 1, 149 (1967)

[13] J.Lu, Q. Liang, Y. Zhang, Z. Ye, S. Fujita, *J. Phys. D: App. Phys*, **40**, 3177-3181 (2007)

[14] W. Shan, W. Walukiewicz, J.W. Ager, H.B. Yuan, H.P. Xin, G. Cantwell, J.J. Song, *App. Phys. Lett.* **89**, 19, 191911 (2005)

[15] D.A. Lucca, D.W. Hamby, M.J. Klopfstein, G. Cantwell, *Phys. Stat. Sol. (b)*, **229**, 2, 845-838 (2002)

[16] J. Lu, Q. Liang, Y. Zhang, Z. Ye, S. Fujita, *J. Phys. D: App. Phys.* **40**, 3177-3181 (2007)

[17] J. Grabowska, K.K. Nanda, E. McGlynn, J-P. Mosnier, M.O. Henry, A. Beaucamp, A. Meaney, *J. Mat. Sci: Mat. in Elec.* **16**, 397-401 (2005)

[18] M-S. Oh, S-H. Kim, T-Y. Seong, *App. Phys. Lett.* **87**, 122103 (2005)

[19] A. Meaney, J-R. Duclere, E. McGlynn, J.-P. Mosnier, R. O'Haire, M.O. Henry, S*uperlatt. and Micro.* **38**, 256–264, (2005)

[20] M. Watanabe, M. Sakai, H. Shibata, C. Satou, S. Satou, T. Shibayama, H. Tampo, A. Yamada, K. Matsubara, K. Sakurai, S. Ishizuka, S. Niki, K. Maeda, I. Niikura, *Physics B*, **376-377**, 711-714 (2006)

[21] D. Stichtenoth, J. Dürr, C. Ronning, L. Wischmeier, T. Voss, *J. App. Phys.* **103**, 083513 (2008)

[22] A. Nakagawa, F. Masuoka, S. Chiba, H. Endo, K. Megro, Y. Kashiwaba, T. Ojima, K. Aota, I. Niikura, Y. Kashiwaba, *App. Sur. Sci.* **254**, 164-166 (2007)

[23] D-K. Hwang, H-S. Kim, J-H. Lim, J-Y. Oh, J-H. Yang, S.J. Park, K-K. Kim, D.C. Look, Y.S. Park, *App. Phys. Lett.* **86**, 151917 (2005)

[24] E. Tournie, C. Morhain, G. Neu, J-P Faurie, *Phys. Rev. B*, **56** 4, R1657 – R1660 (1997)

[25] R. Triboulet, J. Perriére, *Prog. in Crys. Growth and Char. Mater.* **47**, 2-3, 65-138 (2003)

[26] T. Aoki, Y. Shimizu, A. Miyake, A. Nakamura, Y. Nakanishi, Y. Hatanaka, *Phys. Stat. Sol. (b)* , **229**, 2, 911-914 (2002)

[27] D.C. Look, R.L. Jones, J.R. Sizelove, N.Y. Garces, N.C. Giles, L.E. Halliburton, *Phys. Stat. Sol (a)* **195**, 1, 171-177 (2003)

[28] H-J. Ko, M-S. Han, Y-S. Park, Y-S. Yu, B-I. Kim, S. S. Kim, J-H. Kim, *J. Crys. Growth*, **269**, 493-498 (2004)

[29] B. Xiang, P. Wang, X. Zhang, S. A.Dayeh, D.P.R. Alpin, C. Soci, D. Yu, D. Wang, *Nano Letters*, **7**, 2, 323-328 (2007)

[30] B.T. Adekore, J.M. Pierce, R.F. Davis, D.W. Barlage, F. Muth, *J. App. Phys.* **102**, *024908* (2007)

[31] Y.S. Park, C.W. Litton, T.C. Collins, D.C. Reynolds, *Phys. Rev.* **143**, 2 (1966)

[32] S. Limpijumnog, S.B. Zhang, Su-Huai, C.H. Park, *Phys. Rev. Lett.* **92**, 15 (2004)

[33] S.B. Zhang, S-H. Wei, A. Zunger, *Phys. Rev. B.* **63,** 075205 (2001)

[34] F. H. Leiter, H. R. Alves, A. Hofstaetter, D. M. Hofmann, B. K. Meyer, *Phys. Stat. Sol. (b)*, **226**, 1, R4-R5 (2001)

[35] T.M. Børseth, B.G. Svensson, A.Y. Kuznetsov, *App. Phys. Lett.* **89**, 262112 (2006)

[36] P. Klason, T. M. Børseth, Q. X. Zhao, B. G. Stvensson, A. Y. Kuznetsov, P. J. Bergman, M. Willander, *Solid State Comm.* **145**, 321-326 (2008)

[37] A. Janotti, C.G. Van de Walle, *J. Crys. Growth.* 287, 58-65 (2006)

[38] S. Hullavarad, N. Hullavarad, D. Look, B. Claflin, *Nanoscale Res. Lett.* **4**, 1421–1427 (2009)

[39] B. Doggett, S. Chakrabarti, R. O'Haire, A. Meaney, E. McGlynn, M.O. Henry, J-P. Mosnier, *Superlat. and Micro.* **42**, 74-78 (2007)

[40] Z. Fan, P-c. Chang, J.G. Lu, E. C. Walter, R.M. Penner, C-h. Lin, H.P. Lee, *App. Phys. Lett.***85**, 25 (2004)

Chapter 3: Growth and Preparation

3.1 – Good Quality ZnO

ZnO fabrication with respect to the semiconductor industry has always been with a view towards material of high optical and electrical quality and of suitable scale with potential for efficient production. These are essential qualities of a growth method if ZnO-based semiconductor devices are to be made commercially available. As detailed in section 1.1, a great deal of research activity took place concerning the production of large-scale ZnO wafers with Look *et al* [1] publishing preliminary work on vapour-phase-transport (VPT) grown ZnO as grown by E.P.™. Other manufacturers have since produced high-quality, large area ZnO wafers, employing their preferred growth methods; Tokoyo Denpa™ for example use hydrothermal seeded growth and Cermet™ produce films with a melting process. Although exceptional quality ZnO was produced from these companies, amongst others, difficulty in aspects of growth such as the high ZnO vapor pressure hindering melt growth [3], slow growth rate for hydrothermal growth (as low as 10 μm/hr [4]) or a need for extensive post-growth treatment for an epi-ready surface [5] resulted in material that was not economically or efficiently produced for any possible device application.

A lack of single crystal ZnO available cheaply for large-scale homo-epitaxy prompted much activity in other growth processes. The much cheaper and more widely available sapphire still commonly takes the role of substrate for ZnO growth across a range of growth processes including CVD, RF magnetron sputtering, both fast and slow PLD, MBE, MOVPE and more. The nature of hetero-epitaxy though, gives rise to the possibility of induced thermo-mechanical strain, which can give rise to defect species.

Some single crystal growth methods do not suffer from such a difficulty due to seeded growth, or melting. Most do require a substrate for growth, but lattice mismatching can severely hinder epitaxial quality of the ZnO produced. Although some such as $ScAlMgO_4$ (SCAM) offer mismatch as low as ~0.1% [6,7], such near ideal substrates presented the same difficulty as single crystal ZnO, often prohibitively expensive for large scale production of thin films or nano-structures.

a-, *c*- and *r*-plane sapphire were used as substrates in this study with much work examining the fine-tuning of growth parameters to result in best-case material. The method employed here for growth of thin films was PLD, which offers fast material production with a low growth temperature. Nano-structures were also fabricated via PLD but were primarily grown using the VPT growth mechanism using an Au catalyst.

These are the two growth processes in focus here, and as such examination of other methods is outside the scope of this work. An extensive ZnO review by Özgür *et al* [8] discusses many of these other grow processes not covered here.

3.1.1 – Pulsed Laser Deposition

PLD growth of semiconductor thin films rely on inducing a plasma in an evacuated chamber, sourced directing a laser toward a solid target. The resulting plume is guided toward a heated substrate allowing films to form via condensation. Typically for ZnO preparation, high purity 5-9's purity targets are used, with ablation via Nd:Yag (Neodymium: yttrium aluminium garnet) laser with plume directed to the substrate in oxygen ambient. The set-up employed for thin films grown for this study is described in J-R. Duclére *et al* [9]. Control of growth conditions is essential for systematic analysis of material. Considering first the PLD system employed for ZnO production in this study, the conditions for growth were; target ablation by a 266 nm, 150 mJ Nd:YAG laser at a frequency of 2 Hz with a target surface fluence of ~2 $mJcm^{-2}$. These parameters are typical of a PLD system employing Nd:YAG-based ablation [12,13]. The principal variation in fabrication conditions occurs where temperature, ambient, annealing treatment and substrate are concerned. A schematic for the PLD chamber is shown in figure 3.i.

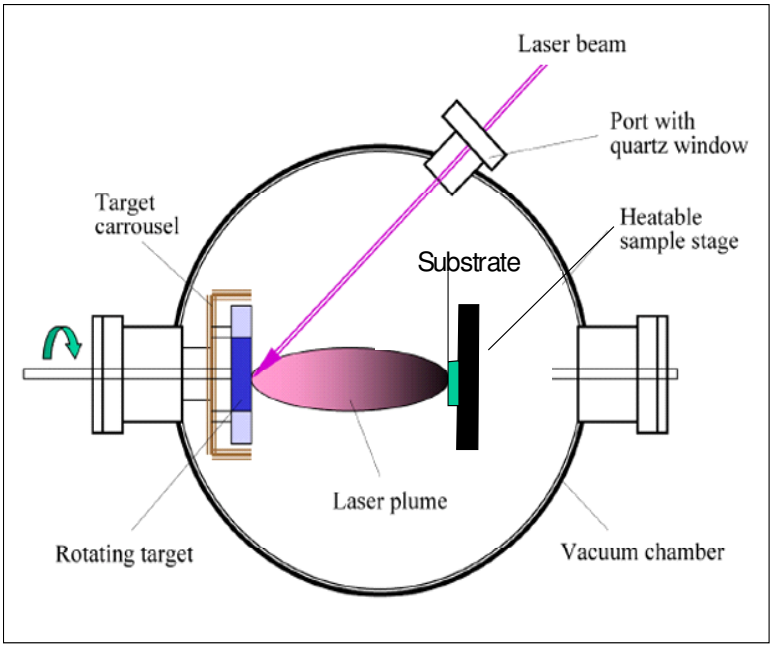

Fig. 3.i: PLD apparatus arrangement.

Minor changes in some growth conditions often result in large variation in material quality and characteristics. Typically in PLD, thin films are sensitive to target purity, ambient pressure and constituents, substrate, base vacuum level, and temperature

at various times and localities during growth. These parameters were altered carefully and systematically for growth here. Successful and best-case growth regimes were identified from characterisation, allowing growth conditions to be tuned for optimisation of material characteristics.

Dopant incorporation was achieved by employing additional targets to the Zn block, or from incorporation of N using an ECR plasma source. N^+/ N_2^+ ions with energies of the order of tens of eV were extracted with the magnetron unit providing microwave power of 250 W at 2.45 gHz.

3.1.2 – Vapour Phase Transport

Vapour, liquid and solid (VLS) phases of ZnO from 5-9's purity powders were used to grow nano-structures. Deposition of Au onto substrates via evaporation followed by annealing resulted in Au droplet clusters, which acted as seeds for ZnO growth. Equal parts ZnO and C powders were first vaporised at high temperatures of ~ 1400K with subsequent condensation of ZnO onto the droplets. The ambient was a controlled flow of Ar gas, which reduced the potential impurity incorporation. This resulted in Au catalysed growth of ZnO nano-structures, with dimensions laterally and vertically tuneable from droplet diameter and growth time respectively. Figure 3.ii shows a schematic of the typical set-up employed with full details described in Grabowska *et al* [14].

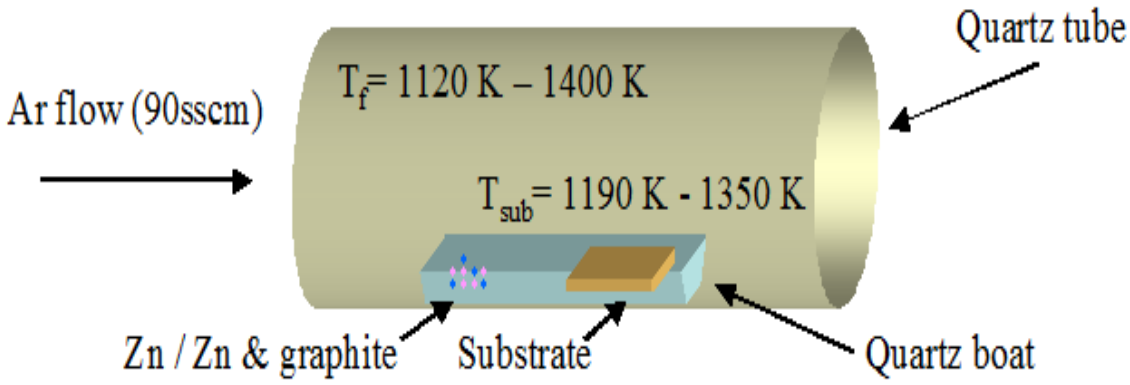

Fig. 3.ii: Schematic of typical VPT growth set-up.

Many temperature schemes were considered in discovering the conditions more favourable for growth of high quality nano-structures. A 2-step process was eventually settled on, producing improvement in quality compared to some other methods [10, 11]. The source materials within the furnace are heated to some 1000 K and then cooled to ~50 K above room temperature before finally being ramped up to the high 1500 K

above growth temperature. Once a scheme was identified that resulted in nano-structure growth, only slight tuning of substrate and growth temperature was performed thereafter. Even mild changes in VPT growth parameters can dramatically alter the resulting character of nano-structures, most notably the type of nano-structure formed. An example of this sensitivity can be found with comparison of the final material produced here [14,15] with nano-rods linked by a nano-wall membrane when a 2-step temperature scheme was introduced.

3.2 –Material Sensitivity to Growth Parameter

As it will be shown in subsequent sections, very slight modification in growth parameters resulted in drastically different sample characteristics. To demonstrate the sensitivity of film quality to growth, two particular growth regimes were examined, both employing a P_2O_5 dopant source but where significant variation in temperature schemes resulted in films that presented very different PL data. The conditions are compared in table 3.i below, followed by schematics of the growth regimes in figure 3ii. Figure 3.iii shows PL data of the two samples demonstrating the resulting differences in film properties.

Sample	**Substrate**	**wt% P_2O_5**	**Growth Temp.**	**Annealing**	**Cooling**
86	*c*-Sapphire	1.25	800K	*in-situ* 30 min in 0.5atm O_2.	280 K/min for 96 min
228	*c*-Sapphire	1.00	1170K at max. in stepped temp. scheme.	*in-situ* temp. stepping.	280 K/min for 120 min

Table 3.i: Growth conditions for samples 86 and 228. Both samples grown at based pressure of 10Pa.

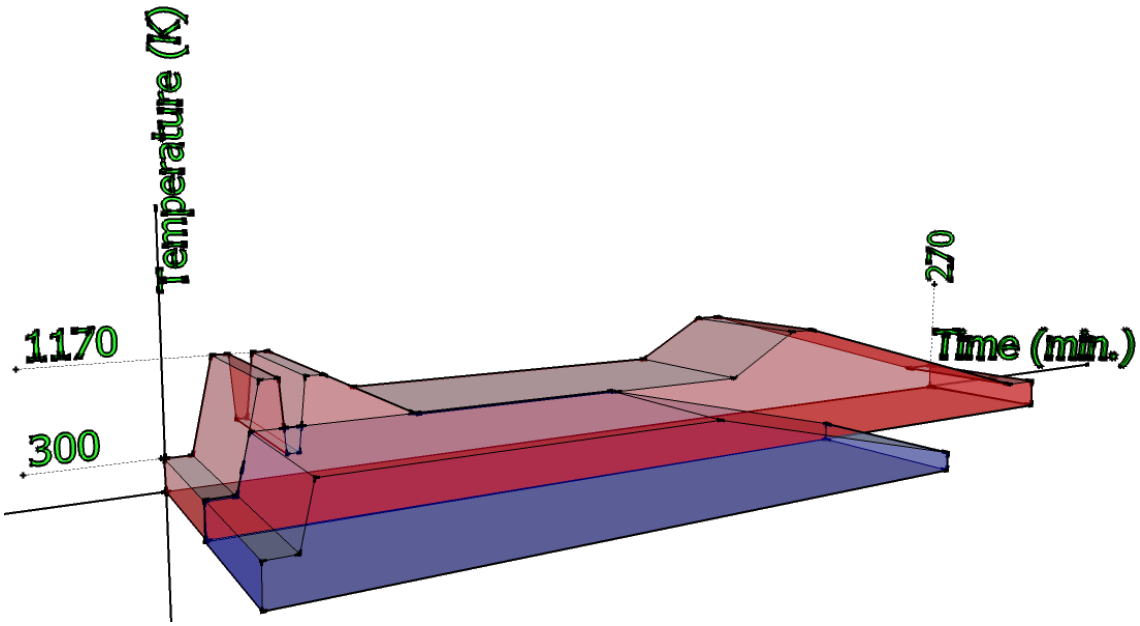

Fig. 3.ii: Growth regime for sample 86 (blue) and 228 (red).

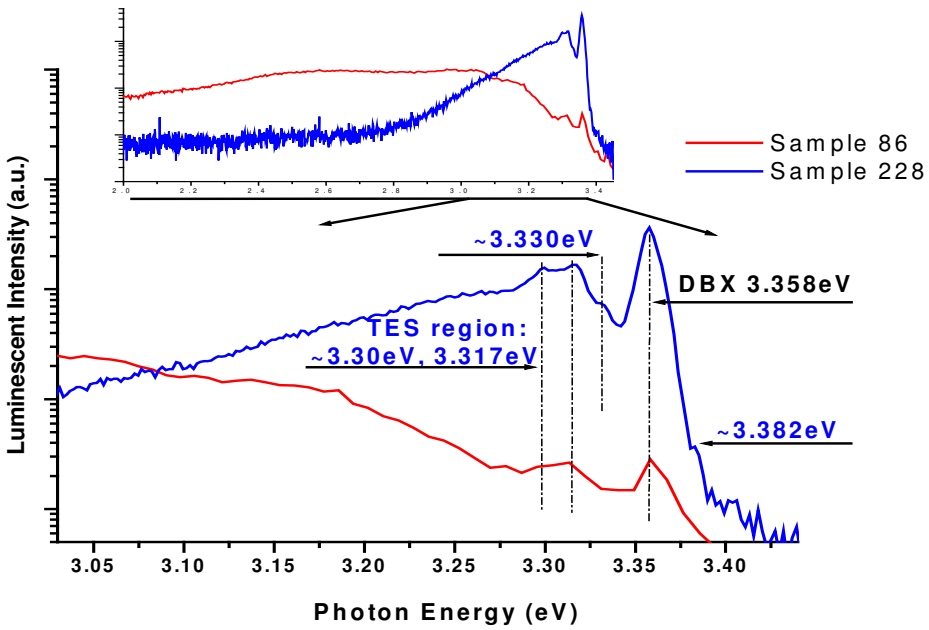

Fig. 3.iii: PL comparison of samples number 86 and 228. Inset: Deeper emission, from 2.0eV.

Considering first the relative intensities, it is clear that there are two very distinct PL profiles in this data. The relative intensities indicate the data were recorded at different temperatures with reduction in intensity predicted from equation 2.viii. With regard to comparability of data, it is necessary to ensure that any different features are not related to acquisition parameters. Over the acquisition temperature difference, ΔE_{Gap} is at most 0.3 meV for ZnO [16] at the moderate difference of 8 K. This is not expected to result in either significant intensity quenching, appearance of newer features

or significant spectral red-shift. NBE PL features are generally stable in PLD material for temperatures up to 30 K [17, 18.19].

Secondly, the PL data show very different relative intensities between the ratios of 3.358 eV DBX to 3.317 eV TES emission - 2.18:1 for sample 228 and half that for sample 86. This far more intense DBX emission together with the narrower FWHM of TES and DBX features and suppression of deeper emission extending from ~ 2.8 eV indicates that overall, sample 228 was grown to a higher quality than sample 86. Moreover, it is indicative of introduction of a lower number of different defect centres The different temperature schemes used during growth and the presence of a stepped temperature regime for sample 228 are the most dissimilar of the growth parameters and so the most likely candidates for causing the disparity in data with in-growth heating and cooling promoting migration of various species and their relaxation to lower energy or native configurations. The affect of the stepped temperature regime applied during growth is now examined.

3.2.1 – Annealing as a Consequence of Temperature Ramping

Several authors have demonstrated the beneficial and sometimes necessary effects of annealing steps in dramatically altering sample character and quality. Viathanian *et al* [19] demonstrate the need for a post-growth rapid thermal anneal at some 1000K to activate the P-dopant as an acceptor. Ip *et al* [20] discussed an *in situ* annealing step required to convert n-type conducting to p-type conducting for P-doped $Zn_{0.9}Mg_{0.1}O$. In Kim *et al* [21] it was also observed that conversion from n-type conducting to p-type conducting occurred at temperatures greater than 1100 K in an N_2 ambient due to greatly reduced electron concentration in their films. These works evidenced the dramatic alteration in film quality and character with a dedicated annealing step. The addition of a stepped growth in sample #228 is therefore a likely candidate for alteration of the films' optical properties with individual ramping and cooling steps acting as an annealing process.

The stepped temperature regime for sample 228 involves regular temperature ramping to 1180 K. This procedure encourages inter-diffusion of the ZnO and ZnO : P_2O_5 but is absent in the growth of sample 86. Considering PL data of a similar nominally undoped film with a temperature-stepped growth regime, emission observed at 3.284 eV and 3.211 eV also appeared for ZnO PL in Henseler *et al* [22] for material that underwent a dedicated annealing procedure. This further supports the annealing-

nature of a temperature-stepped growth regime with a comparison of these spectra provided in figure 3.iv below. The typical DBX-1,2LO emission is induced in the spectrum, likely from the annealing process.

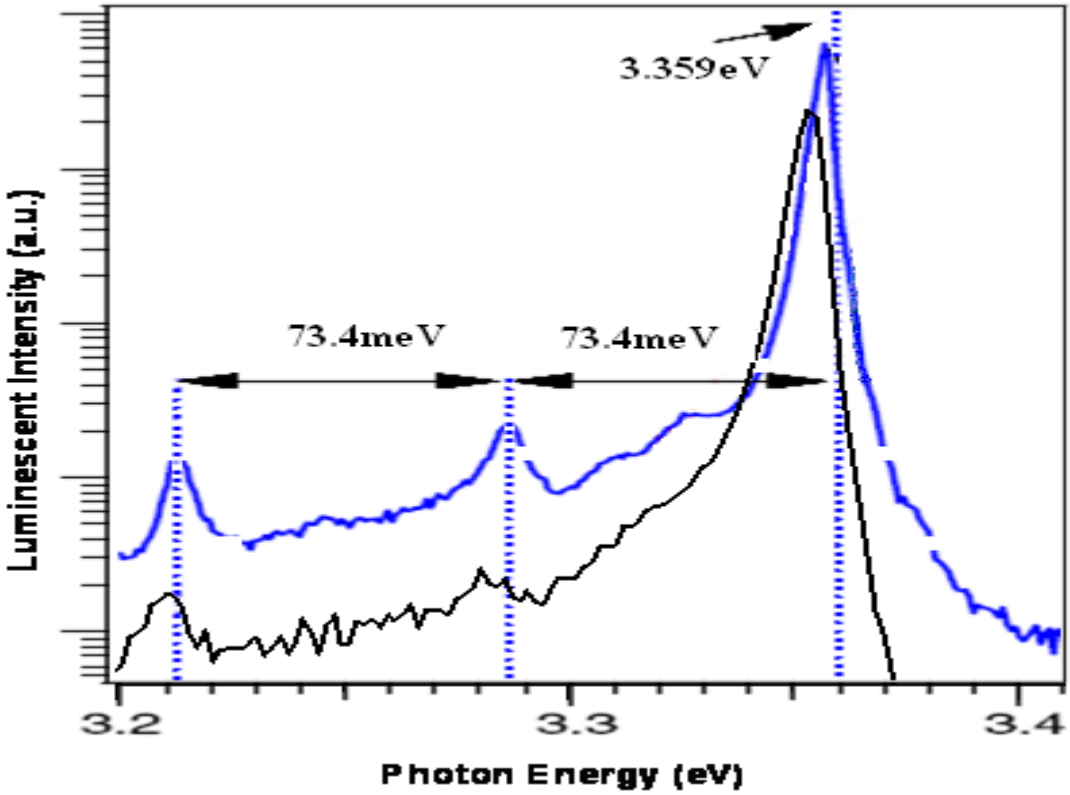

Fig. 3.iv: PL emission of a film grown with a ramped temperature scheme (black) compared to a similar undoped film grown with dedicated annealing step (blue)[22].

3.3 – References

[1] D.C. Look, D.C. Reynolds, J.R. Sizelove, R.L. Jones, C.W. Litton, G. Cantwe11, W.C. Harsch, *Solid Stat. Comm.* **105**, 6, 399-401 (1998)

[3] J. Nause, *III-Vs Review,* **12**, 28 175 (1999)

[4] M. Suscavage, M. Harris, D. Bliss, P. Yip, S-Q. Wang, D. Schwall, L. Bouthillette, J. Bailey, M. Callahan, D.C. Look, D.C. Reynolds, R.L. Jones, C.W. Litton, MTG Internet *J. Nitride Semicond. Res*, **4S1**, 1 (1999)

[5] M.W. Cho, C. Harada, H. Suzuki, T. Minegishi, T. Yao, H. Ko, K. Maeda, I. Nikura, *Superlatt. & Micro.* **38**, 349-363 (2005)

[6] K. Tamura, T. Makino, A. Tsukazaki, M. Sumiya, S. Fuke, T. Furumochi, M. Lippmaa, C. H. Chia, Y. Segawa, H. Koinuma, M. Kawasaki, *Solid Stat. Comm.* **127**, 4 (2003)

[7] A. Ohtomo, K. Tamura, K. Saikusa, K. Takahashi, T. Makino, Y. Segawa, H. Koinuma, M. Kawasaki, *Appl. Phys. Lett.* **75**, 2635 (1999)

[8] Ü. Özgür, Y. I. Alivov, C. Liu, A.Teke, M.A. Reschikov, S. Doğan, V. Avrutin, S-J. Cho, H. Morkoç, *J. App. Phys.* **98**, 041301 (2005)

[9] J-R Duclére, R. O'Haire, A. Meaney, K. Johnston, I. Reid, G. Tobin, J-P. Mosnier, M. Guilloux-Viry, E. McGlynn, M.O. Henry, *J. Mater. Sci: Mat. In Elec.* **16,** 421– 427 (2005)

[10] H.T. Ng, J. Li, M.K. Smith, P. Nguyen, A. Cassell, J. Han, M. Meyyappan, *Science*, **300**, 1249 (2003)

[11] J.Y. Lao, J.Y. Huang, D.Z. Wang, Z.F. Ren, D. Steeves, B. Kimball, W. Porter, *App. Phys. A: Mater. Sci. Process.* **78**, 539 (2004)

[12] X.M. Fan, J.S. Lian, Z.X. Guo, H.J. Lu, *App. Sur. Sci.* **239**, 176-181 (2005)

[13] E. M. Kaidashev, M. Lorenz, H. von Wenckstern, A. Rahm, H.-C. Semmelhack,K.-H. Han, G. Benndorf, C. Bundesmann, H. Hochmuth, M. Grundmann, *App. Phys. Lett.* **82**, 22 (2003)

[14] J. Grabowska, K.K. Nanda, E. McGlynn, J-P. Msonier, M.O. Henry, A. Beaucamp, A. Meaney*, J. Mater Sci: Mater. In Elec.* **16**, 397-301 (2005)

[15] J. Grabowska, A. Meaney, K. K. Nanda, J-P. Mosnier, M. O. Henry, J.-R. Duclère, E. McGlynn, *Phys. Rev. B*, **71**, 115439 (2005)

[15] Y.P. Varshni, *Physica A*, **34**, 1, 149 (1967)

[16] K. Thonke, T.H. Gruber, N. Teofilov, R. Schonfelder, A. Waag, R. Sauer, *Physica B.* **308 – 310** 945 – 948 (2001)

[17] M-Z Lin, C-T Su, H-C Yan, M-Y Chern, *J. J. App. Phys.* **44**,31, L995-L997 (2005)

[18] A. Meaney, J-R. Duclere, E. McGlynn, J.-P. Mosnier, R. O'Haire, M.O. Henry, S*uperlatt. And Micro.* **38**, 256–264, (2005)

[19] V. Vaithianathan, Y. H. Lee, B-T. Lee, S. Hishita, S. S. Kim, *J. Crys. Growth,* **287,** 85 – 88 (2006)

[20] K. Ip, Y.W. Heo, D.P. Norton, S.J. Pearton, J.R. LaRoche, F. Ren, *App. Phys. Lett.* **85**, 1169 (2004)

[21] K-K. Kim, H-S. Kim, D-K. Hwang, J-H. Lim, S-J. Park, *App. Phys. Lett.* **83**, 1 (2003)

[22] M.J. Henseler, W.C.T. Lee, P. Miller, S.M. Durbin, R.J. Reeves, *J. Crys. Growth*, **287**, 48-53 (2006)

Chapter 4: Thin Films and Nano-Structures

Preface

This chapter takes the form of a set of papers as originally published followed by a brief summary of and commentary on their main findings. In some cases, the conclusions at the time of publishing have been amended on consideration of subsequent work. The citation details for these are listed below together with the respective digital object identifier (DOI) links. The author's personal contributions to each of the papers are also listed.

Papers, Contributions and DOI Numbers

[1] R. O'Haire, A. Meaney, E. McGlynn, M.O. Henry, J-R. Duclere, J-P. Mosnier, *Superlatt. and Micro.* **39**, 153-161 (2006)

"Growth of crystalline ZnO nanostructures using pulsed laser deposition" with contributions including:

- Aspects of PL laboratory such as:
    - Data acquisition
    - Laboratory equipment operation and maintenance
    - Spectral calibration
    - Processing and presentation of data
- Analysis of data, especially with respect to identification of common trends between optical and structural / micro-structural data.

http://dx.doi.org/10.1016/j.spmi.2005.08.071

[2] J. Grabowska, K.K. Nanda, E. McGlynn, J-P. Msonier, M.O. Henry, A. Beaucamp, A. Meaney, *J. Mater Sci: Mater. in Elec.* **16**, 397-301 (2005)

"Synthesis and photoluminescence of ZnO nanowires/nanorods" with contributions including:

- Aspects of PL laboratory including:
    - Data acquisition
    - Laboratory equipment operation and maintenance
    - Spectral calibration

    - Processing and presentation of data
- Analysis of data, especially with respect to identification of features unique to VPT nano-structured ZnO

http://dx.doi.org/10.1007/s10854-005-2304-6

[3] J. Grabowska, A. Meaney, K. K. Nanda, J-P. Mosnier, M. O. Henry, J.-R. Duclère, E. McGlynn, *Phys. Rev. B*, **71**, 115439 (2005)
"Surface excitonic emission and quenching effects in ZnO nanowire/nanowall systems: Limiting effects on device potential" with contributions including:

- Aspects of PL laboratory including:
    - Data acquisition
    - Laboratory equipment operation and maintenance
    - Spectral calibration
    - Processing and presentation of data
- Discussion and analysis of data, especially with respect to identification of features unique to VPT nano-structured ZnO

http://dx.doi.org/10.1103/PhysRevB.71.115439

[4] J-R. Duclère, C. McLoughlin, J. Fryar, R. O'Haire, M. Guilloux-Viry, A. Meaney, A. Perrin, E. McGlynn, M.O. Henry, J-P. Mosnier, *Thin Sol. Films*, **500**, 78-83 (2006)
"ZnO thin films grown on platinum (111) buffer layers by pulsed laser deposition" with contributions including:

- Aspects of PL laboratory including:
    - Data acquisition
    - Laboratory equipment operation and maintenance
    - Spectral calibration
    - Processing and presentation of data
- Discussion and analysis of data, especially with respect to affect of Pt (111) buffer layer on optical data
- Identification of common trends between optical and structural data

http://dx.doi.org/10.1016/j.tsf.2005.11.017

[5] A. Meaney, J-R. Duclere, E. McGlynn, J-P. Mosnier, R. O'Haire, M.O. Henry, *Superlatt. and Micro.* **38**, 256-264 (2005)

"Comparison of structural, optical and electrical properties of undoped ZnO thin films grown on *r*- and *c*-Al_2O_3 substrates using pulsed laser deposition" with contributions including:

- Aspects of PL laboratory including:
    - Data acquisition
    - Laboratory equipment operation and maintenance
    - Spectral calibration
    - Processing and presentation of data
- Feedback to growth team for fine-tuning of growth parameters based on optical data, in order to improve material properties, specifically with respect to identifying optimum substrate for growth
- Aspects of Hall laboratory including:
    - Electrical measurement
    - Laboratory equipment operation and maintenance
    - Processing and presentation of data
- Discussion and analysis of data, especially with respect to identification of common trends between optical, electrical, structural and micro-structural data
- Writing and editing in conjunction with 2nd author

http://dx.doi.org/10.1016/j.spmi.2005.08.024

4.1 – A Commentary on Publications in this Chapter

Material characterisation using a variety of techniques showed evidence that good quality thin films were grown via PLD and that both PLD and VPT techniques were successful in producing nano-structured ZnO. All samples displayed epitaxial relationships to the substrate but the microstructures and optical properties were observed to depend greatly on the substrate choice. Analysis of ZnO properties identified a stepped growth process as one of great benefit to the material quality. A characteristic PL feature due to surface excitons SX was identified in nano-structured

materials. Similarly, PL data provided evidence of good homogeneity in thin films. The commentary following the papers includes consideration of growth and characterisation of ZnO thin films and nano-structures with a focus on how particular parameters altered the material properties.

4.2 – Growth Parameters

Many techniques have proven successful for ZnO fabrication and details of these have been discussed in depth with summaries available elsewhere [6]. A brief review of laser-based techniques appears in O'Haire *et al* [1] while an in-depth report on growth of epitaxial ZnO appears in Triboulet *et al* [7]. Common to many methods for production is the high degree to which the final material is affected by very minor changes in a growth parameter. While most parameters require fine-tuning, others are simply fixed for an operable regime such as successful PLD where temperatures of the order of a few hundred Kelvin up to 1000 K. Similarly, a controlled supply of high purity oxygen is used to minimize troublesome oxygen vacancies.

ZnO thin films and nano-structures studied here were successfully grown with a variety of conditions employing two principal growth techniques. VPT was used for nano-structured ZnO, producing both nano-wires and nano-wire / nano-wall arrays with VLS growth identified. Nano-structured ZnO was also achieved using PLD but this technique focused primarily on thin-film fabrication. A systematic approach was undertaken to identify how a particular change in a growth parameter affected the final material [1-5]. Studies were directed toward understanding how optical and electrical properties depended upon choice of growth parameters, with a focus toward the affect of substrate choice on final material. Some authors have established successful hetero-epitaxial growth regimes using substrates such as Si [8], GaAs [9] or GaN [10]. Many reports on successful hetero-epitaxial ZnO thin films employ sapphire substrates [11-15]. It remains extremely popular and was the substrate of choice here.

The degree to which changing the mechanism influences the characteristics of ZnO is clearly apparent when comparing PL data of PLD nano-structures to VLS grown samples. It is not sufficient to just identify either a unique set of parameters for a given growth mechanism that result in good ZnO or an individual parameter that produces a particular characteristic. It is instead necessary to identify the manner in which such a particular growth parameter has changed the final material characteristics. Examination of ZnO was performed in order to identify changes caused by the fine-tuning necessary

in order to achieve desirable material and where possible, offer a mechanism for such changes.

4.3 – Epitaxial and Crystalline Quality

Sapphire was employed for most ZnO grown here due to availability of large area substrates and a reasonably low lattice mismatch [16]. The (11-20), (0001) and (1-102) - or *a*-, *c*- and *r*-plane - orientations were employed for PLD growth with AFM images showing ZnO grown on sapphire to be far better aligned compared to those grown on Si / SiO_2 [2]. The epitaxial relationship was verified here using XRD using Cu K_α radiation generated in a commercial texture X-ray diffractometer.

VPT and PLD nano-structures on *a*-Al_2O_3 demonstrated highly crystalline material with exceptionally low value for the (0002)-ZnO rocking curve FWHM (ω_{FWHM}) of 0.15 ° on *a*- Al_2O_3 and 0.36 ° on *r*-Al_2O_3 [1]. In Kawakami *et al*, growth temperatures of 780 K were shown to eliminate secondary reflections other than those associated with minor secondary ZnO planes but PLD nano-structures here, grown at 980 K show substrate reflections of similar intensity to primary ZnO reflections [2]. Thin film $\theta - 2\theta$ measurements are dominated by sapphire reflections at least an order of magnitude greater than the ZnO peaks [7]. Some thin film data show very minor peaks in addition to ZnO and Al_2O_3 reflections, around 10^{-4} of maximum intensity. In XRD data for ZnO grown on a Pt buffer layer [6] these are expected, with minor Pt-(200), Pt-(220) peaks and Al_2Pt peaks present. Data from XRD measurements do show the crystalline quality of thin film material is good overall with ω_{FWHM} values for primary reflections broadly comparable to nano-structured material at some 0.45 ° for *a*-Al_2O_3 or 0.34 ° for ZnO on a Pt buffer layer.

X-ray φ scans of these films show that they demonstrate good alignment for a particular growth direction with epitaxial relationship to substrate identified. Films including a Pt-buffer for example, demonstrate six (10-11)-ZnO diffraction peaks separated by 60 ° at the same angle as Pt-(002) peaks and shifted some 30 ° to the substrate reflections. A similar trend in ZnO–substrate reflections was observed in *a*-Al_2O_3 thin films and nano-structures grown on *a*- Al_2O_3. This six-fold symmetry confirms an epitaxial relationship between the ZnO film and crystalline substrate [5-7].

4.3.1 – Influence of Substrate on Morphology

A low value for ω_{FWHM} shows the ZnO grown was of good quality but the overall microstructure in both nano-structures and thin films is substantially changed depending on choice of sapphire plane. PLD nano-rods were found to have dimensions greatly dependant on the substrate plane with particles produced ranging in width / height of an order of 150 / 100 nm on *a*- Al_2O_3 to 400 / 300 nm on *r*- Al_2O_3. Similar dimensions of tens to low hundreds of nm were observed for ZnO nano-structures grown by VPT on *a*- Al_2O_3 as well as for the periodicity of terraces in thin films demonstrating striated surface morphology [4,7]. These dimensions are quite similar to those reported in Munuera *et al* [17] where ZnO was found to form periodic lines mimicking the substrate.

Such growth patterns are observed for thin films on (11-20) sapphire with striations evident of film mimicking the non-contiguous nature of the substrate. Steps and terraces in the plane are reflected in the surface morphology as shown in figure 4.i-left below. For films grown on *a*- Al_2O_3, a clustering of ZnO is instead evident, aligned along the C-axis that is perpendicular to the substrate plane as in figure 4.i-right. This columnar growth is apparent from the white termination points.

There exists a 50% r_{rms} increase for films grown on *c*- Al_2O_3 as compared to *a*- Al_2O_3. The higher r_{rms} indicates a non-uniform deposition of ZnO onto the substrate.

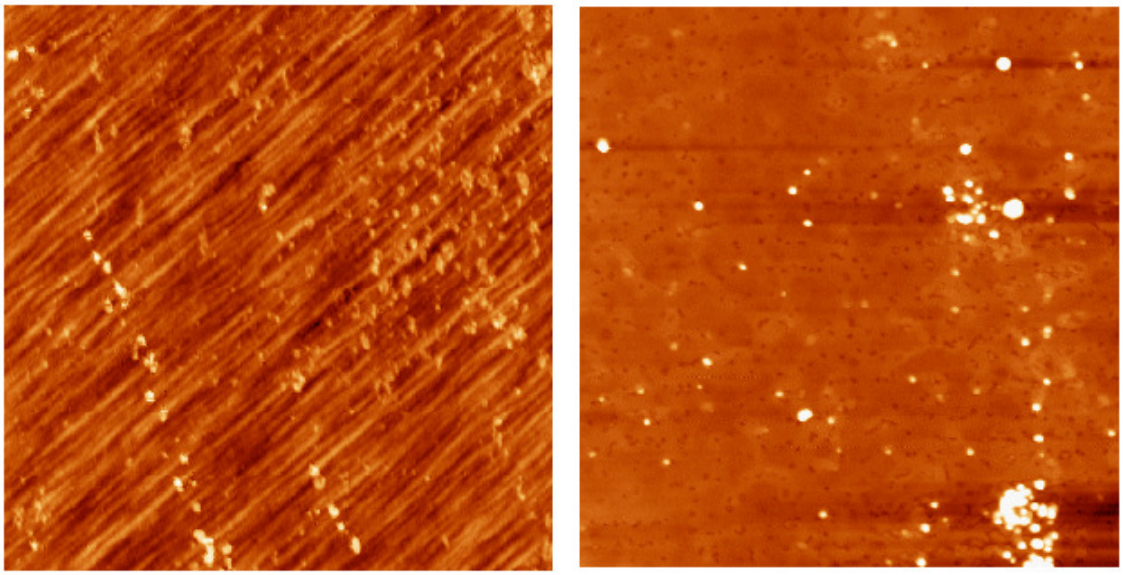

Fig. 4.i - AFM images of ZnO thin films on (11-20) Al_2O_3 - left and (0001) Al_2O_3 - right. Scan areas are 1 μm^2 and 5 μm^2 respectively.

If the ZnO mimics the substrate steps / terraces then it is necessary for the substrate to demonstrate a similar periodicity of steps / terraces. We do not observe such surface morphology in our films grown on *c*- Al_2O_3. The surface of *c*- Al_2O_3 has been shown to be smooth to near atomic flatness following high temperature annealing [18]. We find a higher ω_{FWHM} [2] and r_{RMS} for *c*- Al_2O_3 than *a*- Al_2O_3 so it can be concluded that *c*- Al_2O_3 substrates here did not exhibit periodic striation. The XRD data support this hypothesis with ω_{FWHM} 2.33 times greater for ZnO on *c*- than *a*- Al_2O_3 as the substrate striations provide natural nucleation points. Figure 4.ii illustrates the sapphire planes highlighting the non-contiguous *a*- and *r*- Al_2O_3 planes and the relatively smooth *c*- Al_2O_3 surface.

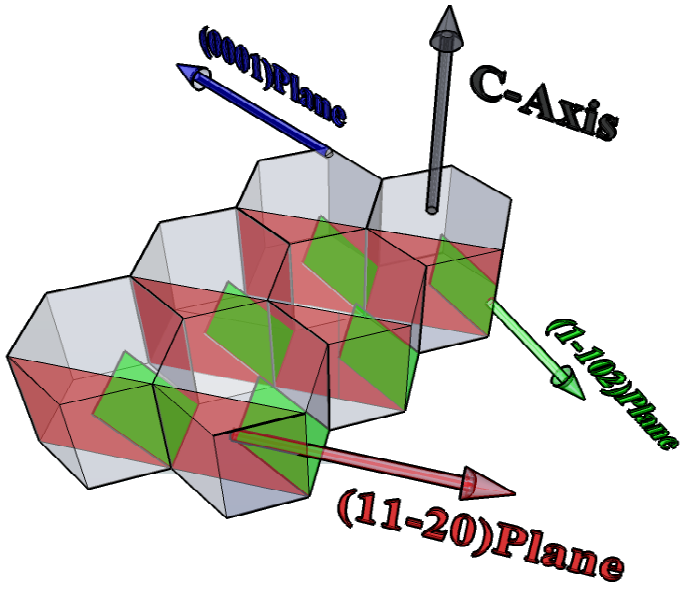

Fig. 4.ii: Sapphire cells with of a-, r- and c-planes displayed in red, green and blue respectively. Substrate steps / terraces are visible along the X-Y direction

4.4 – Optical Characteristics of Thin Films

The effect of varying the substrate on a film's microstructure is evident from the above, and strongly supported by luminescence data. Considering first the thin films produced here, the PL data exhibit evidence of shallower, more donor-like traps [19,20] when deposited on *a*- Al_2O_3 in comparison to either ZnO / *c*- Al_2O_3 or ZnO / Pt / *a*- Al_2O_3 hetero-structures. The addition of a Pt buffer layer appears to create deeper excitonic centres in the NBE region, and quench emission from the ionised DBX centres. Characteristics of these thin films and questions arising from the data are now examined.

4.4.1 – PL Energy Assignments of Thin Films

PL data of the ZnO / *c*- Al_2O_3, ZnO / *a*- Al_2O_3 and ZnO / Pt / *a*- Al_2O_3 hetero-structures were compared to identify features common to the various preparations. Initial analysis of the three spectra [6,7] assigned primary NBE emission in each to I_4, to $I_{6/6A}$ and to I_{11}, I_{10} and I_9 respectively. In making comparisons, the measurement temperature is crucial as E_{Gap} decreases with increasing temperatures, resulting in line-shifts. The PL emission are not directly comparable because of this, having been recorded at 6.7 K for ZnO / *c*- Al_2O_3, ZnO / *a*- Al_2O_3 and 28 K for ZnO / Pt / *a*- Al_2O_3. Further doubts over the assignments arise because they originate from comparison to *I*-line values for E.P.™ material recorded at 4.2 K [6,21].

According to the Varshni equation [22] a red shift of 0.8 meV takes place for a change of 4 K to 28 K. In Meyer *et al* [21] a more moderate shift is predicted over this temperature difference by the function:

$$E_{Gap}(T) = \frac{E_{Gap}(0) \cdot 5.05 \cdot 10^{-4} T^2}{900 - T} \qquad \text{Eqn: 4.i}$$

which results in ΔE_{Gap} and consequently DBX positions of 0.45 meV. We find from experiment[8] that $E_{Gap}(T)$ is more accurately described by equation 4.i in than by the Varshni equation - a change of 0.42 meV experimentally as compared to the 0.8 meV shift predicted by equation 2.vii.

The data in the following figures were energy-shifted to compensate for different measurement temperatures. They indicate the emission originates from a number of defect centres but with a broad spread. A different defect could be expected for Pt-buffer thin films but in the case of the others, only the substrate orientation changes. Such differences in optical characteristics are unexpected for material with only this growth parameter altered. Assignments are especially peculiar when the chemical origins of defect centres are considered. The dominant emission identified as H-related for ZnO / *c*- Al_2O_3 with Al and / or Ga impurities for ZnO / *a*- Al_2O_3 offer no agreement between emissions from very similar films.

[8]Refer to figure 2.vii.

4.4.1.i – Pt Buffer Layer ZnO

Examination of the energy separation between primary PL emission peaks for ZnO / Pt / *a*- Al_2O_3 films and comparing to those at 28 K results in I_8 and I_9 as the most probable contributions for the curve-fit emission. Bulk E.P.™ material typically shows I_8 and I_9 separated by 3.4 eV with I_{10} deeper by 3.6 meV. A good coincidence exists between these energy separations and those for ZnO / Al_2O_3 hetero-structures as in figure 4.iii.

4.4.1.ii – ZnO / *c*, *a*-Al_2O_3

The most intense NBE emission from ZnO / *c*- Al_2O_3 thin films was originally assigned to $I_{6/6a}$. A relatively large FWHM of 4.3 meV makes particular *I*-line contributions difficult to determine. This broad emission encompasses possible contributions from many of the *I*-line series, but the most intense emission is centred around I_8 / $I_{6/6a}$ with a shoulder on the high energy side. These assignments are reasonably sound especially considering a source of Al is readily available from the sapphire substrate. An $I_{6/6a}$ contribution is supported with analysis of ZnO / *a*- Al_2O_3 films, which were prepared in a similar fashion. The likelihood of I_4 H-related bound exciton recombination contributing to the NBE emission on ZnO / *a*- Al_2O_3 is low considering that the films underwent an *ex-situ* anneal. Several authors detail the elimination of hydrogen from ZnO during annealing in oxygen ambient [23,24]. Such an annealing treatment was performed for the ZnO / *a*- Al_2O_3 at ~ 1000 K for 90 minutes in oxygen at a pressure of ~ 0.5 atmospheres. The dominant DBX emission persisted. Pre- and post- anneal data are compared in fig. 4.iv.

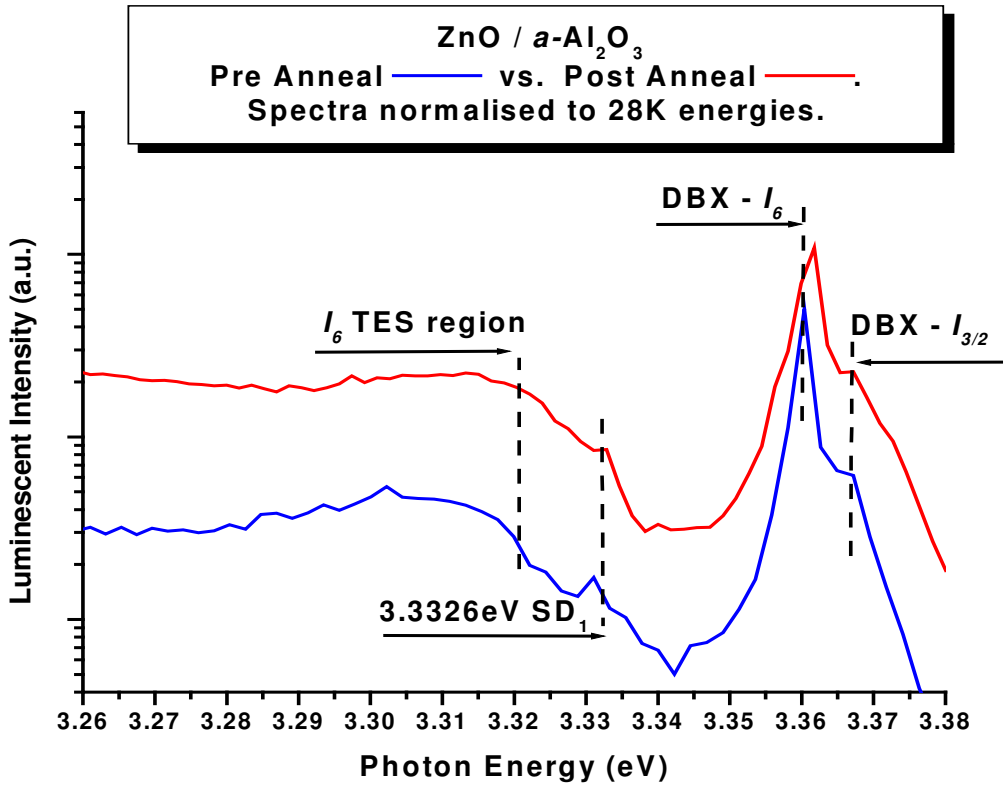

Fig. 4.iv: Pre- and post- anneal spectra of ZnO / a- Al_2O_3 recorded at 12 K.

The dominant NBE feature centred at 3.36036 eV remained despite thermal treatment, although there is a relative reduction in intensity ratio of DBX to TES region emission of 65% after annealing. The ratio of dominant I_6 DBX emission to the higher energy $I_{3/2}$ DBX peak reduces by 53%. These are marked reductions but the emission is still present post-anneal. Attributing any of the emission to H in the films is therefore questionable, as near total quenching is expected for H-related DBX after an oxygen-based anneal. The TES emission and exciton-to-structural defect contribution or SD_1 - see section 4.4.2 - remain after the annealing step [21].

Temperature dependence measurements for the dominant DBX emission in ZnO / *c*- Al_2O_3 and ZnO / *a*- Al_2O_3 reveal nearly identical - 3.54 meV and 3.6 meV respectively - activation energies for the bound exciton emission from plots of $Ln((I_0 / I_T) - 1)$ vs. $1/kT$ shown in figure 4.v. A second region of linearity for the ZnO / *c*- Al_2O_3 is observed at higher temperature - above 30 K - with greater energy required for thermalisation of bound excitons as the CB fills. Higher temperature data were not recorded for ZnO / *a*-Al_2O_3.

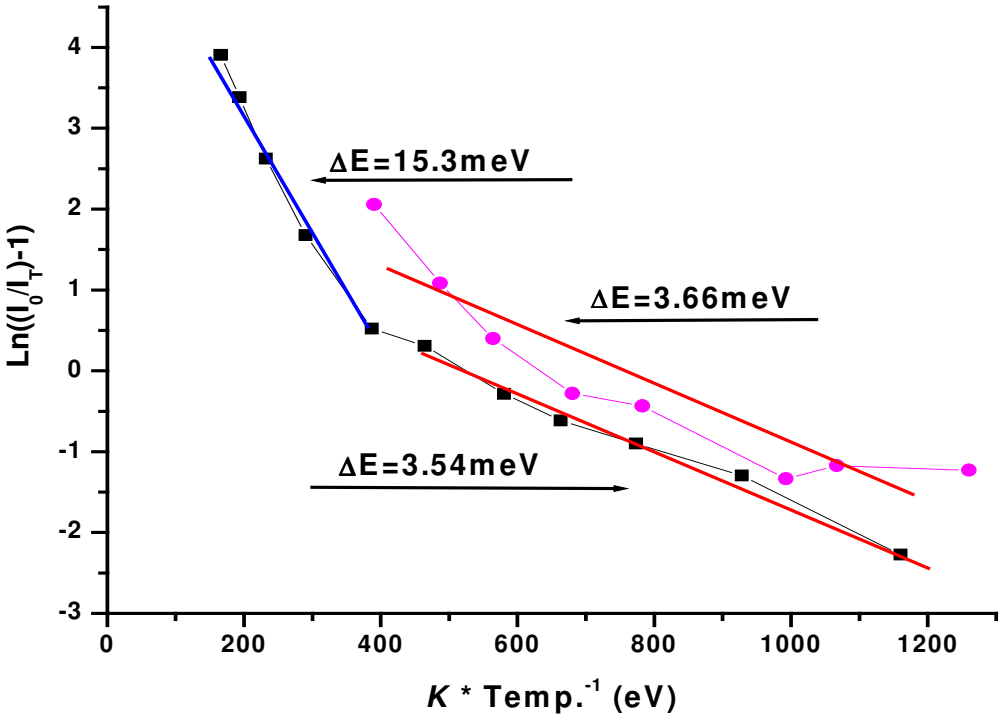

Fig. 4.v: Intensity ratio of primary DBX emission vs. k/Temp showing ΔeV for particular bound excitons.

The original analysis [4] is therefore considered incorrect. The data were processed by introducing a 1.54 meV red shift and 2.24 meV blue shift for the ZnO / *a*- Al_2O_3 and ZnO / Pt / *a*- Al_2O_3 respectively. Fig. 4.vi shows the spectra with the revised assignments and presented at energies for the 28K acquisition temperature. ZnO / *a*- Al_2O_3 and ZnO / *c*- Al_2O_3 both display strong emission understood to originate from an Al defect, suggesting defect diffusion from the substrate as a likely source. The presence of this allows for some interesting observations regarding the sample growth. The 325 nm laser used in PL studies of the films has a penetration depth of some 60 nm. It follows that if Al diffuses from the substrate, defects would need to penetrate some 90% of the film for a nominal 500 nm thickness. Even offering a low mismatch to ZnO, Al_2O_3 substrates do appear to have an unfavourable affect on the films because of abundant Al defects, specifically the donor nature of Al_{Zn} [25].

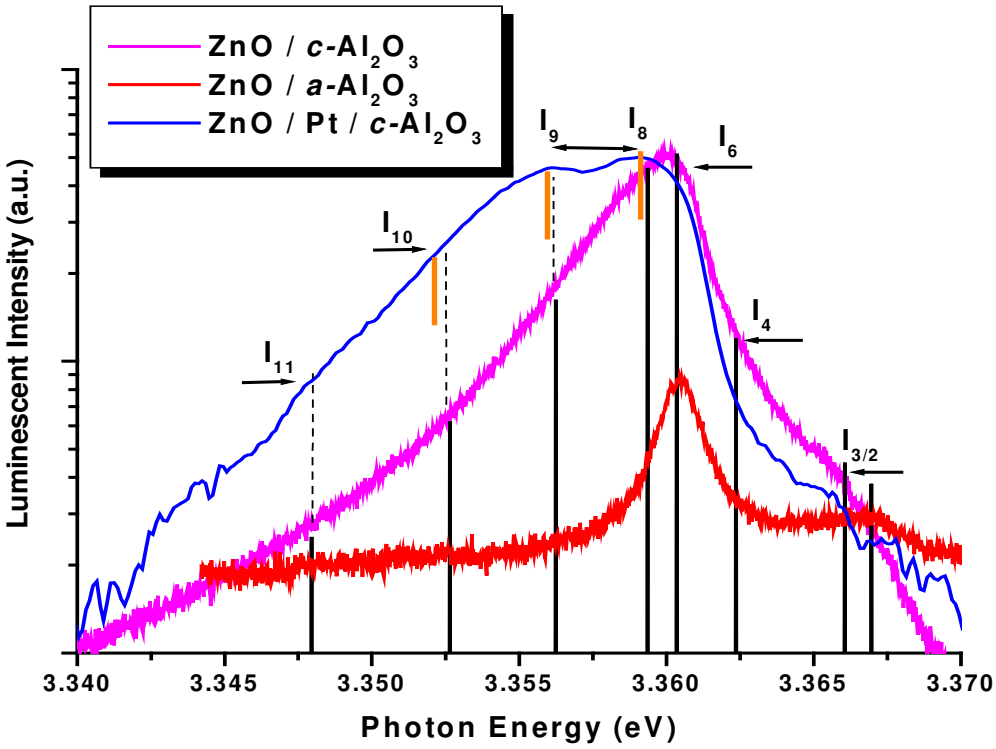

Fig. 4.vi: Revised PL spectra for ZnO films. Orange bars denote curve-fit contributions assigned above as I_{10}, I_9 and I_8 after 2.24 meV blue-shift. Energies normalised to those at 28K.

A possible source for this data adjustment are effects of charges trapped at grain boundaries, which were confirmed as present in these samples by AFM images, known to cause red shift of the ~1 meV [26]. The remaining shift of some 1.2 meV must be account for, and it is the presence of the buffer layer to which this is attributed.

The lattice parameters of ZnO are reasonably constant over a large temperature range, reducing to not less than 3.242 Å along the ZnO *a*-axis and not less than 5.188 Å along the ZnO *c*-axis [27]. The corresponding value for (111)-Pt is some 3.98 Å [28]. It is known that E_{Gap} decreases under tensile strain while a compressive strain causes an increase of the band gap [29]. XRD analysis of ZnO / Pt / *c*- Al_2O_3 films here shows peaks from a variety of Pt planes, (111)-Pt reflections the most intense of these with (220)-Pt some 3 orders of magnitude lower in intensity. As a reduction in E_{Gap} was observed and a tensile strain expected from the Pt buffer due to larger bond length of 0.74Å, it is likely that the buffer layer played some part in the observed shift.

4.5 – PL Comparison of PLD Thin Film vs. PLD Vertical Nano-Systems

Considering nano-structures and their higher surface to volume ratio than thin films they exhibit, a higher likelihood of homogeneity exists over such a smaller volume and because of this a propensity for fewer defects. The optical properties in particular are typically superior in the case of nano-structures than of thin films. PL data of PLD nano-structured and thin film ZnO on a-Al_2O_3 are compared in figure 4.vii. The comparable FWHM of the dominant DBX emissions are apparent. Indeed, the PLD thin films demonstrated a sharper dominant feature in this region, underlining the high quality of the thin film material produced.

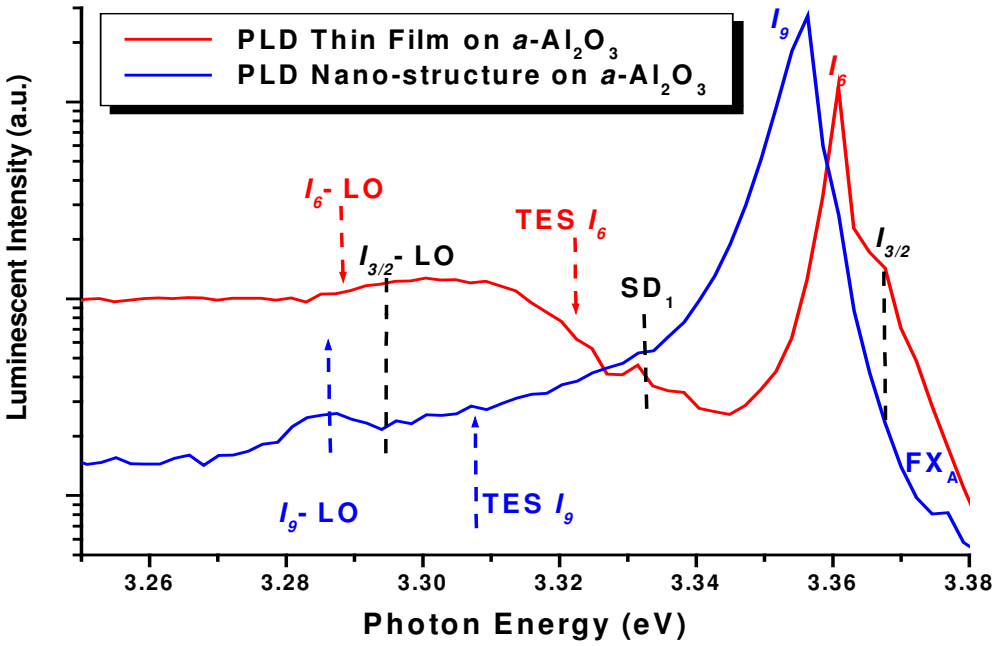

Fig. 4.vii: NBE region PL data recorded at low temperature for thin film and nano-structured PLD ZnO.

This NBE emission consists of an Al-based bound-exciton emission with a FWHM of 1.7 meV together with a shallow and broader shoulder in the ionised DBX, or $I_{3/2}$ region. No other distinct lines are observed for the thin film. There are hints of both I_6 and $I_{3/2}$ on the shallow shoulder of the primary DBX for the nano-structured ZnO. Similarly, a subtle indication of FX emission is observed in the thin film material. At deeper emission, typical LO replicas are apparent, more from the nano-structured PL. Typical energies for emission from TES processes are indicated but no peak is especially marked.

In data from the films SD_1 band, which appears common to many of our PLD grown ZnO, was observed. It appeared to remain in the PLD nano-structured material

and the significant increase in intensity is noteworthy. The significance of this result has not been explored.

The variation in optical properties of ZnO was not limited to thin films as in fig. 4.vi with nano-structured PLD material varying in quality depending on the substrate employed. This above case considered ZnO on *a*-Al_2O_3 but nano-structures grown on *r*-Al_2O_3 displayed similar NBE emission to that in fig. 4.vii but with more numerous and well-defined peaks. The additional features included emission from TES 2S and 2P states in the deeper energies and excited excitonic emission at higher DBX energies. The PL of PLD nano-structures acts as a good reference and comparator for other PL spectra. Examination of the two primary regions – DBX and deeper emissions – follows figure 4.viii below. The inversion of relative intensities for I_6 and I_9 indicated of a greater influence from the substrate-based Al-diffusion. This was supported from XRD data in section 4.2.1, which showed a lower ω_{FWHM} for nano-structured material on *a*-Al_2O_3.

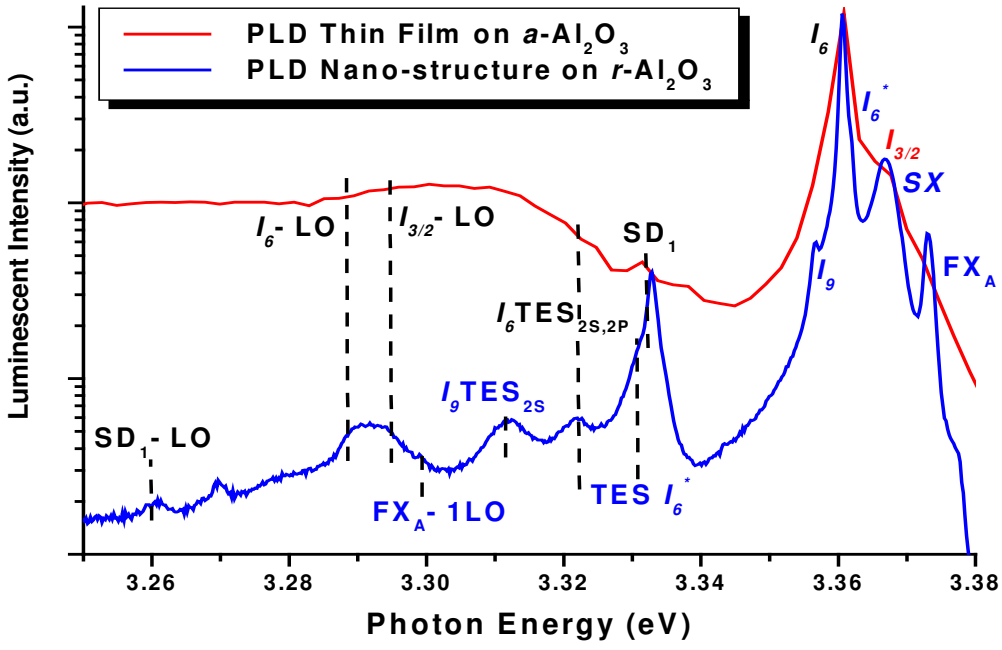

Fig. 4.viii: NBE region PL data recorded at low temperature for thin film and nano-structured PLD ZnO. Inset: Primary DBX emission.

4.5.1 – DBX Region of PLD Thin Film vs. PLD Vertical Nano-Systems

The PL of nano-structured ZnO also exhibits a dominant Al DBX line but with a 52% reduction in FWHM to 0.79 meV, such sharper emission indicative of a reduction in carrier density [21]. A slightly shallower shoulder on this DBX line at around 3.362

eV is also present whose origin was considered as due to I_4 because of its proximity to the known 3.3628eV line and the presence of a band in the locality of typical TES $_{I_4}$. A high annealing temperature of 980 K in a pressure of $5x10^4$ Pa raise doubt over this assignment because of known quenching of emission from excitons bound to hydrogen defects with annealing at even moderate temperature [23].

In Meyer *et al* [21] this emission was presented as originating from excitons in an excited state, specifically I_6^* for this energy. Rotational and vibrational resonances of the bound excitons were considered in Gutowski *et al* [30] as responsible for this emission, typically 1 – 3 meV higher that the ground-state recombination emission which is in good coincidence with data here. Figure 4.ix which follows, shows the primary DBX emission for *a*-Al_2O_3 thin film *r*-Al_2O_3 nano-structures including I_6^*.

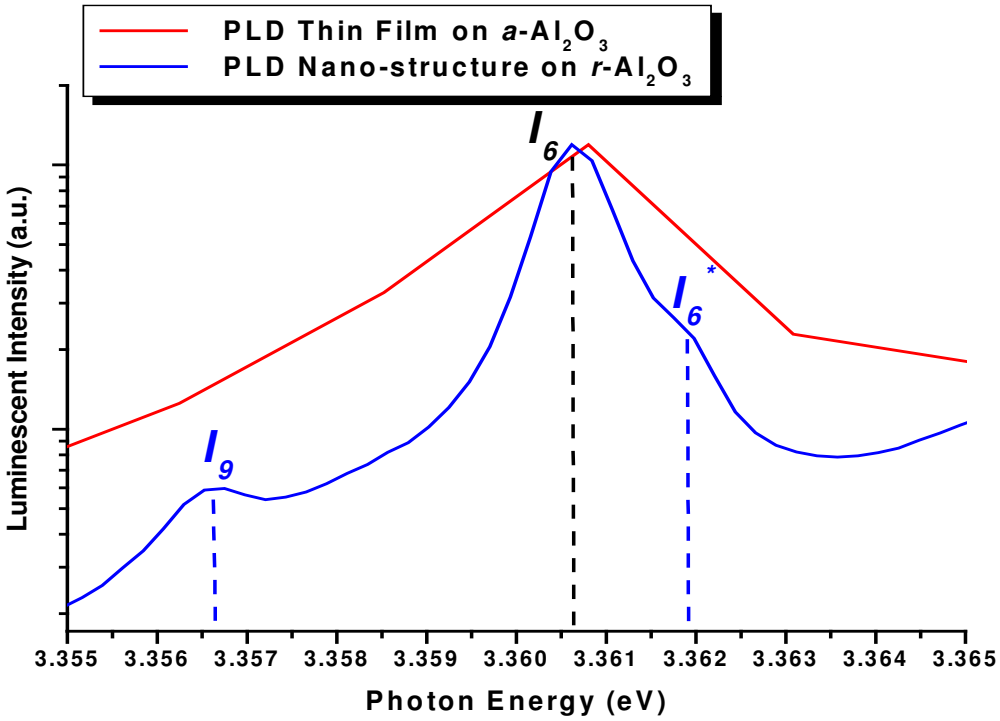

Fig. 4.ix: High-resolution spectra of primary DBX emission from figure 4.viii distinguishing I_6 *and* I_6^*.

Applying equation 2.iv[9] with DBX at 3.3618 eV and TES at 3.331 eV resulted in E_{B_D} of 41 meV, 5.1meV lower than that for I_4 [21] indicative of a different process. An exciton binding energy of 11.21 meV was found with extrapolation of tabulated values in [21]. Two other emission lines at 3.357 and 3.373 eV in the nano-PLD ZnO spectrum

[9] $E_{B_D} = (E_{DBX} - E_{TES})4/3$

are almost certainly I_9 and FX_A. The nano-structured PL data also displays a band in the ionised DBX region and may contain contributions from such. It has been noted in figure 4.vii as due to the surface exciton (SX). This particular emission, whose presence has been attributed to a high surface-to-volume ratio of ZnO, is the subject of an in-depth discussion in section 4.5.2. It can be concluded that the nano-structured ZnO displayed optical quality superior to thin films because of better defined defects as evidenced by sharper emission lines and presence of FX and excited-state bound exciton (DBX^*) emission.

4.5.2 – TES / LO Region of PLD Thin Film vs. PLD Vertical Nano-Systems

The thin film PL data displays a broad band, centred around 3.31 eV in which likely contributions from DBX, LO and TES bands are present, but not individually defined, possibly due to concealment from the presence of a deeper broad band as shown in figure 4.iv. The only clearly defined emission in the thin film spectrum is that of SD_1. The ratio of its intensity to the dominant DBX emission is almost the same for nano-structures and thin films, suggesting the structural defect is not a surface-related one and is very easily produced in even low-volume ZnO. Similar but better-defined emissions are observed in PLD nano-structures with SD_1 of comparable intensity to the deepest DBX line. It's LO phonon replica as well as those for FX, I_6 and ionised DBX are visible. I_6 $TES_{2S,2P}$ contributions are not distinguishable, but for I_9 TES, a distinct 2S state band is observed. These spectra emphasise the difficulty in identification of particular features in PL spectrum with a broad band, which may contain many contributions from separate processes

Interesting distinctions between the PL of PLD and VPT nano-structure ZnO are revealed from the presence of DBX^* in PLD but not VPT nano-structures together with a sharper emission in the SX region in VPT than in PLD nano-structures. These emission lines indicate high optical quality of very differing types and are examined together with other characteristics below.

4.6 – Optical Characteristics of Vertical Nano-Systems

Nano-rods of some 100 nm in diameter and reasonably uniform lengths of 1 μm were prepared with VPT using VLS phase growth. These nano-rods were connected by a network if ZnO membranes creating a foam-like structure [5]. PLD nano-structures, also on a-Al_2O_3, consisted of densely packed clusters of hexagonal nano-rods with a

relatively bottom-heavy structure with heights of no more than around 100 nm and widths of some 150-250 nm [2]. The growth of the PLD structures was similar in nature to that reported in Kawakami *et al* [16] with hexagonal islands of ZnO seeding the nano-structure growth.

The VLS phase nano-structures were grown using an Au catalyst with nano-structure diameter discretely controlled by the Au droplet volume and height by growth time. PLD nano-structures were grown atop a ZnO precursor on *a*-, *c*- and *r*-plane sapphire. Luminescence studies provided spectra of nano-structured material in which several NBE features as well as evidence of FX emission are observed.

Optical data show the nano-structured ZnO compares favourably to that of bulk and in the case of VPT grown nano-structures, equally well-defined DBX emission lines were observed. The bulk ZnO spectrum PL data in figure 4.x display typical I_9, I_8 and $I_{6/6a}$ lines, together with DBX* emission, shallow I_{3a}, I_1, I_0 and peaks at the FX energies.

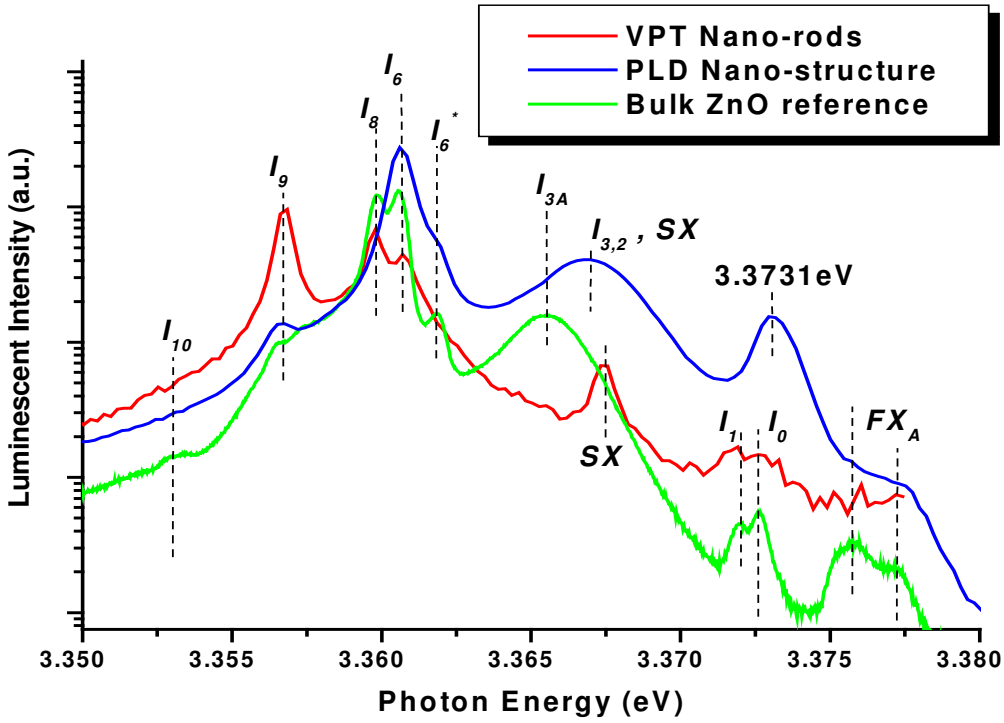

Fig. 4.x: NBE emission from VPT (red) and P LD (blue) nano-structures compared to a bulk ZnO reference spectrum (green).

The optical characteristics of nano-structured material grown by PLD have been previously examined. Many of its emission lines are present in the bulk ZnO reference

spectrum and readily identifiable, including indications of free-excitons. A curious broad band centred at 3.3731 eV with FWHM of 6.5 meV is unidentified. It resides ~0.6 meV above the I_0 DBX line but likely contains contributions from this. The principal difference in optical properties between our nano-structured material and the bulk reference sample is the presence of a peak at 3.3675 eV. It appears sharper in VPT material than PLD nano-structures with FWHM values of 3.0 meV and 7.3 meV respectively but as noted previously, the band for PLD nano-structures likely includes some ionised DBX contributions. The nature of this emission is revealed with TD studies, in which it is observed to quench at temperatures as low as 30K [3]. Evolution of integrated intensities of this emission with temperature shows it to be excitonic in nature with activation energy comparable to that of the typical DBX emission from these nano-structures of 5 - 6 meV. 3.3674(1) eV has been previously assigned to a surface exciton in Savikhin and Frieberg [31] and Trankinov *et al* [32]. Its absence in the bulk reference sample lent weight to assignment of this as a process related to large surface area ZnO [3]. Evidential deductions from the occurrence of low temperature quenching, low activation energy, presence only in nano-structured ZnO and via comparative analysis to other surface-related emission indicate that this feature is present as a consequence of films that display a very high surface-to-volume ratio.

The absence of FX emission is also indicative of non-radiative processes governing the VPT nano-structure PL. The only bound excitonic emissions shallower than SX are those understood as I_1 at 3.3717 eV and I_2 at 3.3725 eV. Though not as well defined as the SX emission peak, these do share the property of following a similar trend and quenching completely at a modest 20K.

4.7 – Conclusions

The above data displayed strong evidence that thin films grown via PLD and both PLD and VPT nano-structured ZnO were of very high quality. All samples displayed epitaxial relationships to the substrate but the microstructures and optical properties were observed to depend greatly on the substrate choice. PL data provided evidence of good homogeneity in thin films with some of comparable optical quality to nano-structures for *c*-Al_2O_3 ZnO. The substrate effect was especially acute with inclusion of a Pt-buffer layer with resulting strain due to bond-length mismatch resulting in a reduction in E_{Gap}. Analysis of ZnO properties identified a stepped growth process as one of great benefit to the material quality. A characteristic PL feature due to

surface excitons SX was identified in nano-structured materials for both PLD and VPT materials. PLD nano-structures were of sufficient optical quality to allow identification of the DBX^{*}.

4.8 – References

[1] R. O'Haire, A. Meaney, E. McGlynn, M.O. Henry, J-R. Duclere, J-P. Mosnier, *Superlatt. and Micro.* **39**, 153-161 (2006)

[2] J. Grabowska, K.K. Nanda, E. McGlynn, J-P. Msonier, M.O. Henry, A. Beaucamp, A. Meaney*, J. Mater Sci: Mater. in Elec.* **16**, 397-301 (2005)

[3] J. Grabowska, A. Meaney, K. K. Nanda, J-P. Mosnier, M. O. Henry, J.-R. Duclère, E. McGlynn, *Phys. Rev. B*, **71**, 115439 (2005)

[4] J-R. Duclère, C. McLoughlin, J. Fryar, R. O'Haire, M. Guilloux-Viry, A. Meaney, A. Perrin, E. McGlynn, M.O. Henry, J-P. Mosnier, *Thin Sol. Films*, **500**, 78-83 (2006)

[5] A. Meaney, J-R. Duclere, E. McGlynn, J-P. Mosnier, R. O'Haire, M.O. Henry, *Superlatt. and Micro.* **38**, 256-264 (2005)

[6] Ü. Özgür, Ya. I. Alivov, C. Liu, A.Teke, M.A. Reschikov, S. Doğan, V. Avrutin, S-J. Cho, H. Morkoç, *J. App. Phys.* **98**, 041301 (2005)

[7] R. Triboulet, J. Perriére, *Prog. in Crys. Growth and Char. Mater.* **47**, 2-3, 65-138 (2003)

[8] Y.C. Liu, S.K. Tung, J.H. Hsieh, *J. Crys. Growth*, **287**, 105 - 111 (2006)

[9] Y.R. Ryu, S. Zhu, D.C. Look, J.M. Wrobel, H.M. Jeong, H.W. White, *J. Crys. Growth*, **216** 330–334 (2000)

[10] C.J. Pan, C.W. Tu, J.J. Song, G. Cantwell, C.C. Lee, B.J. Poong, G.C. Chi, *J. Crys. Growth*, **282**, 112-116 (2005)

[11] M.J. Henseler, W.C.T. Lee, P. Miller, S.M. Durbin, R.J. Reeves, *J. Crys. Growth*, **287**, 48-53 (2006)

[12] A.Y. Polyakov, N.B. Smirnov, A.I. Belogorokhov, A.V. Govorkov, E.A. Kozhukhova, A.V. Osinsky, J.Q. Xie, B. Hertog, S.J. Pearton, *J. Vac. Sci and Tech. B.* **25**, 6, 1794-1798 (2007)

[13] C. Sui, N. Chen, X. Xu, G. Wie, P. Cai, H. Zhou, *Thin Sol. Films*, **516**, 1138-1141 (2008)

[14] S. Gangil, A. Nakamura, Y. Ichikawa, K. Yamamoto, J. Ishihara, T. Aoki, J. Temmyo, *J. Crys. Growth*, **298**, 486-490 (2007)

[15] S. Liang, C.R. Gorla, N. Emmanetoghi, Y. Liu, W.F. Mayo, Y. Lu, *J. Electron. Mater*. **27**, L72 (1998)

[16] J.B. Baxter, E.S. Aydil, *J. Crys. Growth,* **274** 407 (2005)

[16] M. Kawakami, A. B. Hartanto, Y. Nakata, T. Okada, *J. J. App. Phys.* **42**, 1A/B, L 33–L35 (2003)

[17] C. Munuera, J. Zúñiga-Pérez, J.F. Rommeluerec, V. Salletc, R. Tribouletc, F. Soriaa, V. Muñoz-Sanjosé, C. Ocal, *J. Crys. Growth.* **264**, 70-78 (2004)

[18] M. Yoshimoto, T. Maeda, T. Ohnishi, H. Koinuma, O. Ishiyama M. Shinohara, M. Kubo, R. Miura, A. Miyamoto, *Appl. Phys. Lett.* **67,** 18 (1995)

[19] D. M. Hofmann, A. Hofstaetter, F. Leiter, H. Zhou, F. Henecker, B. K. Meyer, S. B. Orlinskii, J. Schmidt, P. G. Baranov, *Phys. Rev. Lett.* **88**, 4 (2002)

[20] M.D. McCluskey, S.J. Jokela, W.M. H. Oo, *Physica B*, **376–377**, 690–693 (2006)

[21] B.K. Meyer, H. Alves, D.M. Hofmann, W. Kriegseis, D. Forster, F. Bertram, J. Christen, A. Hoffmann, M. Strassburg, M. Dworzak, U. Haboeck, A.V. Rodina, *Phys. Stat. Sol. (b),* **241**, 2, 231-260 (2004)

[22] Y.P. Varshni, *Physica A*, **34**, 1, 149 (1967)

[23] D.C. Look, R.L. Jones, J.R. Sizelove, N.Y. Garces, N.C. Giles, L.E. Halliburton, *Phys. Stat. Sol. (a)*, **195**, 1, 171-177 (2003)

[24] A. Dadgar, N. Oleynik, J. Blasing, S. Deiter, D. Forster, F. Bertram, A. Diez, M. Seip, A. Greiling, J. Christen, A. Krost, *J. Crys. Growth*, **272**, 800 – 804 (2004)

[25] S.B. Zhang, S-H. Wei, A. Zunger, *Phys. Rev. B.* **63**, 075205 (2001)

[26] D.F. Blossey, *Phys. Rev. B*, **3**, 1382 (1971)

[27] J. Albertson, S.C. Abrahams, A. Kvick, *Acta Cryst.* **B45**, 34-40 (1989)

[28] S.R. Calvo, P.B. Balbuena, *Sur. Sci.* **601**, 4786-4792 (2007)

[29] D.G. Zhao, S.J. Yu, M.H. Xie, S.Y.Tong, H. Yang, *App. Phys. Lett.* **83**, 4 (2003)

[30] J. Gutowski, N. Presser, I. Broser, *Phys. Rev. B* **38**, 9746 (1988)

[31] V. V. Travnikov, A. Freiberg, S. F. Savikhin, *J. Lumin.* **47**, 107 (1990)

[32] S. F. Savikhin, A. Freiberg, *J. Lumin.* **55**, 1 (1993)

Chapter 5: Doped ZnO Thin Films

Preface

This chapter takes the form of a set of papers as originally published followed by a brief summary of and commentary on their main findings. In some cases, the conclusions at the time of publishing have been amended on consideration of subsequent work. The citation details for these are listed below together with the respective digital object identifier (DOI) links. The author's personal contributions to each of the papers are also listed.

Papers, Contributions and DOI Numbers

[1] S. Chakrabarti, B. Doggett, R. O'Haire, E. McGlynn, M.O. Henry, A. Meaney, J-P. Mosnier, *Superlat. and Micro.* **42**, 21-25 (2007)

"Characterization of nitrogen-doped ZnO thin films grown by plasma-assisted pulsed laser deposition on sapphire substrates" with contributions including:

- Aspects of PL laboratory including:
    - Data acquisition
    - Laboratory equipment operation and maintenance
    - Spectral calibration
    - Processing and presentation of data
- Discussion and analysis of data, especially with respect to identification of acceptor-related optical features and of common trends between optical and structural / electrical data
- Feedback to growth team for fine-tuning of growth parameters based on optical data, in order to improve material properties, specifically with respect to the presence of acceptor species

http://dx.doi.org/10.1016/j.spmi.2007.06.003

[2] S. Chakrabarti, B. Doggett, R. O'Haire, E. McGlynn, M.O. Henry, A. Meaney, J-P. Mosnier, *Elec. Lett.* **42**, 20 (2006)

"*p*-type conduction above room temperature in nitrogen-doped ZnO thin film grown by plasma-assisted pulsed laser deposition" with contributions including

- Aspects of PL laboratory including:
    - Data acquisition
    - Laboratory equipment operation and maintenance

    - Spectral calibration
    - Processing and presentation of data
- Discussion and analysis of data, especially with respect to identification of acceptor-related optical features and of common trends between optical and structural / electrical data.
- Feedback to growth team for fine-tuning of growth parameters based on optical data, in order to improve material properties, specifically with respect to the presence of acceptor species and photoconductive affect

http://dx.doi.org/10.1049/el:20062161

[3] J-R. Duclère, R.O'Haire, A. Meaney, K. Johnston, I. Reid, G. Tobin, J-P. Mosnier, M. Guilloux-Viry, E. McGlynn, M.O. Henry, *J. Mater Sci: Mater. In Elec.* **16**, 421-427 (2005)
"Fabrication of p-type doped ZnO thin films using pulsed laser deposition" with contributions including:

- Aspects of PL laboratory including:
    - RT Data acquisition
    - Laboratory equipment operation and maintenance
    - Spectral calibration
    - Processing and presentation of data
- Discussion and analysis of data, especially with respect to identification of acceptor-related optical features and of common trends between optical and structural / electrical data
- Feedback to growth team for fine-tuning of growth parameters based on optical data, in order to improve material properties, specifically with respect to dopant choice

http://dx.doi.org/10.1007/s10854-005-2308-2

[4] J-R. Duclère, M. Novotny, A. Meaney, R. O'Haire, E. McGlynna, M.O. Henry, J-P. Mosnier, *Superlat. and Micro.* **38**, 397-405 (2005)
"Properties of Li-, P- and N-doped ZnO thin films prepared by pulsed laser deposition" with contributions including:

- Aspects of PL laboratory including:
    - Data acquisition

    - Laboratory equipment operation and maintenance
    - Spectral calibration
    - Processing and presentation of data
- Discussion and analysis of data, especially with respect to identification of acceptor-related optical features and of common trends between optical and structural / electrical data
- Feedback to growth team for fine-tuning of growth parameters based on optical data, in order to improve material properties, specifically with respect to dopant choice

http://dx.doi.org/10.1016/j.spmi.2005.08.011

[5] B. Doggett, S. Chakrabarti, R. O'Haire, A. Meaney, E. McGlynn, M.O. Henry, J-P. Mosnier, *Superlat. and Micro.* **42**, 74-78 (2007)
"Electrical characterisation of phosphorus-doped ZnO thin films grown by pulsed laser deposition" with contributions including

- Discussion and analysis of data, especially with respect to identification of acceptor-related features and of common trends between data from differt measurement techniques

http://dx.dio.org/10.1016/j.spmi.2007.04.028

5.1 – Commentary on Publications in this Chapter

Evidence is obtained of good quality ZnO thin films with epitaxial relationships to the substrates. The crystalline quality was found to deteriorate with high doping, but lower dopant concentrations were found beneficial for maintaining crystalline quality and improving optical and electrical characteristics. Phosphorous or nitrogen doping resulted in acceptor-related characteristics. For instance, the p-type behaviour, although short lived upon exposure of the material to UV radiation, was identified in ZnO with a 0.01 wt% P_2O_5 dopant. P-type photoconductive effects were also observed in N-ZnO films. ABX emission lines were present in films even with high concentrations of dopant. Li and Bi were also employed as dopant sources but neither produced evidence of a p-type film and were not considered in details in this dissertation.

5.2 – Dopant Sources

PLD films were grown using a variety of dopants in an attempt to create p-type ZnO. Films were doped with Bi, N, P and Li of various concentrations and grown on various substrate orientations to identify favourable growth conditions. Films were prepared either using the sequential growth technique as described in 3.2 to layer nominally undoped ZnO with material from dopant target ablation, or with N ions supplied from an ECR source. T_{Grow} varied from one series to another, ranging from 500K for P-doped films to 1000K for N-doped samples with even higher temperatures for *in-situ* post-growth annealing. The remaining case used $LiNbO_3$ substrates to achieve Li-doping by means of diffusion. Film properties were examined using XRD, PL and Hall Measurement with data compared to that of control samples.

5.3 – Crystalline Quality

The degree of crystalline quality in doped films was affected by a combination of factors, including but not limited to: substrate plane orientation, dopant, film thickness and annealing treatment. Considering first the substrate, the typical choice for Bi-, P- and N-doped films was (0001)-Al_2O_3 with (11-20)-Al_2O_3 and (1-102)-Al_2O_3 used for some N-doped films. The ω_{FWHM} for films grown on (0001)-Al_2O_3 were found within the limits of 0.30 ° to 0.60 ° for undoped and moderately doped films [1] which indicated a good reproducibility in crystalline quality from sample to sample. Although this is a doubling of ω_{FWHM} , the low absolute value of 0.60 ° is indicative of a good retention in crystalline quality at lower dopant concentrations. Increasing the amount of dopant was found to reduce the crystalline quality for films grown on similar substrates. Values for ω_{FWHM} broadened to as high as 3.0 ° in the case of a film with 2.6 wt% dopant from an InP target. The evolution in ω_{FWHM} with increasing P_2O_5 content is shown in figure 5.i below. The data indicate a lower dopant concentration is preferred in maintaining film quality. Rocking curves broadened universally. The increase in ω_{FWHM} was smallest for low dopant concentration. N-doping caused a similar increase in ω_{FWHM} to over double that of the same reflection from an undoped film. This is illustrated clearly in figure 5.ii with ω_{FWHM} plotted as a function of ion beam density.

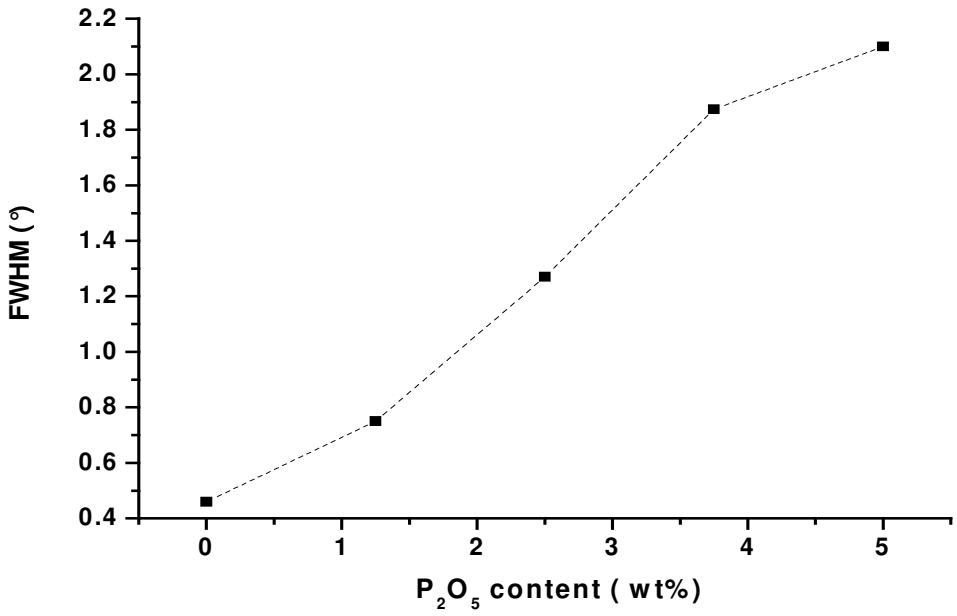

Fig. 5.i: ω_{FWHM} of primary ZnO reflection for P-doped samples with increasing wt% dopant.

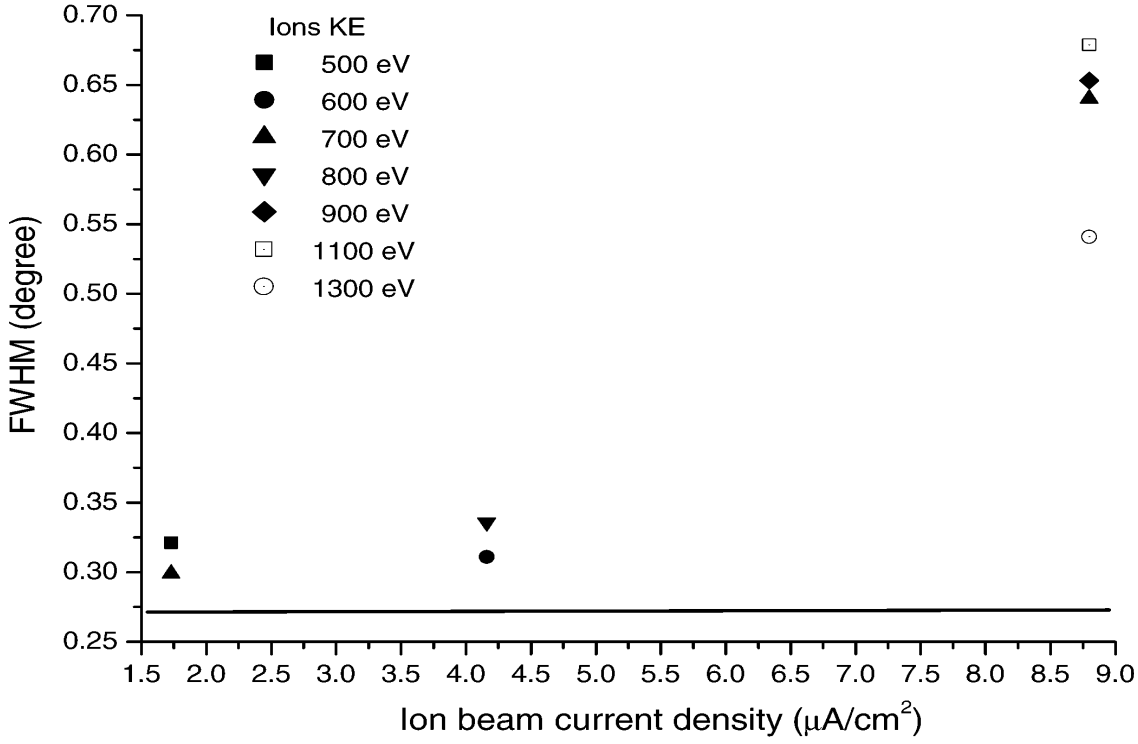

Fig. 5.ii: ω_{FWHM} as a function of ion beam density for N-doped films. Line shows ω_{FWHM} for undoped film.

N-doped films demonstrated a doubling of ω_{FWHM} when film thickness increased from 550 nm to 800 nm [2]. As this trend was not detected in undoped films, where

ω_{FWHM} fluctuated as films thickness was increased from 350 nm to 800 nm with a minimum film thickness of ~540 nm with a 13nm buffer layer [1], the data appear to have indicated that an ideal thickness for a given dopant concentration exists to minimize the increase in ω_{FWHM} . The thickness of individual films was not examined beyond this observation.

Considering the relationship of annealing treatment to crystalline quality, XRD θ - 2θ scans universally display intense substrate reflections for the thin films, up to 100 times the intensity of the primary ZnO reflection [1]. These substrate reflections were present throughout the doped ZnO data, including those which underwent a post-growth *ex-situ* annealing treatment, a step reported as aiding in intensity reduction of substrate reflections [6]. This showed the correct annealing parameters were elusive.

Treatments were varied to examine which conditions increased the crystalline quality. The annealing conditions were chosen generally, such that they were carried out at or just above T_{Grow}. The other annealing conditions for a specific sample were chosen to best aid improvement of its crystalline quality encourage diffusion and migration of non-native complexes and reduce the influence of substrate on defect formation.

There are further variables in a thermal treatment that affect sample's crystalline quality beyond ambient, temperature and time. In section 3.2, the advantage of a ramped temperature scheme during growth was discussed. The disadvantage of omitting such steps was again evidenced when XRD data for P-doped films with InP as a dopant source were examined. InP-doped films of various wt% dopant on a *c*-Al_2O_3 and annealed *in-situ* for 15 minutes at T_{Grow} in 50 kPa O_2 resulted in a non-uniform treatment throughout the film. Surfaces underwent a very different treatment to the central volume of the film. Figure 5.iii below depicts the layered planes of ZnO and ZnO / InP with a central region highlighted, partially shielded from annealing treatments.

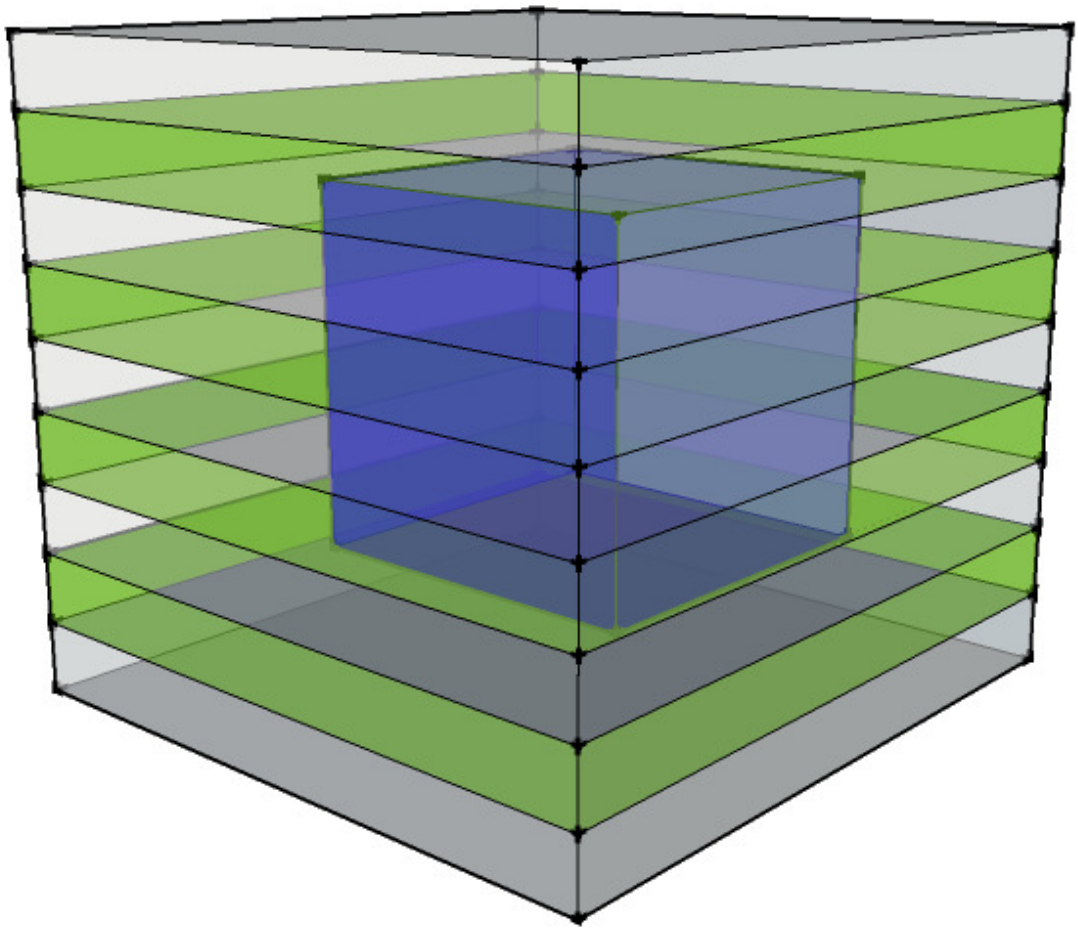

Fig. 5.iii: Schematic of ZnO / ZnO : InP layers illustrating non-uniform thermal treatment during anneal process – central blue cubic outline not undergoing same treatment as surfaces.

Layering the film and performing a post-growth anneal with an associated shielding effect contributed greatly to the observed five-fold increase in ω_{FWHM} for the primary ZnO reflection at 2.6 wt% InP, increasing from 0.6 ° to 3.0 °. Reflections from very different materials were a result of the layering coupled with low diffusion as evidenced from SIMS measurement recorded from a commercial Quadrupole SIMS apparatus. [3].

What was apparent from these data overall is the marked proportional increase in ω_{FWHM} values. Although annealing treatment parameters and choice affect ω_{FWHM} values, the above data appeared primarily influenced by dopant concentration. Highly-doped films grew with the micro-structure tending toward no longer mimicking substrate morphology, ω_{FWHM} increasing and the film becoming less crystalline overall. This was evidenced further by XRD data for films doped with Bi- [3] and N- [2] doped ZnO with ω_{FWHM} values increasing to 0.78 ° and 1.24 ° respectively. Even though this evidence pointed to a reduction in crystalline quality with dopant addition, it also

suggested lower dopant concentrations resulted in lowest reduction of crystalline quality.

5.4 – Electrical Characteristics of InP-Doped Thin Films

P_2O_5 and InP were used as phosphorous sources for films grown on both *a*- and *c*- plane sapphire. Evidence of acceptor incorporation in P-doped films was achieved to varying levels of success. The undoped films were grown under 10 Pa O_2 at 800K on *a*-Al_2O_3 and annealed *in-situ* 30 minutes at T_{Grow} in an oxygen-rich 50 kPa ambient. They demonstrated an overall n-type conducting with a carrier concentration of $-9.4x10^{15}\,cm^{-3}$ but a reasonably high resistivity of 460Ωcm and mobility of 1.5 $cm^2V^{-1}s^{-1}$ with Hall measurement considered with respect to a nominally undoped control.

The data indicate doping from an InP source did not result in overall p-type conduction. Indeed, the carrier concentration was observed to increase from $-1.4\,x10^{18}$ cm^{-3} to $-1.7x10^{18}$ cm^{-3} over the range 100 K to 300 K. Mobility values were comparable in magnitude to undoped films but showed an overall reduction from low to high temperatures. Increasing from 77 K to 150 K in this material resulted in a reduction in carrier concentration and increase in mobility although only very slight changes observed in each case, as shown in figure 5.iv below.

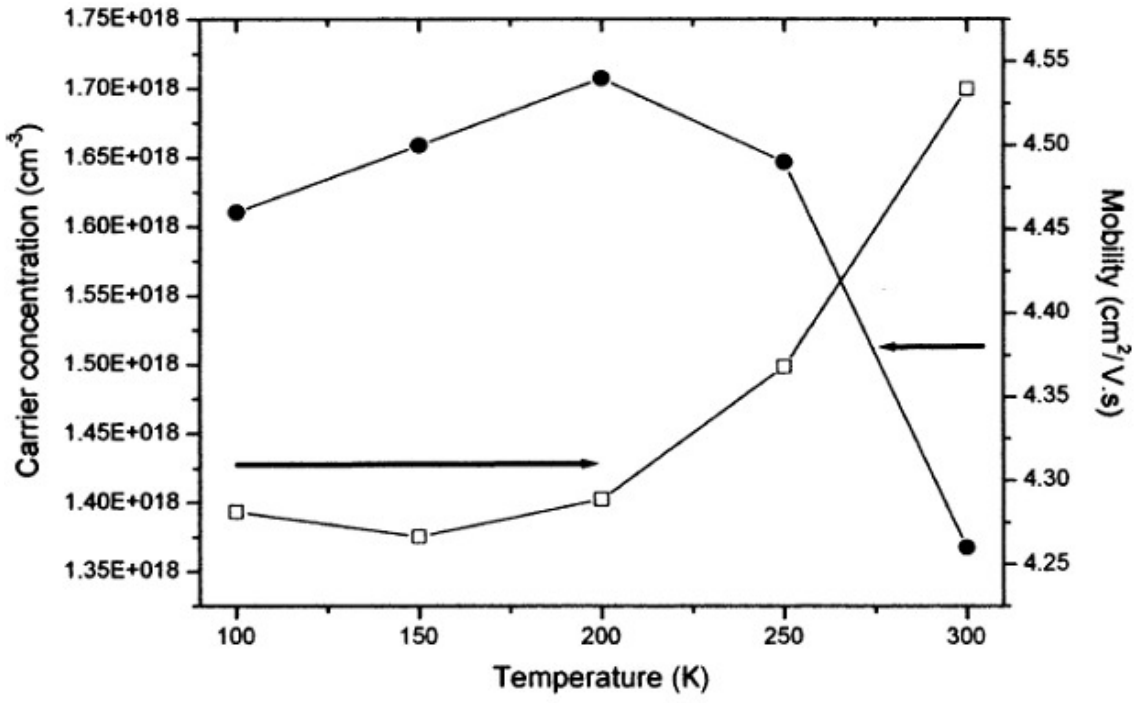

Fig. 5.iv: TD mobility and carrier concentration for InP-doped ZnO thin films prepared via PLD.

As a consequence of low sublimation temperatures for P and related oxides and n-type conduction increase, it can be concluded that In was more plentiful than P with any successful P-related acceptors likely compensated by In_i and / or In_{Zn} centres.

An interesting observation was made at the temperature where carrier concentration begins to increase, tending toward demonstrating greater n-type conduction. At 150 K, P-doped ZnO has been reported to change its overall conductivity from p- to n-type [8]. This effect was been attributed to surface band-bending, whereby electrons produced from UV-illumination, become trapped locally at the surface while holes remain the dominant carriers in the bulk [9]. Moreover, a similar model was considered with respect to persistent photoconductivity observed in some ZnO with a lower P_2O_5 concentration.

5.5 – Electrical Characteristics of P_2O_5 Doped Thin Films

Films with 1.25 – 3.75 wt% of dopant [3] displayed inconsistent conductivity data with both p- and n-type measured for the same film. Mobility within the range of 0.8-4.5 $cm^2 V^{-1} s^{-1}$ and resistivity between 26 - 406 Ωcm were broadly agreeable with the values for nominally undoped samples, offering little information as to how P_2O_5 affected the film. The 5.0 wt% P_2O_5 film presented a consistent conductivity type and a departure in electrical characteristics from nominally undoped ZnO. It was prepared under different conditions to films with a lower dopant concentration at a low 540 K in 2.66 Pa of oxygen and annealed *in-situ* for 60 minutes in $1.33x10^5$ Pa of the same ambient.

This film displayed carrier density of $-1.1x10^{20}$ cm^{-3}, an increase of almost 12000 times that of the control. Mobility doubled to 3.5 $cm^2 V^{-1} s^{-1}$, while resistivity reduces in this 5 wt% dopant film by some 40000 to $1.2x10^{-2}$ Ωcm [3]. These marked changes in electrical properties together with the 5-fold increase in ω_{FWHM} indicated that doping to levels of the order of a number of wt% was much too large to beneficially adjust film properties. This was a primary consideration in the decision to fabricate a 2nd series of P-doped ZnO films. The high phosphorous content alone cannot be considered entirely responsible for these changes, as nominally undoped ZnO was also found to display different mobility and resistivity values depending on the substrate plane. The nominally undoped *a*-Al_2O_3 films showed a propensity for higher resistivity and lower mobility than those on *c*-Al_2O_3. Films on *a*-Al_2O_3 with 5 wt% P_2O_5 demonstrated

similar mobility to the undoped film, but with resistivity closer to that of undoped *c*-Al_2O_3 indicating the inclusion of P-dopant was primarily responsible for influencing film resistivity.

Lower concentrations of P_2O_5 proved far more successful with regard to evidence of p-type behaviour. Mobility values were greatly reduced in comparison to the control with a corresponding increase in resistivity. The magnitude of change in these characteristics was again found to be very dependant on measurement conditions. Specifically, an N- based measurement ambient promoted the tendency to p-type behaviour with introduction of an exceptionally high 1800 Ωcm resistivity [5], an observation consistent with electrical data from films of higher dopant content. Most interesting was the observation of an inversion in conductivity type upon exposure to an incandescent light source, again with minimum carrier concentration of recorded at 150 K of $6*10^{16} cm^{-3}$, as in the InP-doped films. The p-type behaviour was reversible however, with films displaying n-type conductivity after a few minutes.

Recent models have attributed the origins of persistent photoconductivity to the effect of chemisorbed oxygen on the surface acting as an e^- trap, depleting the film of negative carrier. Under illumination, the photo-excited holes allow the trapped e^- increase the conductivity [10]. A similar phenomenon has been reported to affect the characteristics of ZnO in aqueous solution under UV illumination [11].

The p-type photo-induced conductivity here was measured in an N-ambient which may provide a layer analogous to the O layer but increasing resistivity and hole concentration with illumination. Whatever mechanism causes the p-type conductivity, it is a short lived one with all films which displayed this property reverting back to n-type ZnO after a matter of minutes, suggesting a very dissimilar process involved to the persistent n-type photoconductivity, decaying over a matter of days [8].

5.6 – Optical Characteristics of 1.25 -5.0 wt% P_2O_5 Doped Thin Films

The *a*-Al_2O_3 plane was employed for films containing 1.25 – 5.0 wt% P_2O_5, maintained at a constant temperature of 790 K in a 10 Pa O_2 ambient. Films of a nominal 500nm thickness were produced, comprising of a substrate and a number of sequential layers of ZnO / ZnO : P_2O_5 depending on desired dopant content and finally a ZnO capping layer. *In-situ* annealing was performed post growth in 50 kPa oxygen at 800K for 30 minutes. The 5 wt% P_2O_5 film was subject to different annealing and

growth conditions, prepared at a lower 540 K in 20 mPa O_2 with *in-situ* annealing treatment in relatively oxygen-starved ambient of 10 Pa over 60 minutes. The affect of P addition and the films characteristic changes produced together with indication as to their origins clearer with examination of PL evolution with increasing P-content. This data is shown in figure 5.v with spectra recorded at 10 K.

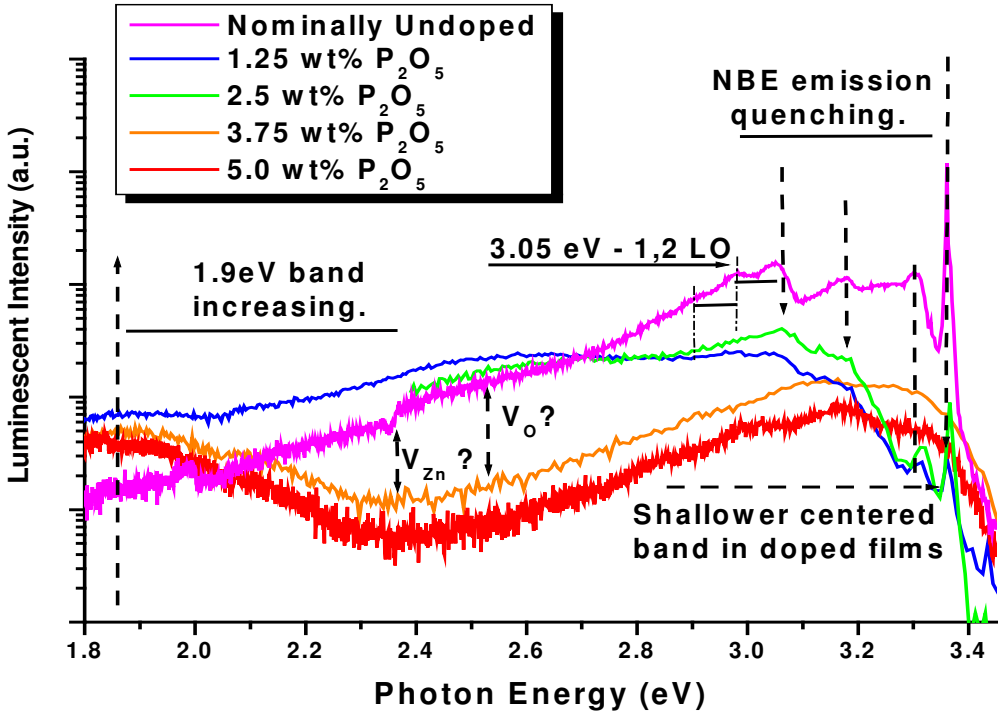

Fig. 5.v: PL spectra for P-doped ZnO thin films compared to that of control sample.

A striking difference in spectra was observed from undoped to doped material with further PL deterioration with increasing P_2O_5 content. There is completely quenching of features at shallow energies in films with greater than 2.50 wt% P_2O_5 with lower dopant concentrations preserving some of DBX emission. An as yet unidentified feature at 3.05 eV demonstrates LO replica for the nominally undoped film. Persistence of this emission but the absence of replica in spectra from doped ZnO suggests replicas are weakly coupled to the zero-phonon line (zpl). Emission in the TES region is the subject of later discussion in this section.

P-doping has been reported to quench the bound exciton lines together with deep emission centred at around 1.9 eV [12]. At this energy in figure 5.v, the emission exhibits a reasonably regular 5-fold increase across the various dopant concentrations. Annealing under very similar conditions to those employed here was shown to promote this deeper emission, with high temperature treatment oxygen ambient introducing a

deep acceptor level consistent with a low electron carrier concentration resulting in fewer occupied deep centres [13]. A higher carrier concentration as listed in 5.3.2 is consistent with the relatively lower increase in 1.9 eV intensities here, across all dopant concentrations. The distinct spectral intensity increases of doped compared to undoped ZnO however, indicate some success with P-incorporation if these deeper states are indeed P donor-related.

There is a persistence of typical green emission at ~2.5 eV up to 2.50 wt% P_2O_5 whose origin remains controversial [14-16]. Børseth [17] argued that a number of processes contribute to this band with annealing treatments in Zn and O rich environments leading to identification of V_{Zn} and V_O as primary contributors at 2.35 eV and 2.53 eV respectively. Hoffmann *et al* supported assignment of the band around 2.45 eV to V_O, identifying a donor level lying 530 meV below the CB [18]. Others have shown evidence for the deep band emission (DBE) having its origins in the Cu_{Zn} acceptor, though the band typically displays fine-structure in this case [19].

The broad nature of DBE in figure 5.v does not permit identification of two or more individual contributions. The band overall[10] displays an increasing intensity with respect to the spectrum of nominally undoped ZnO. Dissociated oxygen species from dopant together with the oxygen-rich preparation and annealing ambient suggest oxygen deficiency is extremely unlikely. If other classifications of these bands in the literature are considered correct then V_{Zn} may be considered the majority contribution. The small but distinct increase in intensity across the entire band indicates that some contribution in the V_O region be present and increasing. This offers some information about the growth and annealing processes, suggesting that the 10 Pa growth pressure was too low and / or the annealing treatment was not especially successful in passivating this native defect, even considering the annealing gas pressure of 50 kPa. This further substantiates the benefit of applying multi-stage annealing treatments during growth.

At 3.75 wt% P_2O_5 there is a sudden quenching of the DBE. A P_{Zn} centre or related complex can explain this decrease with higher dopant content. The V_{Zn} defect is occupied by the abundant P since P_{Zn} exhibits far lower formation energy than either native vacancy. This model is supported by the occurrence of a higher carrier

[10] V_{Zn} band energies were not recorded for the 2.5 wt% P_2O_5 film but all other features follow similar trend to those of 1.25 wt% P_2O_5 film.

concentration since P_{Zn} acts as a triple donor. A focus on NBE emission is shown in figure 5.vi below, the data recorded at 10 K.

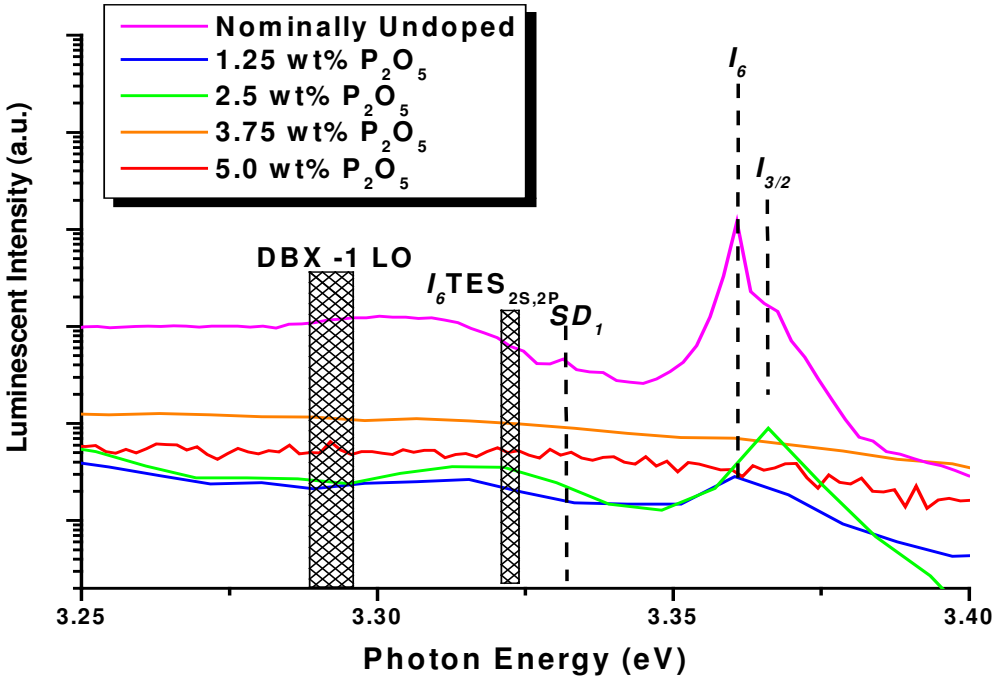

Fig. 5.vi: PL for thin films in NBE region for control sample and various wt% dopant.

The spectra show substantial reduction in optical quality at greater than 2.50 wt% P_2O_5, a trend consistent with the relative growth of deeper emission bands. No distinctive ZnO DBX emission is visible at 3.75 or 5.0 wt% P_2O_5; the absence of both TES and DBX-LO emission in spectra from doped film corroborates this. The Al-related I_6 DBX line persists in moderately-doped films with a suggestion of ionised DBX emission remaining in PL from the 1.25 wt% P_2O_5 film. The apparent shift of the primary DBX line for data from the 2.50 wt% P_2O_5 film and the intensity increase in emission for the 1.25 wt % P_2O_5 sample are attributed to changes in data acquisition parameters. It should be noted though that with P-addition increased P-diffusion, DBX lines have been observed to blue-shift [13, 20].

The distinctive SD_1 feature is not identifiable in any spectrum of doped ZnO shown above; a band at around 3.3 eV – 3.33 eV emerges. SD_1 is removed with introduction of dopant, suggesting the native structural defect is a centre at which phosphorous or a related complex resides. Energy of ~3.3 eV is too shallow to be categorised as a BX LO replica but falls within the typical $I_{8/9}TES_{2S}$ energy region but

no I_9 or I_9 emission is visible. The I_6 TES at 3.322 eV also needs consideration as a possible classification for this band. Curve-fitting from fig. 5.vi produces a centre at 3.317 eV with only a 0.3% deviation from r^2. TES contributions may play some part in this emission band, but from the evidence above, another classification for the primary contribution must be considered with the P-based complexes the most probable candidate.

A quenching of V_{Zn} centres at high wt% P_2O_5 due to formation of P_{Zn} is suggested. At lower dopant concentration formation of P_{Zn}-2 V_{Zn} is more probable. As E_f increases in O-rich films, the formation energy for V_{Zn}, and with it that of the P_{Zn}-2 V_{Zn} shallow acceptor, reduces [7]. Recent data in Yao *et al* [21] also shows E_B for $P_{2p1/3}$ as very close to that for P-O-Zn bonds in zinc phosphate glasses suggesting that the P_{Zn}- 2 V_{Zn} acceptor forms preferentially when ZnO : P is prepared in O-rich conditions. If this acceptor is indeed introduced into the ZnO films here resulting in a PL band from 3.3 eV – 3.33 eV, the defect E_B may be calculated as between 110 and 150 meV.

Others have classified this band as the DAP / e^-A transition over a temperature range for P-doped ZnO PL [22,23] with E_B in the range of 150 meV – 200 meV. This would indicate a different acceptor process involved. This observation is supported when the dominant BX feature is considered, with an ABX identified in [22,23] whereas an Al-based DBX appears in fig.5.vi. The origin of this band is considered further in samples with a lower wt% of dopant.

5.6.1 – Post-Anneal Optical Characteristics of P_2O_5 Doped Thin Films

Figure 5.vii shows PL spectra of 1.25 – 5.0 wt% P_2O_5 films that have undergone a post-growth *ex-situ* anneal. The additional anneals were performed to allow characterisation of films with respect to changes brought about from this process. An *ex-situ* anneal in 50.6 kP O_2 over 90 minutes at 890 K was performed for all but the 3.75 wt% P_2O_5 film, which was treated at 100 K higher. It is noteworthy that 800K is a comparable temperature to that reported as required for thermal activation of the P-dopant [24].The data are again shown compared to that of the nominally undoped ZnO. The spectra follow a reasonably similar trend to those of pre-anneal samples with a quenching of DBX emission together with a slight tendency for increased intensity in

the deep 1.9 eV centred band. The changes in optical character are not all linearly dependant on P-content. ZnO with 3.75 wt% P_2O_5 for instance, shows a persistence of the ~2.35 eV band as in the control, re-emerging for this wt % but quenching again as P-content is increased to 5.0 wt%. The only parameter changed for this treatment was the annealing temperature.

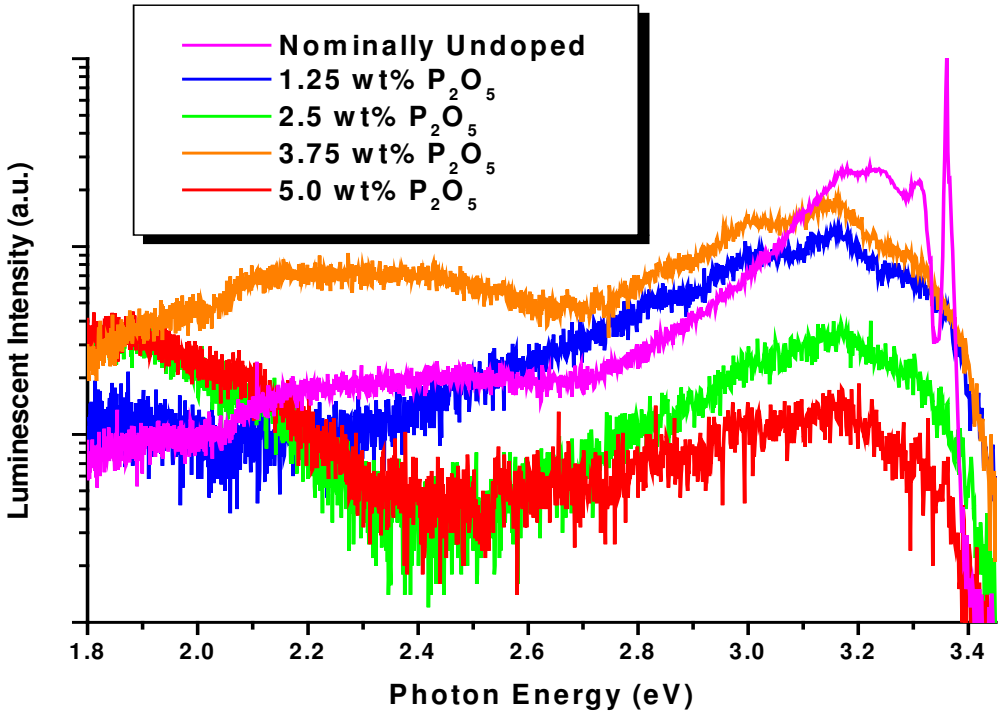

Fig. 5.vii: PL of 1.25 to 5 wt% P_2O_5 sample post ex-situ annealing with reference to a nominally undoped control.

It is apparent from this that a higher temperature annealing treatment promotes the V_{Zn} defects; as wt% P_2O_5 is increased, the DBE re-emerges with an intensity maximum distinctly deeper than the energy for the reported V_O band. The 3.32 eV – 3.33 eV emission previously assigned as due to P_{Zn} - 2 V_{Zn} complexes does not re-emerge, suggesting the conditions of annealing / high wt% of dopant do not lend themselves to preferential formation of the P_{Zn} anti-site.

Considering the re-emerging DBE energy range of 2.10 eV to 2.60 eV and plotting the integrated area with respect to wt% of dopant, an approximate linear dependence is initially apparent for all except the anomalous 3.75 wt% P_2O_5 spectrum as shown in figure 5.viii. Curve-fitting produces a relatively low r^2 value of 0.82

however, showing this relationship to be unlikely but the four-fold increase in integrated intensity of the DBE for 3.75 wt% P_2O_5 spectrum is certain.

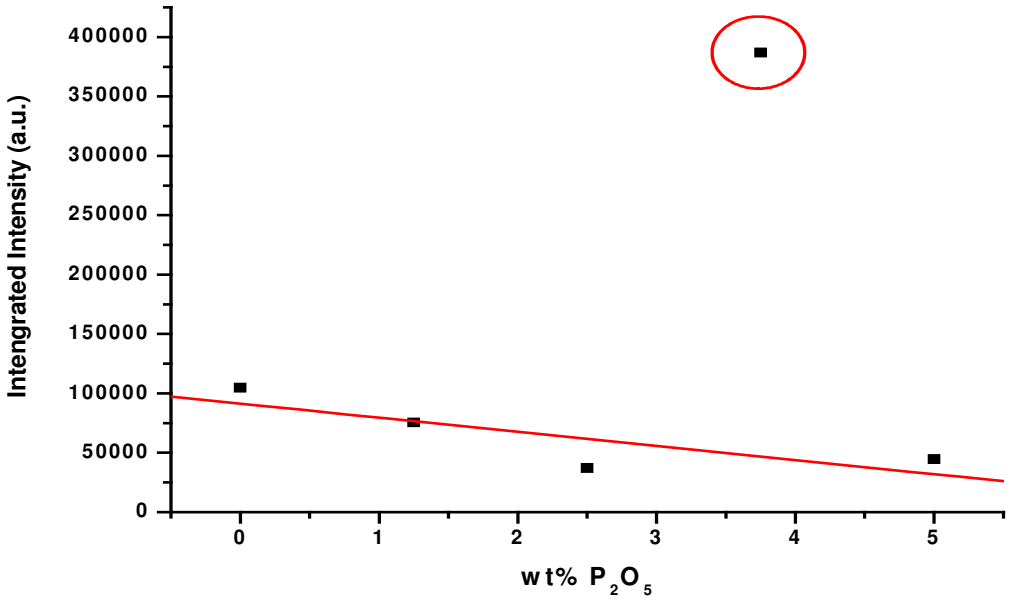

Fig. 5.viii: Integrated intensity of DBE band for P_2O_5 doped ZnO thin films post ex-situ anneal. Anomalous increase for highest temperature anneal circled.

5.6.2 – Reduced Dopant Content

Fabricating a 2nd series of P-doped films was warranted given the low quality characteristics of those with 1-5 wt% dopant. Lower P_2O_5 concentrations were expected to improve crystalline, optical and electrical quality. The reduction in ω_{FWHM} and photo-induced p-type conductivity in low-dopant ZnO has been previously discussed[11]. A spectrum with features which were overall better-defined and more numerous was obtained from PL measurements of films with lower dopant concentration. Features were assigned with respect to nominally undoped control. Figure 5.ix below shows spectra of undoped and doped thin films with wt% dopant in the limits of $0.01 \leq P_2O_5 \leq 1.25$ wt%. The spectra photon energies were normalised to those of nominally undoped PLD films on *c*-Al_2O_3, from figure 4.vi.

[11]Refer to sections 5.2 and 5.4 respectively.

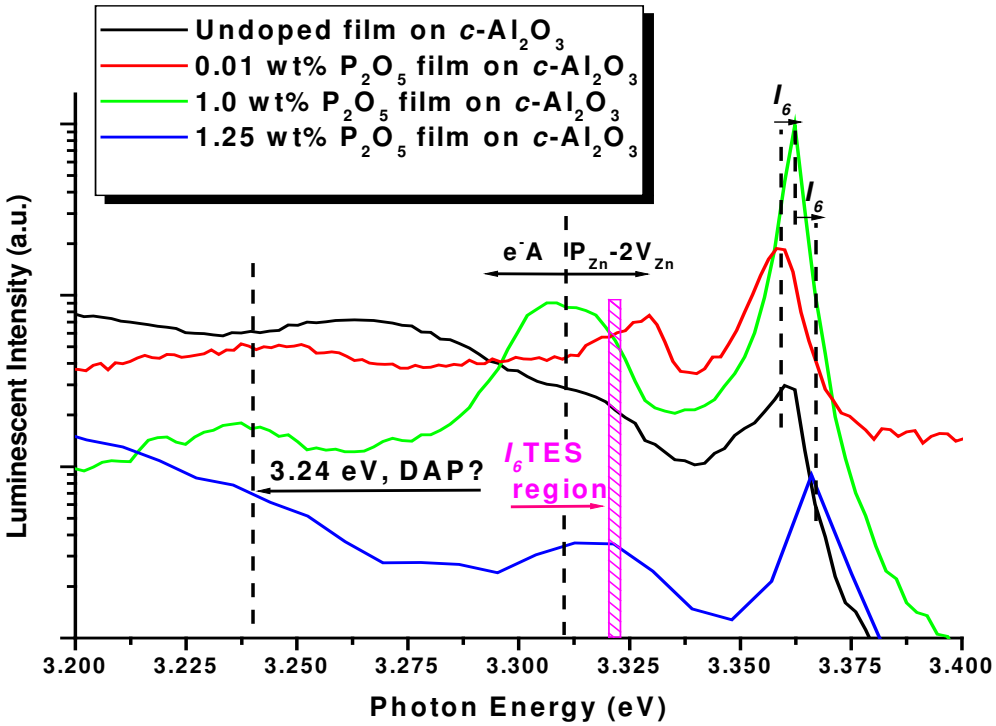

Fig. 5.ix: PL of 0.01 and 1 wt% P_2O_5 ZnO compared to that of nominally undoped thin film.

The familiar DBX emission is apparent in all spectra with substantial influence from the substrate evident due from strong I_6 emission and perhaps some evidence of I_9 In defects in undoped and 0.01 wt% P_2O_5 films. The feature(s) in the ~3.29 eV – 3.33 eV deservers some further consideration in light of a band in the typical DAP region, most clearly noticeable in the spectrum of 1.0 wt% P_2O_5 film. A range of 110 meV to 150 meV was calculated for E_{B_A} from eqn. 2.1 – $E_{e^-A} = E_{Gap}(T) - E_{B_A} + k_B T/2$.

This band in emission from the 1.0 wt% P_2O_5 film was curve-fit for two separate contributions at 3.306 eV and 3.315 eV, the latter previously assigned to a P_{Zn}-2 V_{Zn} acceptor which appears for other moderately doped films as in fig. 5.x. The former energy however, does have a good coincidence with e^-A as reported in the literature [22,23]. It appears that under the correct conditions, with ~ 1.0wt% of dopant, that acceptor levels are incorporated into the film while still maintaining high enough optical quality to allow the e^-A.

5.7 – P-type Conducting N-doped Films

Nitrogen doping was achieved in thin films with incorporation from an ECR plasma source as detailed in 3.1.1.

5.7.1– An Important Process in Growth

Growth involved a substrate grown at a low 580 K and subsequently anneal at 300 K higher [1,2] and a cooling followed, a step reported as key for production of p-type ZnO from N-doping [25]. Film thickness has been previously attributed to crystalline quality but the electrical data were not especially dissimilar for films of varying thickness. This appears to indicate the growth produced a homogenous film. The electrical data will show that ramping step was an improvement on earlier N-doping [4] attempts, with a far higher mobility acquired with it's inclusion The mechanism may be similar to the stepped temperature scheme resulting in annealing as detailed previously in 3.2.1. The N-doped materials from this growth demonstrated p-type conductivity from 220 K to RT. The p-type behaviour was found augmented by illumination, similar to that as outlined in 5.4.

5.7.2 – Electrical Characterisation

N-doped films displayed a nominal carrier concentration at RT of $5*10^{15}\,cm^{-3}$. Over a temperature range of 200 – 450 K this value remained reasonably constant. Illuminating under similar conditions as for P_2O_5 film analysis caused a slight reduction in carrier concentration, as shown in figure 5.xi below. The reduction suggests the mechanisms responsible for the conductivity changes for P- and N-doped materials were different. Indeed, the model of adsorbed oxygen acting as a hole-drain reported in Hullavarad *et al* fits the observation [26]. The TD carrier concentration for such N-films is displayed in figure 5.x with data for both measurements in dark and under illumination

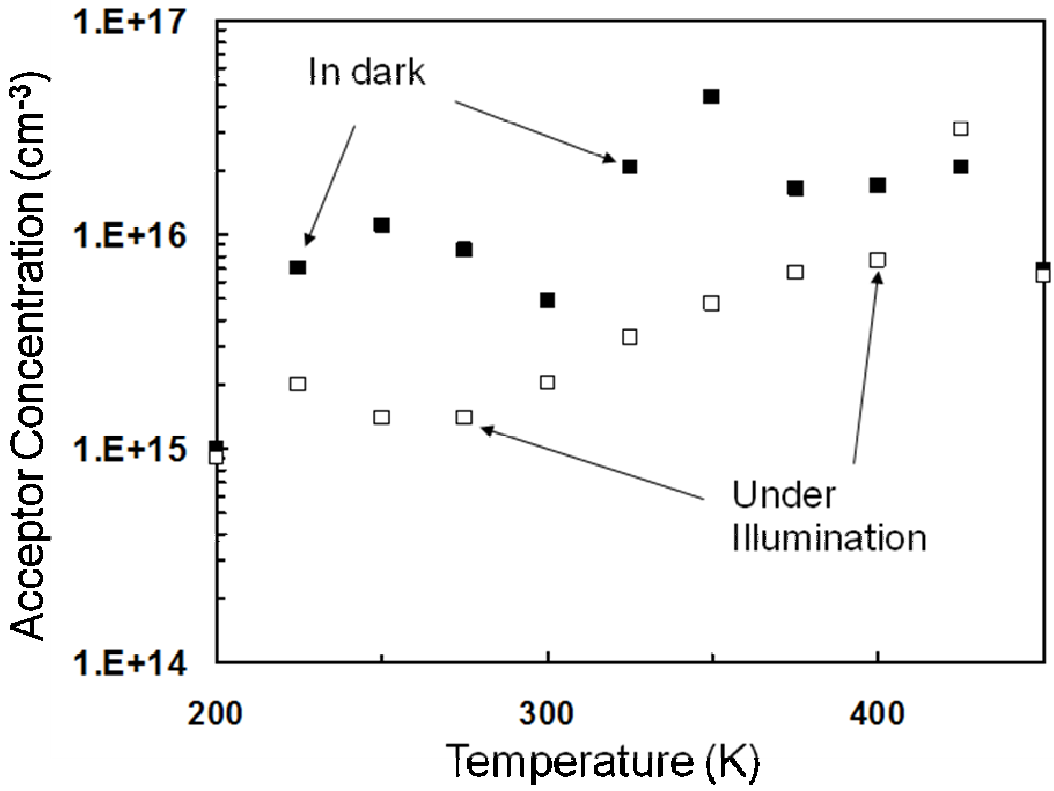

Fig. 5.x: Temperature dependant carrier concentration for N-doped thin films.

The changing electrical character of N-doped films due to illumination was again observed with mobility measurements as shown in figure 5.xii below. The increase under illumination displayed is not wholly consistent with the changes apparent in fig. 5.xi but the change is not significantly different enough to warrant further consideration. The data do indicate that the affect of illuminating the sample do alter the electrical properties, but not substantially, and not to the point of conduction type conversion.

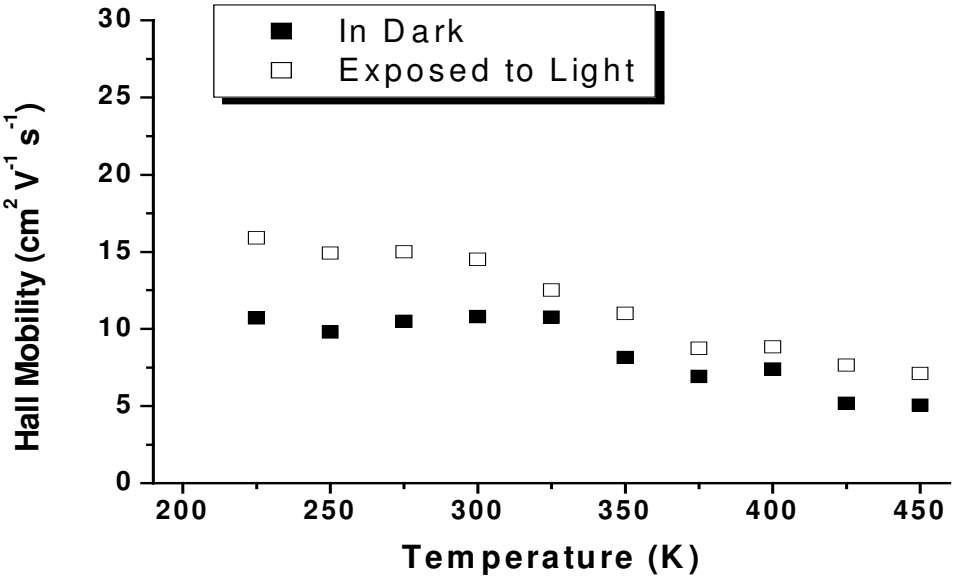

Fig. 5.xi: TD of mobility for N-doped thin films measured under illumination and in the dark.

Overall, there is clear evidence for p-type behaviour in these films. The data is substantiated by the underlying difficulties in consistent Hall Measurement as outlined in 2.4, as consistent p-type measurement was none-the-less achieved. The data also indicated that the films were quite homogeneous as evident from only moderate changes in electrical behaviour with illumination and no conductivity type inversion.

5.8 – A Return to the DAP

Fig. 2.ix showed PL TD data of N-doped films, prepared under similar conditions to those above but fabricated subsequent to the report data [1,2]. These included addition of a ZnO capping layer above the N-doped film at the end of growth. The original optical data recorded at RT displayed some slight indications of emission classified as acceptor-related. More current optical measurements resulted in bands at 3.213 eV and 3.24 eV which were considered as possibly displaying e^- / DAP behaviour respectively, over the temperature range. Fig. 5.xii below shows these data again, and is followed by a more considered classification of the features with respect to position, electrical data, and features observed in other reports.

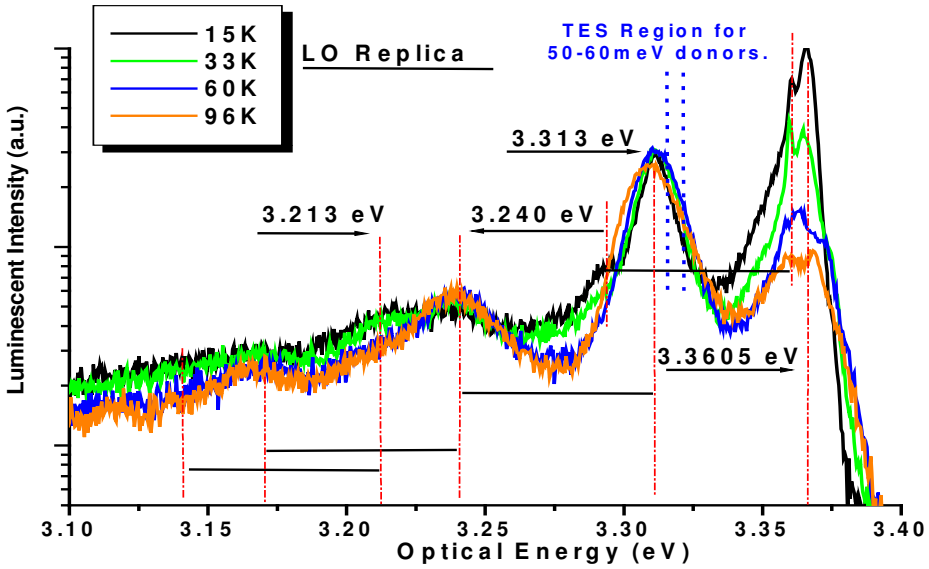

Fig. 5.xii: TD PL of N-doped ZnO

The similar trend observed in intensity with temperature change for the 3.24 eV and 3.313 eV bands together with the energy differences lends weight to a classification of the former to an LO of 3.313 eV. The DBX and 3.213 eV band also display distinct LO replica. The 3.313 eV emission persists over the temperature range, similar to other reports of acceptor-related emission [27].The 3.24 eV band however, may contain other contributions as well as 3.313 eV – 1LO. A band in this region has also been assigned as a typical DAP position in the literature [28,29]. Considering the evolution of intensity over the temperature range, as in fig. 2.x where characteristic intensity inversion from DAP to e^-A was not observed, the classification of this to a band to DAP was unsuitable. A calculation of E_{B_A} from eq. 2.ii - $E_{e^-A} = E_{Gap}(T) - E_{B_A} + k_B T/2$ - given the E_{Gap} and E_{e^-A} results in a ~127meV value, agreeable to the typical range of E_{B_A} for the N-acceptor [22]. As such, the 3.313 eV band may be assigned as e^- to a N-based acceptor transition. The 3.213 eV band remains without assignment, although it has been observed in N-doped ZnO films, remaining stable to higher temperatures, as observed here [27].

5.9 – Conclusions

Dopant introduction was found to deteriorate film crystalline quality but low concentrations maintained a reasonably low ω_{FWHM} values and also enhancing electrical properties. Optical data showed acceptor-related features even at higher concentrations

of P-dopant. Acceptor-related characteristics were found for both P- and N- dopants. Electrical measurements were exceptionally sensitive to ambient for P-doping, with p-type photoconductivity introduced under UV illumination. A change was also apparent for N-doped films under illumination with a reduction in dominant carrier concentration, but the majority carrier remained holes, as when measured in the dark. Other dopants (Li and Bi) did not display any indication of acceptor incorporation with negative carrier concentrations of the order of $10^{17}\,\mathrm{cm}^{-3}$ measured.

5.10 – References

[1] S. Chakrabarti, B. Doggett, R. O'Haire, E. McGlynn, M.O. Henry, A. Meaney, J-P. Mosnier, *Superlat. and Micro.* **42**, 21-25 (2007)

[2] S. Chakrabarti, B. Doggett, R. O'Haire, E. McGlynn, M.O. Henry, A. Meaney, J-P. Mosnier, *Elec. Lett.* **42**, 20 (2006)

[3] J-R. Duclère, R.O'Haire, A. Meaney, K. Johnston, I. Reid, G. Tobin, J-P. Mosnier, M. Guilloux-Viry, E. McGlynn, M.O. Henry, *J. Mater Sci: Mater. In Elec.* **16**, 421-427 (2005)

[4] J-R. Duclère, M. Novotny, A. Meaney, R. O'Haire, E. McGlynna, M.O. Henry, J-P. Mosnier, *Superlat. and Micro.* **38**, 397-405 (2005)

[5] B. Doggett, S. Chakrabarti, R. O'Haire, A. Meaney, E. McGlynn, M.O. Henry, J-P. Mosnier, *Superlat. and Micro.* **42**, 74-78 (2007)

[6] M. Kawakami, A. B. Hartanto, Y. Nakata, T. Okada, *J. J. App. Phys.* **42**, 1A/B, L 33–L35 (2003)

[7] W-J. Lee, J. Kang, K.J. Chang, *Physica B*, **376-377**, 699-702 (2006)

[8] B. Clafin, D.C. Look, S.J. Park, G. Cantwell, *J. Crys. Growth*, **287**, 16-22 (2006)

[9] D.C. Look, *Semicon. Sci.and Tech.* **20**, S55–S61, (2005)

[10] Z. Fan, P-c. Chang, J.G. Lu, E. C. Walter, R.M. Penner, C-h. Lin, H.P. Lee, *App. Phys. Lett.***85**, 25 (2004)

[11] J. Domenech, A. Prieto, *J. Phys. Chem.* **90**, 6, 1123–1126, (1986)

[12] G. Hu, H. Gong, E.F. Chor, P. Wu, *App. Phys. Lett.* **89**, 251102 (2006)

[13] Y.W. Heo, K. Ip, S.J. Pearton, D.P. Norton, *phys. Stat. Sol. (a)*, **201**, No.7, 1500 – 1509 (2004)

[14] D. Li, Y.H. Leung, A.B. Djurišić, Z.T. Liu, M.H. Xie, S.L. Shi, S.J. Xu, W.K. Chan, *App. Phys. Lett.* **85**, 9 (2004)

[15] K. Vanheusden, W.L. Warren, C.H. Seager, D.R. Tallant, J.A. Voigt, B.E. Gnade, *J. App. Phys.* **79**, 10, 7983 (1996)

[16] A.F. Kohan, G. Ceder, D. Morgan, C.G. Van de Walle, *Phys. Rev. B.* **61**, 22 (2000)

[17] T.M. Børseth, B.G. Svensson, A.Y. Kuznetsov, *App. Phys. Lett.* **89**, 262112 (2006)

[18] D.M. Hofmann, D. Pfisterer, J. Sann, B.K. Meyer, R. Tena-Zaera, V. Munoz-Sanjose, T. Frank, G. Pensl, *App. Phys. A.* **88**, 147-151 (2007)

[19] Ü. Özgür, Y. I. Alivov, C. Liu, A.Teke, M.A. Reschikov, S. Doğan, V. Avrutin, S-J. Cho, H. Morkoç, *J. App. Phys.* **98**, 041301 (2005)

[20] S-J. So, C-B. Park, *J. Crys. Growth.* 285, 606-612 (2005)

[21] B. Yao, Y. P. Xie, C. X. Cong, H. J. Zhao, Y. R. Sui, T. Yang, Q. He, *J. Phys. D: Appl. Phys.* **42**, 015407 (2009)

[22] D-K. Hwang, H-S. Kim, J-H. Lim, J-Y. Oh, J-H. Yang, S.J. Park, K-K. Kim, D.C. Look, Y.S. Park, *App. Phys. Lett.* **86**, 151917 (2005)

[23] C.X. Shan, Z. Liu, S.K. Hark, *App. Phys. Lett.* 92, 073103 (2008)

[24] K-K. Kim, H-S. Kim, D-K. Hwang, J-H. Lim, S-J. Park, *App. Phys. Lett.* **83**, 1 (2003)

[25] A. Tsukazaki, A. Ohtomo, T. Onuma, M. Ohtani, T. Makino, M. Sumiya, K. Ohtani, S. F. Chichibu., S. Fuke, Y. Segawa, H. Ohno, H. Koinuma, M. Kawasaki, *Nature Materials* **4**, 42 - 46 (2004)

[26] S. Hullavarad, N. Hullavarad, D. Look, B. Claflin, *Nanoscale Res. Lett.* **4**, 1421–1427 (2009)

[27] J.B. Cui, M.A. Thomas, Y.C. Soo, H. Kandel, T.P. Chen, J. Phys. D: App. Phys. **42**, 155407 (2009)

[28] A. Dadgar, N. Oleynik, J. Blasing, S. Deiter, D. Forster, F. Bertram, A. Diez, M. Seip, A. Greiling, J. Christen, A. Krost, *J. Crys. Growth*, **272**, 800 – 804 (2004)

[29] G. Xiong, KJ.B. Ucer, R.T. Williams, J. Lee, D. Bhattacharyya, J. Metson, P. Evans, *J. App. Phys.* **B**, 043258 (2005)

Chapter 6: The State of the Art & Considerations for Future Work

6.1 – A Doping Problem Unsolved

P and N doped ZnO produced here displayed acceptor-related features, with revised assignments to the P_{Zn}-2 V_{Zn} and $e^{-}A$ acceptor mechanisms respectively. Electrically, both displayed p-type conductivity, but N-doping appeared superior, with p-type behaviour measured at high temperatures. The long-term stability of this doping is still uncertain however, indeed the dopant most suited for achieving p-type ZnO is still yet to be identified experimentally with a recent review discussing P, Li, Sb and N amongst others, in doping of ZnO [2]. Others have reported success with F_i incorporated as an acceptor in ZnO and ZnMgO [3]. ZnO displaying a stable conductivity type that is easy reproduced is still yet to be achieved with many successful reports on mis-matched substrates, which typically introduce a high defect density [4]. The current research has certainly moved in an encouraging direction.

6.2 – A Doping Problem Solved?

Reports in Tsukazi *et al* from 2005 [5,6] showed that ZnO blue-LED homo-junctions were possible for ZnO but suffered from difficulties with electroluminescence shift due to imbalance of majority carrier between the p and n junctions. Although other authors have published ZnO p-n junctions for device application [7] the rectifying characteristics did not better the threshold voltage.

More recent work from the same Nakano, Tsukazi *et al* [8] has concentrated on ZnO devices, but ones which do not require a p-type ZnO film since Shottky diodes are understood to emit light [9]. Other successful work has been published for ZnO used in novel device production. Solar cells for example, which also do not require a p-type layer have been manufactured but efficiency has not been improved substantially in the previous 5 years [10, 11]. This show ZnO device application is still a relatively young field of research with limits of device characteristics still being tested.

These latter reports underline the difficulty to this day in realising reliable and stable good quality p-type material, with research directed toward devices not reliant on p-type ZnO. The material itself though sits with a number of other transparent oxide semiconductors materials attracting attention with a good recent review by Hosono [12]. Indeed, with many nitride-based materials being directed toward realisation of all-phosphor LED-based warm-white lighting, incorporating ZnO with these may offer an

initial niche for the application of ZnO, even if the p-type problem is not solved. Indeed, ZnO has been successfully used in LEDs with materials currently common to such devices, such as a n-ZnO / p-GaN hetero-junction [13].

6.3 – Future Research

Questions still remaining unanswered as to the nature of some of the p-type conduction demonstrated in this dissertation, quite usual for doping studies as discussed above. The difficulties outlined in measuring the electrical characteristics of the material, tuning growth and maintaining optical and electrical characteristics may be teased out with much more extensive, systematic approaches to growth and characterisation. The number of variables present in growth and characterisation, including those outside of experimental control, makes this type of approach difficult. Tackling the issues concerning reproducibility of the p-type behaviour identified here and ensuring material growth is guided to producing p-type materials of long-term stability are natural and achievable steps in further work, followed perhaps by proof-of-concept devices.

6.4 – References

[1] D.C. Look, G.M. Renuld, R.H. Burgener II, J.R. Sizelove, *App. Phys. Lett.* **85**, 22 (2004)

[2] M.D. McCluskey, S.J. Jokela, *J. App. Phys.* **106**, 071101 (2009)

[3] A. Janotti, E. Snow, C.G. Van de Walle, *App. Phys. Lett.* **95**, 172109 (2009)

[4] C.W. Zou, R.Q. Chen, W. Gao, *Solid State Comm.* **149**, 45-46, 2085-2089 (2009)

[5] A. Tsukazi, A. Ohtomo, T. Onuma, M. Ohtani, T. Makino, M. Sumiya, K. Ohtani, S.F. Chichibu, S. Fuke, Y. Segawa, H. Ohno, H. Koinuma, M. Kawasaki, *Nature Materials*, **4**, 42-46 (2005)

[6] A. Tsukazi, M. Kubota, A. Ohtomo, T. Onuma, K. Ohtani, H. Ohno, S.F. Chichibu, M. Kawasaki, *J. J. App. Phys.* **44**, 21, L653-L645 (2005)

[7] J. Huang, L. Wang, R. Xu, K. Tang, W. Shi, Y. Xia, *Semicond. Sci. Technol*. 24, 075025 (2009)

[8] M. Nakano, T. Makino, A. Tsukazaki, K. Ueno, A. Ohtomo, T. Fukumura, H. Yuji, Y. Nishimoto, S. Akasaka, D. Takamizu, K. Nakahara, T. Tanabe, A. Kamisawa, M. Kawasaki, *App. Phys. Exp*. **1**, 12, 121201 (2008)

[9] E.F. Schubert, Light Emitting Diods, **2nd ed**. *Cambridge University Press, Cambridge*, p2, 2006

[10] S. Erten-Ela, S. Cogal, G. Turkmen, S. Icli, *Curr. App. Phys.* **10**, 187-192 (2010)

[11] M. Law, L.E. Greene, J.C. Johnson, R. Saykally, P. Yang, *Nature Materials,* **4**, 455-459 (2005)

[12] H. Hosono, *Thin Solid Films,* **515**, 15 (2007)

[13] J. Y. Lee, J. Hoon Lee, H. S. Kim, C-H. Lee, H-S. Ahn, H. K. Cho, Y. Y. Kim, B. H. Kong, H. S. Lee, *Thin Solid Films*, **517**, 5157-5160 (2009)

Acknowledgements

Having found my way to the end of this, and being certain that I have reached this exact journey's end only because of the influences of others along the way, I wish to extend thanks to those whom I am most indebted.

- Professor Martin Henry for his guidance, time, patience and wealth of advice.

- My colleagues at Dublin City University physics department, with special thanks to Dr. Enda McGlynn, Dr. Jean-Paul Mosnier, Dr. Jean-René Duclére, Dr. Justina Grabowska, Dr. Subho Chakrabrati, Dr. Richard O' Haire and all of the ZnO research group.

- My brother Noel for his unwavering support and my brother Steve for his blind expectation of my reaching this goal.

- Dr. McNamara, Dr. Sheppard and Ms. Rosarie Crowley for their help in overcoming some of life's obstacles outside of academia.

- My friends too numerous to list, that have been there even if they didn't know it.
- Geoff's, suppliers of the caffeine-rich dissertation fuel that is Waterford's best coffee.
- Special recognition to my parents Sarah & Noel, who nurtured the seed of curiosity and understanding that continues to shape me to this day. Mam, Dad…I did it.